Spatiotemporal model-based index development for Bering Sea and Aleutian Islands crab stocks

Update for Crab Plan Team modeling workshop

Caitlin Stern[1,2], Emily Ryznar[3,4], and Jon Richar[3,5]
[1]Alaska Department of Fish and Game
[2]caitlin.stern@alaska.gov
[3]NOAA Fisheries
[4]emily.ryznar@noaa.gov
[5]jon.richar@noaa.gov

January 2025

Introduction

The goal of this investigation was to develop spatiotemporal model-based indices of abundance for three Bering Sea and Aleutian Islands (BSAI) crab stocks: Tanner crab (*Chionoecetes bairdi*), St. Matthew Island blue king crab (*Paralithodes platypus*), and Norton Sound red king crab (*Paralithodes camtschaticus*). Research suggests that spatiotemporal model-based indices can be more robust to survey changes than are design-based indices, though the models must be well-specified (Yalcin et al. 2023). Spatiotemporal model-based indices are used in North Pacific Fishery Management Council (NPFMC) groundfish stock assessments for species including Eastern Bering Sea (EBS) walleye pollock (*Gadus chalcogrammus*) and EBS Pacific cod (*Gadus macrocephalus*), both of which use the vector-autoregressive spatial temporal (VAST) approach (Thorson 2019) to produce indices used in the assessments (Ianelli et al. 2024; Barbeaux et al. 2024). Previous BSAI crab stock assessments have presented models using spatiotemporal model-based indices (e.g., Ianelli et al. 2017), although these models were not accepted for harvest specifications (SSC 2017).

We generated biomass and abundance estimates using the R package *sdmTMB* (Anderson et al. 2022), which uses geostatistical time series data to estimate spatial and spatiotemporal generalized linear mixed effects models. This approach allows for index standardization when the set of stations surveyed is not consistent across years: one can generate a spatial grid that covers the area of interest, predict from the model onto that grid, and sum the predicted abundance/biomass to obtain an area-weighted index that is independent of sampling locations (Anderson et al. 2022).

All three stock assessments for the crab stocks presented here use data from the National Marine Fisheries Service (NMFS) Eastern Bering Sea (EBS) bottom trawl survey (Stockhausen 2024; Hamazaki 2024; Stern and Palof 2024). The St. Matthew Island blue king crab stock assessment also uses data from the Alaska Department of Fish and Game (ADF&G) St. Matthew Island blue king crab pot survey, while the Norton Sound red king crab stock assessment uses data from the NMFS Northern Bering Sea bottom trawl survey and the ADF&G Norton Sound red king crab trawl survey.

Spatiotemporal model-based index development is expected to confer distinct advantages for each of the three stocks. For the St. Matthew Island blue king crab stock, standardizing the survey indices could allow the assessment to use the existing survey data more rigorously. The NMFS EBS trawl survey is undergoing changes including dropping the high sampling density "corner stations" near St. Matthew Island from 2024 onward (DeFilippo et al. 2023; Stern & Palof 2024); index standardization will allow the assessment to

continue using the full time series of data despite changes in the spatial footprint of the survey. For Norton Sound red king crab, a model-based approach could provide a more consistent way to combine the three existing trawl survey data sets into a single index of abundance. For Tanner crab, spatiotemporal model-indices will permit index standardization across the full survey time series despite changes in the survey footprint in early survey years.

Spatiotemporal index standardization can also be accomplished using vector autoregressive spatiotemporal models (VAST). However, compared to *sdmTMB*, VAST is often criticized for having a difficult user interface, slower estimation times, and less-flexible model specification. Therefore, we mainly use *sdmTMB* in the following index standardization.

Methods

We fit models using the R package *sdmTMB*.

A number of decision points arise when fitting models using *sdmTMB*, including:

- The resolution of the spatial mesh used in fitting the model. A higher number of knots, specified when creating the spatial mesh using the make_mesh() function, indicates a higher resolution mesh.

- The spatiotemporal random fields estimation method. The spatiotemporal random fields can be estimated as independent and identically distributed (IID), first-order autoregressive (AR1), a random walk, or fixed at zero. The spatial random fields are estimated for each time slice, the period of which is specified in the model (e.g., time = year).

- The model family. Many options exist, including tweedie(), delta_gamma(), and delta_lognormal().

For each stock, we ran a range of models to examine the effects of choices at each of these decision points on model predictions. After fitting models, we used the following steps for model evaluation:

- First, we checked measures such as model convergence using the sdmTMB::sanity() function. Output of this function for a model that passes all sanity checks is displayed as follows:

✓ Non-linear minimizer suggests successful convergence

✓ Hessian matrix is positive definite

✓ No extreme or very small eigenvalues detected

✓ No gradients with respect to fixed effects are $>= 0.001$

✓ No fixed-effect standard errors are NA

✓ No standard errors look unreasonably large

✓ No sigma parameters are < 0.01

✓ No sigma parameters are > 100

✓ Range parameter doesn't look unreasonably large

- If a model passed all the sanity checks, we used the R package *DHARMa* (Hartig 2022) to calculate the DHARMa residuals using the function DHARMa::dharma_residuals(). Models that did not pass the sanity checks were excluded from further consideration.

- We examined the DHARMa residual Q-Q plots. We tested for quantile deviations, under- or overdispersion, outliers, and zero- inflation using the functions DHARMa::testQuantiles(), DHARMa::testDispersion(), DHARMa::testOutliers(), and DHARMa::testZeroInflation(), respectively. Additionally, we examined plots of DHARMa residuals over space and time for potential patterns of autocorrelation.

- We evaluated model predictive skill (the predictive ability of the model for new observations; Anderson *et al.* 2024) using the cross validation function sdmTMB_cv(). This function measures model predictive skill by holding out subsets of the data in turn and using each as a test set. These subsets of data are termed "folds". To compare models, we did cross validation with the same number of folds for each model then extracted the model's summed log-likelihood value, which represents the model's predictive density. Predictive density values closer to zero indicate better out-of-sample predictive skill. We also plotted model-predicted indices against observed values and examined goodness-of-fit.

- We also compared model-predicted indices using the best model framework for each stock with indices generated in VAST using a comparable framework to evaluate potential differences in index generation between model algorithms.

Tanner crab

We utilized abundance and biomass data collected from the NMFS EBS bottom trawl survey (1975-2024) to fit Tanner crab models in *sdmTMB*. Sex-maturity categories included all males combined, immature females, and mature females, and data were filtered to only include crab with a carapace width greater than or equal to 25mm. As the survey gear and methods were standardized in 1982 (Stauffer 2004), we fit separate models to data before 1982 and data in and after 1982 for each sex-size/maturity category. To evaluate decision points for model formulations, we fit models using a 50-knot, 90-knot, and 120-knot mesh (Figures 2 - 4), a Tweedie or delta-gamma model family, and a IID spatiotemporal random field. Models fit using the delta-lognormal family did not pass initial model sanity checks and models using an AR1 or random walk spatiotemporal random field did not converge. Therefore, we do not discuss these frameworks any further. The best model framework was used to predict Tanner crab abundance and biomass on an EBS-wide survey grid (Figure 1), a grid encompassing the EBS area west of 166° (for the Tanner West stock; Figure 66, Appendix), and a grid encompassing the EBS area east of 166° (for the Tanner East stock; Figure 67, Appendix). Each prediction grid was a resolution of 5 km^2.

Norton Sound red king crab

The Norton Sound red king crab stock assessment includes data from the NMFS trawl survey (1976-1991), ADF&G trawl survey (1996-2024), and NMFS NBS trawl survey (2010-2023). Here, we used abundance data from the NMFS NBS trawl survey to fit models in *sdmTMB*. Future work will address producing model-based indices for the remaining data sets. We filtered the NMFS NBS trawl survey data set to ensure that it included only observations with coordinates falling within the Norton Sound Section of Statistical Area Q. Matching the assessment model, we included abundance information on males with carapace length $\geq$ 64 mm. For model fitting, we used spatial meshes at three resolutions: 100 knots, 50 knots, and 30 knots (Figures 60 - 58). We used a prediction grid with resolution of 5 km^2 (Figure 57). For model cross validation, we used 3 folds.

St. Matthew Island blue king crab

The St. Matthew Island blue king crab stock assessment includes two survey time series: the NMFS summer bottom trawl survey and the ADF&G pot survey. Here, we used biomass data collected during the NMFS summer bottom trawl survey (1978-2024) to fit models in *sdmTMB*; further investigation of how to specify area surveyed for the pot survey is needed before that data set can be analyzed using this approach. Matching

the assessment model, we included biomass information on males with carapace length $\geq$ 90 mm. For model fitting, we used spatial meshes at three resolutions: 120 knots, 90 knots, and 50 knots (Figures 25 - 23). We used a prediction grid with a resolution of 4 km^2 (Figure 26). For model cross validation, we used 3 folds; models did not always converge with 5 or 10 folds.

Results

Tanner crab

Model diagnostics

All models passed sanity checks. Model diagnostics using DHARMa residuals varied among the number of knots specified in the mesh (50, 90, 120), model family (Tweedie, delta-gamma), and data period (pre-1982, 1982 onward) for both abundance (Table 1) and biomass (Table 2) models. For male abundance, a model using a delta-gamma distribution and 50 knots performed the best for both periods in terms of the greatest log-likelihood, with only the post-1982 model showing evidence of outliers, zero-inflation, and quantile deviations. However, this was true regardless of the model family or number of knots used, and this pattern was consistent across other sex-maturity categories. For immature female abundance, a delta-gamma model had the largest log-likelihood across periods, with models using 90 and 50 knots performing best pre-1982 and post-1982, respectively. The best model pre-1982 showed evidence of quantile deviation and dispersion, whereas the best model post-1982 showed evidence of outliers, zero-inflation, and quantile deviation. Contrasting the other two sex-maturity categories, the Tweedie family had the largest log-likelihood for mature female abundance, with 90 and 50 knots performing best pre-1982 and post-1982, respectively. The pre-1982 Tweedie model only showed evidence of zero-inflation, whereas the post-1982 Tweedie model showed evidence of outliers, dispersion, zero-inflation, and quantile deviation.

As with male abundance, a delta-gamma model using 50 knots had the largest log-likelihood for male biomass pre- and post-1982. Models for both periods showed evidence of quantile deviation, dispersion, and outliers, where just the post-1982 model also showed evidence of zero-inflation as was true for other models in this period. For immature female biomass, a Tweedie model using 90 and 50 knots for pre- and post-1982 had the greatest log-likelihood. While the pre-1982 Tweedie model had the largest log-likelihood, it showed evidence of dispersion and zero-inflation whereas the next-best model, a delta-gamma using 90 knots, did not. For immature female biomass post-1982, Tweedie and delta-gamma models using 50 knots had the largest and very similar log-likelihoods, with the Tweedie model showing evidence of quantile deviation, dispersion, outliers, and zero-inflation where the delta-gamma model did not show evidence of dispersion. A similar pattern was seen in diagnostics for mature female biomass models, where Tweedie models using 50 knots had the largest but very similar log-likelihood values to delta-gamma models using 50 knots across both periods. The pre-1982 50-knot Tweedie model showed evidence of dispersion, outliers, and zero-inflation, whereas the 50-knot delta-gamma model did not. The post-1982 50-knot Tweedie model exhibited evidence of all diagnostics, whereas the 50-knot delta-gamma model did not show evidence of dispersion.

Accounting for strong model performance across sex-maturity categories, periods, and response (abundance/biomass), we selected the delta-gamma model family and a 50-knot mesh as a parsimonious model framework for prediction. DHARMa residuals for these models across sex-maturity categories and periods did not strongly diverge from the 1-1 line (Figures 5 - 6) despite some evidence of quantile dispersion. In addition, DHARMa residuals for these models did not show evidence of spatiotemporal autocorrelation (Figures 7 - 12).

Predicted abundance and biomass

Heat maps of EBS-wide predicted abundance for Tanner crab males, immature females, and mature females are shown in figures 13 - 15, respectively, using our chosen model framework (delta-gamma, 50 knots). Heat maps of EBS-wide predicted biomass for Tanner crab males, immature females, and mature females are

shown in figures 16 - 18. Abundance and biomass heat maps for Tanner crab west and east of 166° are shown in Appendix figures 68 - 73 and figures 74 - 79, respectively.

Predicted index fits to observations

The EBS-wide model-predicted indices using a delta-gamma family varied in their fits to survey abundance (Figure 19) and biomass observations (Figure 20) across sex-maturity categories and between model fitting periods. Across sex-maturity categories, model fits with different knots were most variable before 1982, which could be due to high variability in the spatial footprint of the survey in this period. In this period, uncertainty was generally greater in indices predicted using 50 knots, with the majority of survey observations points and associated uncertainty overlapping with model predicted values and uncertainty. From 1982 onward, indices predicted at different knots are less variable compared with each other, with models using 50 knots generally exhibiting greater uncertainty than 90 and 120 knots. As before, the majority of survey observations points and associated uncertainty overlap with model predicted values and uncertainty across knot specifications. Similar patterns across knots and sex-maturity categories were seen for predicted abundance and biomass indices for Tanners west and east of 166° (Figures 80 - 83, Appendix).

Comparison of *sdmTMB* with VAST

For the EBS, abundance and biomass indices were similar between *sdmTMB* and VAST estimates (Figures 21 - 22). Across sex-maturity categories, the greatest differences in *sdmTMB* and VAST estimates were in the pre-1982 period, with *sdmTMB* estimates generally exhibiting greater uncertainty in this period. Among sex-maturity categories, the greatest difference in estimates were for mature females, where *sdmTMB* estimates were generally slightly higher than VAST but still tracking the observed survey values. Similar patterns were seen in *sdmTMB* and VAST estimates for Tanner crab west of 166° (Figures 84 - 85, Appendix) and east of 166°(Figures 86 - 87, Appendix).

St. Matthew Island blue king crab

Model diagnostics

For SMBKC, only models using the Tweedie family passed the sanity checks. Models using the delta gamma and delta lognormal families did not. Models using IID, random walk, and AR1 spatial estimation methods with spatial resolutions of 50, 90, and 120 knots passed the sanity checks.

Results of the tests performed on the DHARMa residuals for each model are displayed in figures 27 - 34 and Table 3. DHARMa residuals for the IID Tweedie model with 50 knots could not be generated and so residual analysis results for that model are not displayed. All models showed evidence of underdispersion, with observed data less dispersed than expected under the fitted models. None of the models showed evidence of outliers. All models showed evidence of quantile deviations. The IID and RW models with 120 knots showed evidence of zero inflation, with the observed data containing more zeros than would be expected under the fitted model.

The spatial distribution of DHARMa residuals for each model is plotted in figures 35 - 42. Spatial residual patterns are satisfactory for all models.

Predictive density (log-likelihood) values for the SMBKC models that passed the sanity checks are shown in Table 3. Predictive density values closer to zero indicate better out-of-sample predictive skill. Models with missing predictive density values are models that did not pass all sanity checks. The three models with the best out-of-sample predictive skill all used the random walk spatial estimation method. The model with 90 knots had the best out-of-sample predictive skill, followed by the models with 50 and 120 knots.

Predicted biomass

The spatial distribution of model-predicted SMBKC biomass for each model is shown in figures 43 - 51.

Model-based index fit to observations

For all three spatial random fields estimation methods (IID, RW, and AR1), the model fitted using a mesh with finer spatial resolution (120 knots) estimated lower blue king crab biomass than the models fitted using coarser spatial resolutions (50 or 90 knots) (Figures 52, 53, and 54). The models with 120 knots showed poorer visual fits to the survey observations, particularly in recent years, in accordance with their relatively lower predictive skill scores. For the IID, RW, and AR1 models, the models with 90 knots estimated higher biomass than did the models with 50 knots. The models with 50 knots had the best predictive skill of the IID and AR1 models, but the model with 90 knots had the best predictive skill of the RW models and overall.

Comparison of *sdmTMB* with VAST

A matched comparison between sdmTMB and VAST for the sdmTMB models with the best predictive skill was not possible because output from random walk, Tweedie VAST models was not available. It was not clear how to implement a random walk in VAST. However, output from IID VAST models using the Tweedie or delta-gamma families was available, and output from the IID and Tweedie VAST models is shown compared to the indices from the two sdmTMB models with best predictive skill in Figures 55 and 56. For the models using a 90-knot mesh, the sdmTMB and VAST predictions for recent years are very similar, with the sdmTMB predictions higher in 2024. For the models using a 50-knot mesh, the sdmTMB and VAST predictions for recent years are more divergent, with the VAST model generally predicting higher abundance.

Norton Sound red king crab

Model diagnostics

We ran models with IID, random walk, and AR1 spatial estimation methods; with the Tweedie, delta gamma, and delta lognormal families; and with spatial resolutions of 30, 50, and 100 knots. Of these 27 models, the only one that passed the sanity checks was the model with random walk spatial estimation, the Tweedie family, and 30 knots.

The DHARMa residuals diagnostic plot showed evidence of quantile deviations for the NSRKC model (Figure 61), with no evidence of over- or underdispersion, outliers, or zero inflation.

Predictive density (log-likelihood) values for NSRKC models are shown in table 4. Models with missing predictive density values are models that did not pass all sanity checks.

Predicted abundance

A heat map of predicted NSRKC abundance for the model with random walk spatial estimation, the Tweedie family, and a 30-knot mesh is show in Figure 63.

Model-based index fits to observations

The predicted index showed a close fit to survey abundance estimates, with the exception of 2022, when the model seems to over-estimate abundance relative to the survey estimate (Figure 64). The random walk, Tweedie models with 100-knot mesh and 50-knot mesh are shown for comparison with the 30-knot mesh model, although only the model with the 30-knot mesh passed sanity checks.

Comparison of *sdmTMB* with VAST

A matched comparison between sdmTMB and VAST was not possible because output from random walk, Tweedie VAST models was not available. VAST models using IID and Tweedie did not converge, and it was not clear how to implement a random walk spatial estimation method in VAST. Available VAST models used IID with a delta-gamma family and the resulting index is show in Figure 65. Recognizing that the comparison is not matched, the sdmTMB-derived index more closely follows the fluctuations in survey abundance estimates, while the VAST-derived index seems to smooth to a greater extent, and tends to estimate lower abundance overall.

Recommended models

For Tanner crab, we recommend a delta-gamma model using a 50-knot mesh as these were consistently top-performing models across sex-maturity categories and periods. However, different best models could be selected by sex-maturity category and fitting period such as delta-gamma models using 90 knots.

For St. Matthew Island blue king crab, on the basis of the predictive skill scores and visual inspection of model fits, we recommend using the index of abundance generated by either the random walk, Tweedie model with a 90-knot mesh or the random walk, Tweedie model with a 50-knot mesh.

For Norton Sound red king crab, only one model passed the sanity checks and thus is the recommended model. That model uses random walk spatial estimation, the Tweedie family, and a 30-knot mesh.

Acknowledgements

References

Anderson, S.C., Ward, E.J., English, P.A., Barnett, L.A.K. 2022. sdmTMB: An R package for fast, flexible, and user-friendly generalized linear mixed effects models with spatial and spatiotemporal random fields. bioRxiv.

Anderson, S.C., Ward, E.J., English, P.A., Barnett, L.A.K., Thorson, J.T. 2024. Cross-validation for model evaluation and comparison. Retrieved from https://pbs-assess.github.io/sdmTMB/articles/cross-validation.html.

Barbeaux, S.J., L. Barnett, P. Hulson, J. Nielsen, S.K. Shotwell, E. Siddon, I. Spies. 2024. Assessment of the Pacific cod stock in the Eastern Bering Sea. In: Stock Assessment and Fishery Evaluation report for the Groundfish Resources of the Bering Sea/Aleutian Islands regions. North Pacific Fishery Management Council, Anchorage, AK.

DeFilippo, L., S. Kotwicki, L. Barnett, J. Richar, M.A. Litzow, W.T. Stockhausen, K. Palof. 2023. Evaluating the impacts of reduced sampling density in a systematic fisheries-independent survey design. Frontiers in Marine Science 10:1219283.

Hamazaki, T. 2024. Norton Sound red king crab stock assessment for the fishing year 2024. In: Stock Assessment and Fishery Evaluation Report for the King and Tanner Crab Fisheries of the Bering Sea and Aleutian Islands: 2024 Final Crab SAFE. North Pacific Fishery Management Council, Anchorage AK.

Hartig, F. 2022. DHARMa: Residual Diagnostics for Hierarchical (Multi-Level / Mixed) Regression Models. R package version 0.4.6, https://CRAN.R-project.org/package=DHARMa.

Ianelli, J., D. Webber, J. Zheng, A. Letaw. 2017. Saint Matthew Island blue king crab stock assessment 2017. In: Stock Assessment and Fishery Evaluation Report for the King and Tanner Crab Fisheries of the Bering Sea and Aleutian Islands: 2017 Final Crab SAFE. North Pacific Fishery Management Council, Anchorage AK.

Ianelli, J., T. Honkalehto, S. Wassermann, A. McCarthy, S. Steinessen, C. McGilliard, E. Siddon. 2024. Assessment of walleye pollock in the eastern Bering Sea. In: Stock Assessment and Fishery Evaluation report for the Groundfish Resources of the Bering Sea/Aleutian Islands regions. North Pacific Fishery Management Council, Anchorage, AK.

SSC. 2017. Scientific and Statistical Committee report to the North Pacific Fishery Management Council, October 2nd-4th, 2017. North Pacific Fishery Management Council, Anchorage, AK.

Stauffer, G.A. 2004. NOAA protocols for groundfish bottom trawl surveys of the Nation's fishery resources. U.S. Dep. Commer., NOAA Tech. Memo. NMFS-F/SPO-65, 205p.

Stern, C., K. Palof. 2024. Saint Matthew Island blue king crab stock assessment 2024. In: Stock Assessment and Fishery Evaluation Report for the King and Tanner Crab Fisheries of the Bering Sea and Aleutian Islands: 2024 Final Crab SAFE. North Pacific Fishery Management Council, Anchorage AK.

Stockhausen, W.T. 2024. 2024 stock assessment and fishery evaluation report for the Tanner crab fisheries of the Bering Sea and Aleutians Islands regions. In: Stock Assessment and Fishery Evaluation Report for the King and Tanner Crab Fisheries of the Bering Sea and Aleutian Islands: 2024 Final Crab SAFE. North Pacific Fishery Management Council, Anchorage AK.

Thorson, J.T. 2019. Guidance for decisions using the vector autoregressive spatio-temporal (VAST) package in stock, ecosystem, habitat, and climate assessments. Fisheries Research 210:143-161. https://doi.org/10.1016/j.fishres.2018.10.013

Yalcin, S., S.C. Anderson, P.M. Regular, P.A. English. 2023. Exploring the limits of spatiotemporal and design-based index standardization under reduced survey coverage. ICES Journal of Marine Sciences 80:2368-2379. https://doi.org/10.1093/icesjms/fsad155

Tables

Table 1: Tanner crab diagnostic values for abundance models fit with Tweedie or delta gamma families and a spatial resolution of 50, 90, or 120 knots across sex-size maturity categories and model-fitting periods (pre-1982, during or after 1982). Log-likelihood values were estimated using the cross-validation function in sdmTMB with 3 folds. Quantile, dispersion, outlier, and zero-inflation diagnostics were estimated from DHARMa residuals, with values below 0.05 indicating significant metrics. Values are ordered within sex-size maturity category and period by decreasing log-likelihood.

Category	Period	Family	Knots	Log-likelihood	Quantiles	Dispersion	Outliers	Zero-inflation
Immature Female	<1982	Delta-gamma	90	-6371.5	0.0	0.0	0.5	0.5
Immature Female	<1982	Tweedie	90	-6475.4	0.0	0.0	0.0	0.1
Immature Female	<1982	Tweedie	120	-6666.0	0.1	0.0	0.4	0.2
Immature Female	<1982	Delta-gamma	50	-6716.3	0.0	0.2	0.2	0.0
Immature Female	<1982	Tweedie	50	-6850.9	0.1	0.0	0.1	0.1
Immature Female	<1982	Delta-gamma	120	-6907.8	0.0	0.0	0.1	0.1
Immature Female	>=1982	Delta-gamma	50	-53281.6	0.0	0.1	0.0	0.0
Immature Female	>=1982	Tweedie	50	-53380.1	0.0	0.0	0.0	0.0
Immature Female	>=1982	Tweedie	90	-53543.3	0.0	0.0	0.0	0.0
Immature Female	>=1982	Delta-gamma	90	-53553.8	0.0	0.2	0.0	0.0
Immature Female	>=1982	Tweedie	120	-53722.7	0.0	0.0	0.0	0.0
Immature Female	>=1982	Delta-gamma	120	-53852.8	0.0	0.7	0.0	0.0
Male	<1982	Delta-gamma	50	-9256.2	0.4	0.5	0.1	0.4
Male	<1982	Tweedie	90	-9339.9	0.0	0.0	0.0	0.1
Male	<1982	Delta-gamma	90	-9349.7	0.0	0.1	0.5	0.3
Male	<1982	Tweedie	120	-9397.7	0.0	0.0	0.0	0.0
Male	<1982	Delta-gamma	120	-9398.7	0.1	0.5	0.4	0.1
Male	<1982	Tweedie	50	-9540.7	0.0	0.0	0.0	0.0
Male	>=1982	Delta-gamma	50	-76006.3	0.0	0.1	0.0	0.0
Male	>=1982	Tweedie	50	-76072.9	0.0	0.0	0.0	0.0
Male	>=1982	Tweedie	90	-76229.4	0.0	0.0	0.0	0.0
Male	>=1982	Delta-gamma	90	-76277.7	0.0	0.1	0.0	0.0
Male	>=1982	Tweedie	120	-76318.2	0.0	0.0	0.0	0.0
Male	>=1982	Delta-gamma	120	-76509.5	0.0	0.1	0.0	0.0
Mature Female	<1982	Tweedie	90	-6089.8	0.1	0.4	0.1	0.0
Mature Female	<1982	Delta-gamma	90	-6097.3	0.0	0.8	0.5	0.6
Mature Female	<1982	Delta-gamma	50	-6097.4	0.0	0.4	0.0	0.0
Mature Female	<1982	Delta-gamma	120	-6108.3	0.2	0.3	0.1	0.0
Mature Female	<1982	Tweedie	120	-6132.7	0.0	0.0	0.8	0.0
Mature Female	<1982	Tweedie	50	-6189.4	0.1	0.0	0.0	0.0
Mature Female	>=1982	Tweedie	50	-43560.9	0.0	0.0	0.0	0.0
Mature Female	>=1982	Delta-gamma	50	-43625.4	0.0	0.0	0.0	0.0
Mature Female	>=1982	Delta-gamma	90	-43803.8	0.0	0.0	0.0	0.0
Mature Female	>=1982	Delta-gamma	120	-43943.3	0.0	0.0	0.0	0.0
Mature Female	>=1982	Tweedie	90	-43837.0	0.0	0.0	0.0	0.0
Mature Female	>=1982	Tweedie	120	-44059.6	0.0	0.0	0.0	0.0

Table 2: Tanner crab diagnostic values for biomass models fit with Tweedie or delta gamma families and a spatial resolution of 50, 90, or 120 knots across sex-size maturity categories and model-fitting periods (pre-1982, during or after 1982). Log-likelihood values were estimated using the cross-validation function in sdmTMB with 3 folds. Quantile, dispersion, outlier, and zero-inflation diagnostics were estimated from DHARMa residuals, with values below 0.05 indicating significant metrics. Values are ordered within sex-size maturity category and period by decreasing log-likelihood.

Category	Period	Family	Knots	Log-likelihood	Quantiles	Dispersion	Outliers	Zero-inflation
Immature Female	<1982	Tweedie	90	-6356.8	0.2	0.0	1.0	0.0
Immature Female	<1982	Delta-gamma	90	-6514.3	0.1	0.3	0.4	0.1
Immature Female	<1982	Delta-gamma	120	-6630.5	0.0	0.1	0.9	0.3
Immature Female	<1982	Tweedie	120	-6823.7	0.1	0.1	0.7	0.8
Immature Female	<1982	Delta-gamma	50	-6874.7	0.0	0.0	0.0	0.0
Immature Female	<1982	Tweedie	50	-7246.5	0.0	0.0	0.2	0.3
Immature Female	>=1982	Tweedie	50	-53292.8	0.0	0.0	0.0	0.0
Immature Female	>=1982	Delta-gamma	50	-53303.1	0.0	0.1	0.0	0.0
Immature Female	>=1982	Tweedie	90	-53587.3	0.0	0.0	0.0	0.0
Immature Female	>=1982	Delta-gamma	120	-53639.8	0.0	1.0	0.0	0.0
Immature Female	>=1982	Tweedie	120	-53652.8	0.0	0.0	0.0	0.0
Immature Female	>=1982	Delta-gamma	90	-53652.9	0.0	0.9	0.0	0.0
Male	<1982	Delta-gamma	50	-9275.5	0.0	0.0	0.0	0.3
Male	<1982	Tweedie	90	-9295.3	0.0	0.0	0.1	0.3
Male	<1982	Tweedie	50	-9309.6	0.0	0.0	0.0	0.1
Male	<1982	Delta-gamma	120	-9343.0	0.0	0.0	0.1	0.7
Male	<1982	Delta-gamma	90	-9349.5	0.0	0.0	0.4	0.0
Male	<1982	Tweedie	120	-9422.2	0.0	0.0	0.5	0.6
Male	>=1982	Delta-gamma	50	-75992.4	0.0	0.0	0.0	0.0
Male	>=1982	Tweedie	50	-76031.1	0.0	0.0	0.0	0.0
Male	>=1982	Delta-gamma	90	-76307.0	0.0	0.0	0.0	0.0
Male	>=1982	Tweedie	120	-76345.7	0.0	0.0	0.0	0.0
Male	>=1982	Delta-gamma	120	-76382.0	0.0	0.0	0.0	0.0
Male	>=1982	Tweedie	90	-76489.4	0.0	0.0	0.0	0.0
Mature Female	<1982	Tweedie	50	-6101.9	0.2	0.0	0.0	0.0
Mature Female	<1982	Delta-gamma	50	-6108.2	0.2	0.1	0.1	0.5
Mature Female	<1982	Delta-gamma	120	-6108.8	0.0	0.4	0.4	0.4
Mature Female	<1982	Delta-gamma	90	-6134.0	0.0	0.3	0.4	0.6
Mature Female	<1982	Tweedie	90	-6135.2	0.2	0.9	0.5	0.0
Mature Female	<1982	Tweedie	120	-6159.8	0.2	0.1	0.0	0.0
Mature Female	>=1982	Tweedie	50	-43735.8	0.0	0.0	0.0	0.0
Mature Female	>=1982	Delta-gamma	90	-43746.8	0.0	0.1	0.0	0.0
Mature Female	>=1982	Tweedie	90	-43818.5	0.0	0.0	0.0	0.0
Mature Female	>=1982	Delta-gamma	50	-43898.4	0.0	0.3	0.0	0.0
Mature Female	>=1982	Delta-gamma	120	-44076.4	0.0	0.0	0.0	0.0
Mature Female	>=1982	Tweedie	120	-44166.4	0.0	0.0	0.0	0.0

Table 3: St. Matthew Island blue king crab fitted model predictive skill (log-likelihood) values, estimated using sdmTMB cross-validation, for models fitted with Tweedie, delta gamma, or delta lognormal model familes; spatial random fields estimated using independent and identically distributed (IID), random walk (RW), or first-order autoregressive (AR1) methods; and spatial resolution of 50, 90, or 120 knots. Predictive skill (log-likelihood) values closer to zero represent better out-of-sample predictive skill. Model configurations with missing log-likelihood values represent models that did not pass sanity checks. Quantile, dispersion, outlier, and zero-inflation diagnostics were estimated from DHARMa residuals, with values below 0.05 indicating significant metrics.

Family	Estimation method	Knots	Log-likelihood	Quantiles	Dispersion	Outliers	Zero inflation
Tweedie	IID	120	-9880.9	0	0	0.6	0.0
Tweedie	IID	90	-9924.0	0	0	0.1	0.6
Tweedie	IID	50	-9732.6				
delta gamma	IID	120					
delta gamma	IID	90					
delta gamma	IID	50					
delta lognormal	IID	120					
delta lognormal	IID	90					
delta lognormal	IID	50					
Tweedie	RW	120	-9646.6	0	0	0.5	0.0
Tweedie	RW	90	-9630.6	0	0	0.5	0.6
Tweedie	RW	50	-9636.0	0	0	0.6	0.7
delta gamma	RW	50					
delta lognormal	RW	50					
Tweedie	AR1	120	-9952.4	0	0	0.8	0.1
Tweedie	AR1	90	-9860.5	0	0	0.4	0.6
Tweedie	AR1	50	-9700.1	0	0	0.4	0.9
delta gamma	AR1	50					
delta lognormal	AR1	50					

Table 4: Norton Sound red king crab fitted model predictive density (log-likelihood) values, estimated using sdmTMB cross-validation with 3 folds, for models fitted with Tweedie, delta gamma, or delta lognormal model familes; spatial random fields estimated using independent and identically distributed (IID), random walk (RW), or first-order autoregressive (AR1) methods; and spatial resolution of 30, 50, or 100 knots. Predictive density (log-likelihood) values closer to zero represent better out-of-sample predictive skill. Model configurations with missing log-likelihood values represent models that did not pass sanity checks. Quantile, dispersion, outlier, and zero-inflation diagnostics were estimated from DHARMa residuals, with values below 0.05 indicating significant metrics.

Family	Estimation method	Knots	Log-likelihood	Quantiles	Dispersion	Outliers	Zero inflation
Tweedie	IID	100					
Tweedie	IID	50					
Tweedie	IID	30					
delta gamma	IID	100					
delta gamma	IID	50					
delta gamma	IID	30					
delta lognormal	IID	100					
delta lognormal	IID	50					
delta lognormal	IID	30					
Tweedie	RW	100					
Tweedie	RW	50					
Tweedie	RW	30	-658.1	0.0	0.2	0.6	0.1
delta gamma	RW	100					
delta gamma	RW	50					
delta gamma	RW	30					
delta lognormal	RW	100					
delta lognormal	RW	50					
delta lognormal	RW	30					
Tweedie	AR1	100					
Tweedie	AR1	50					
Tweedie	AR1	30					
delta gamma	AR1	100					
delta gamma	AR1	50					
delta gamma	AR1	30					
delta lognormal	AR1	100					
delta lognormal	AR1	50					
delta lognormal	AR1	30					

Figures
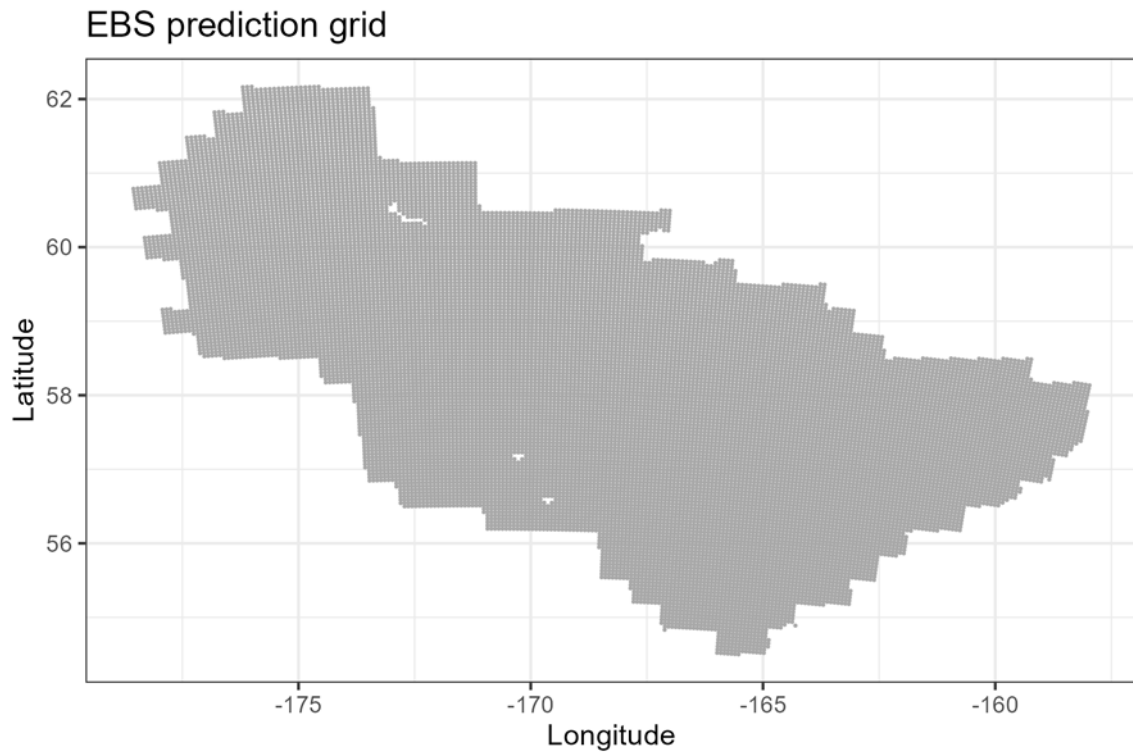
Figure 1: Eastern Bering Sea prediction grid used for Tanner crab spatial abundance and biomass predictions. Spatial resolution is 5km^2 and does not include land.
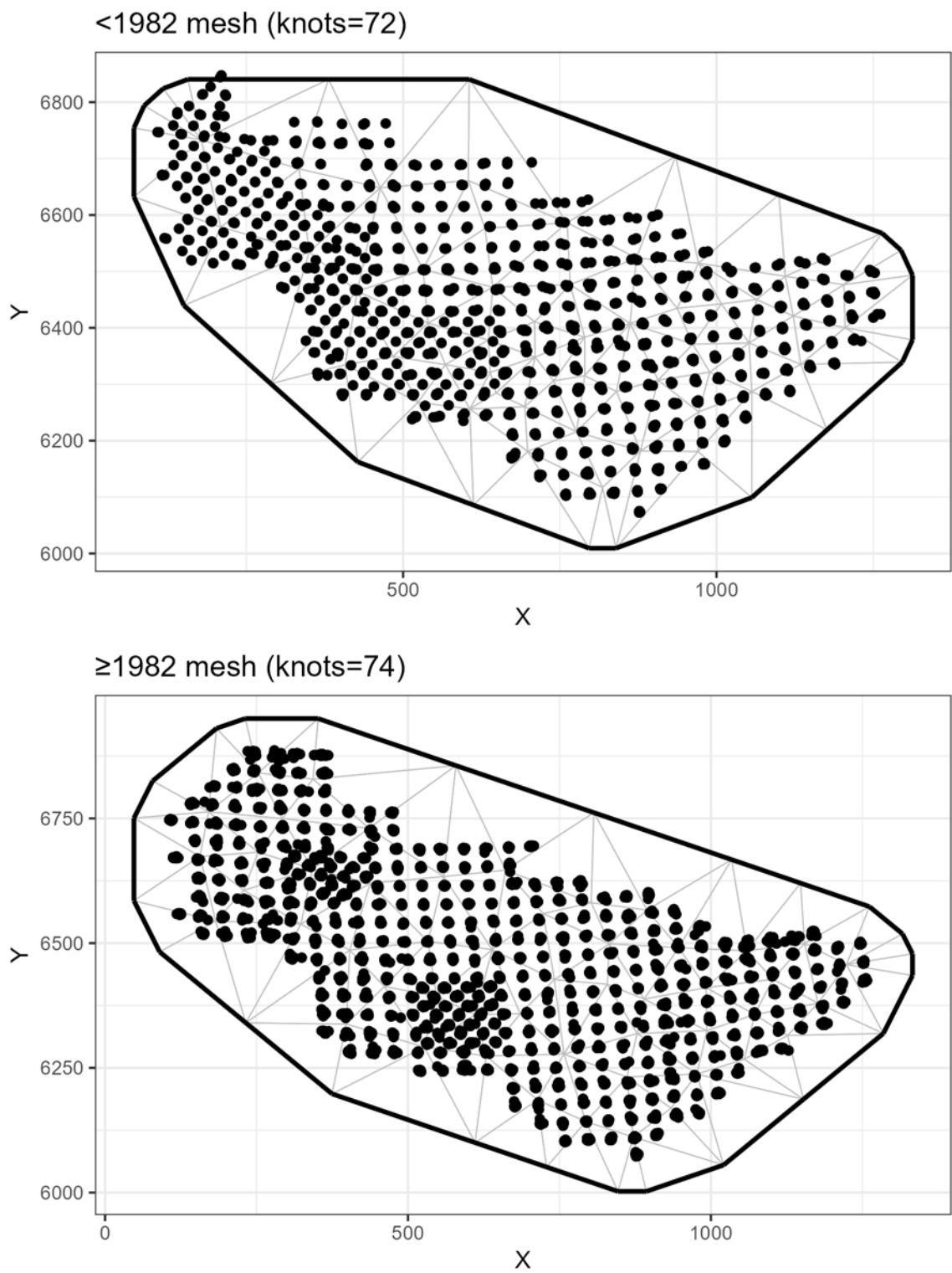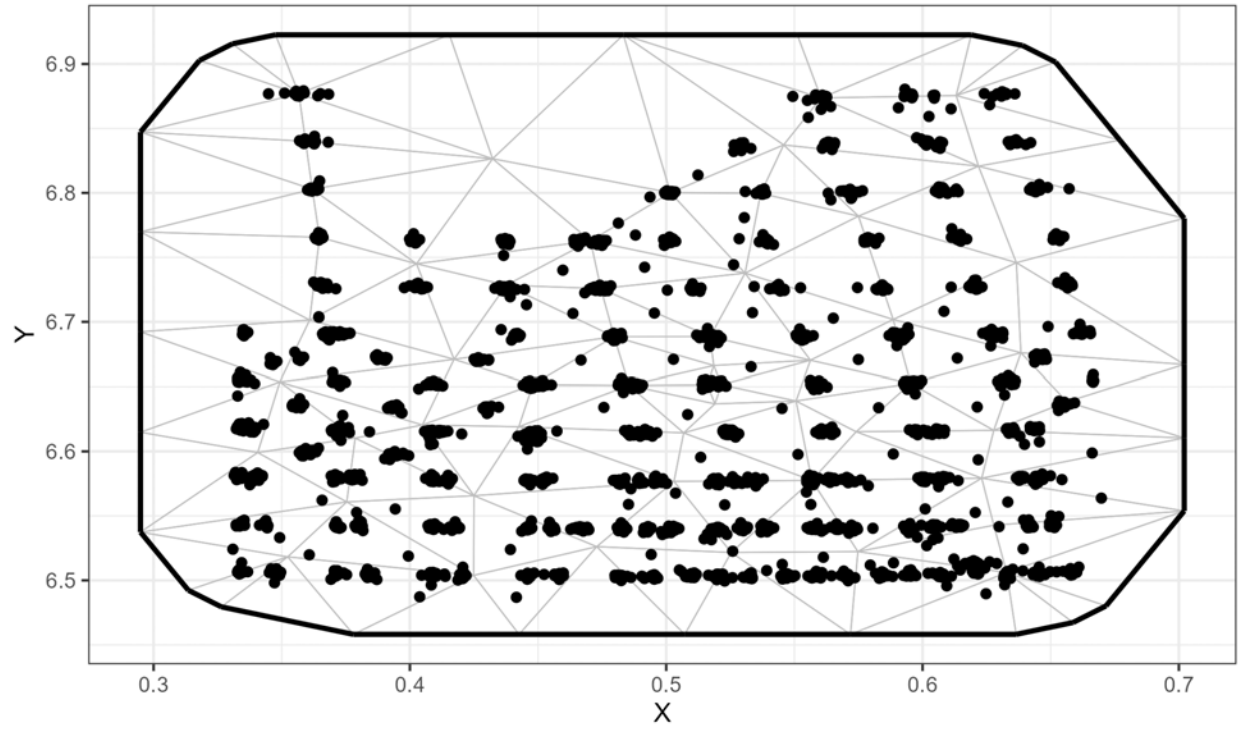
Figure 2: Spatial mesh with 50 knots used for fitting Tanner crab spatial models. Points represent observations and vertices represent knot locations. The title denotes the realized number of knots after mesh generation.
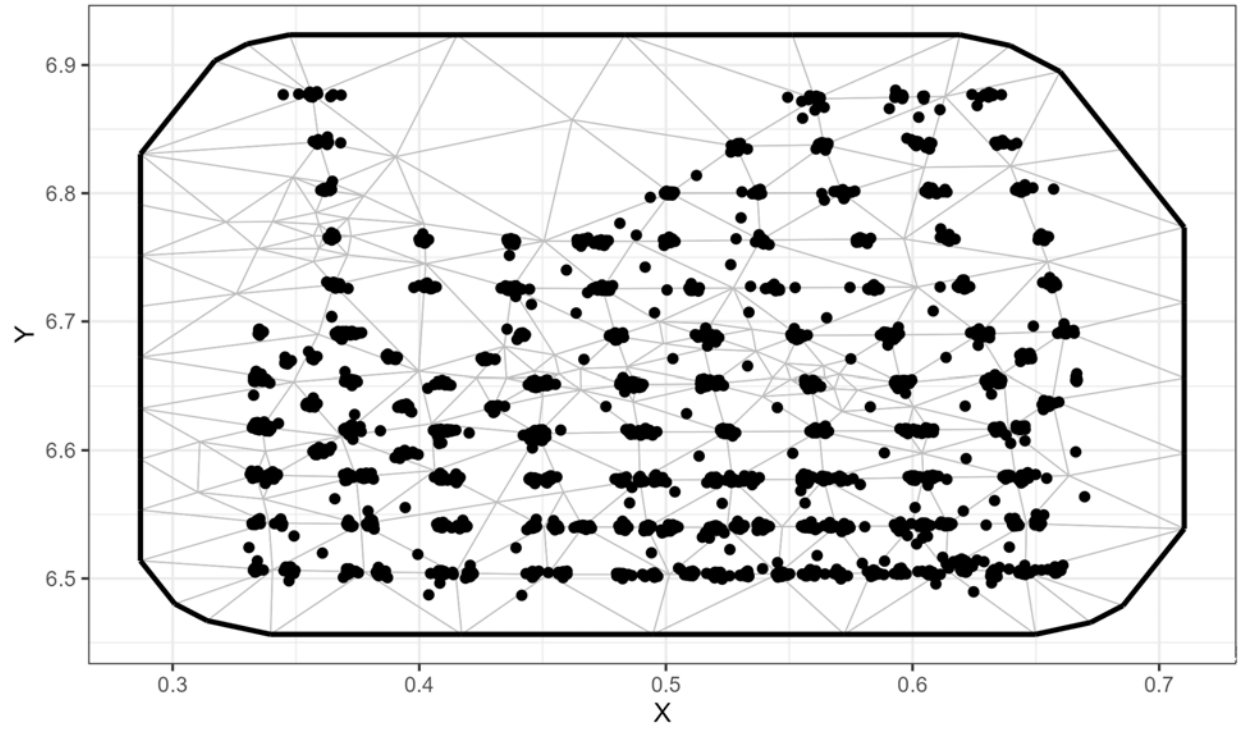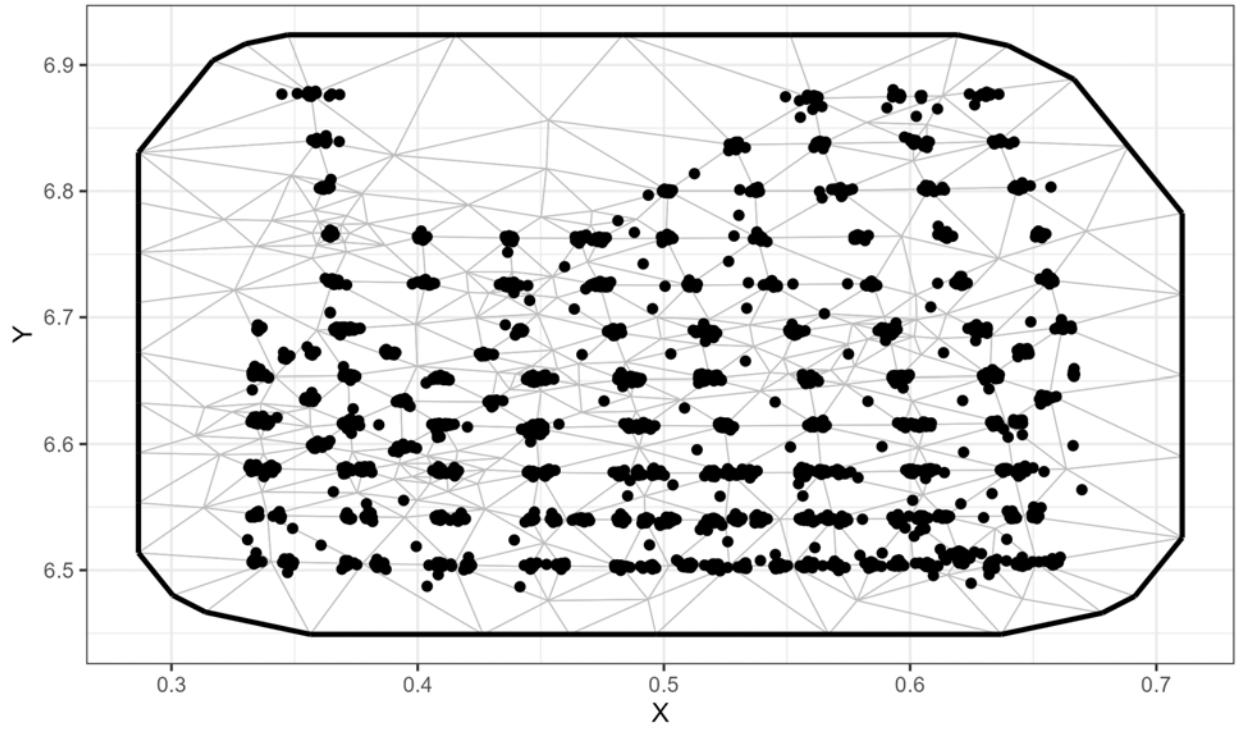
<1982 mesh (knots=122)

≥1982 mesh (knots=122)
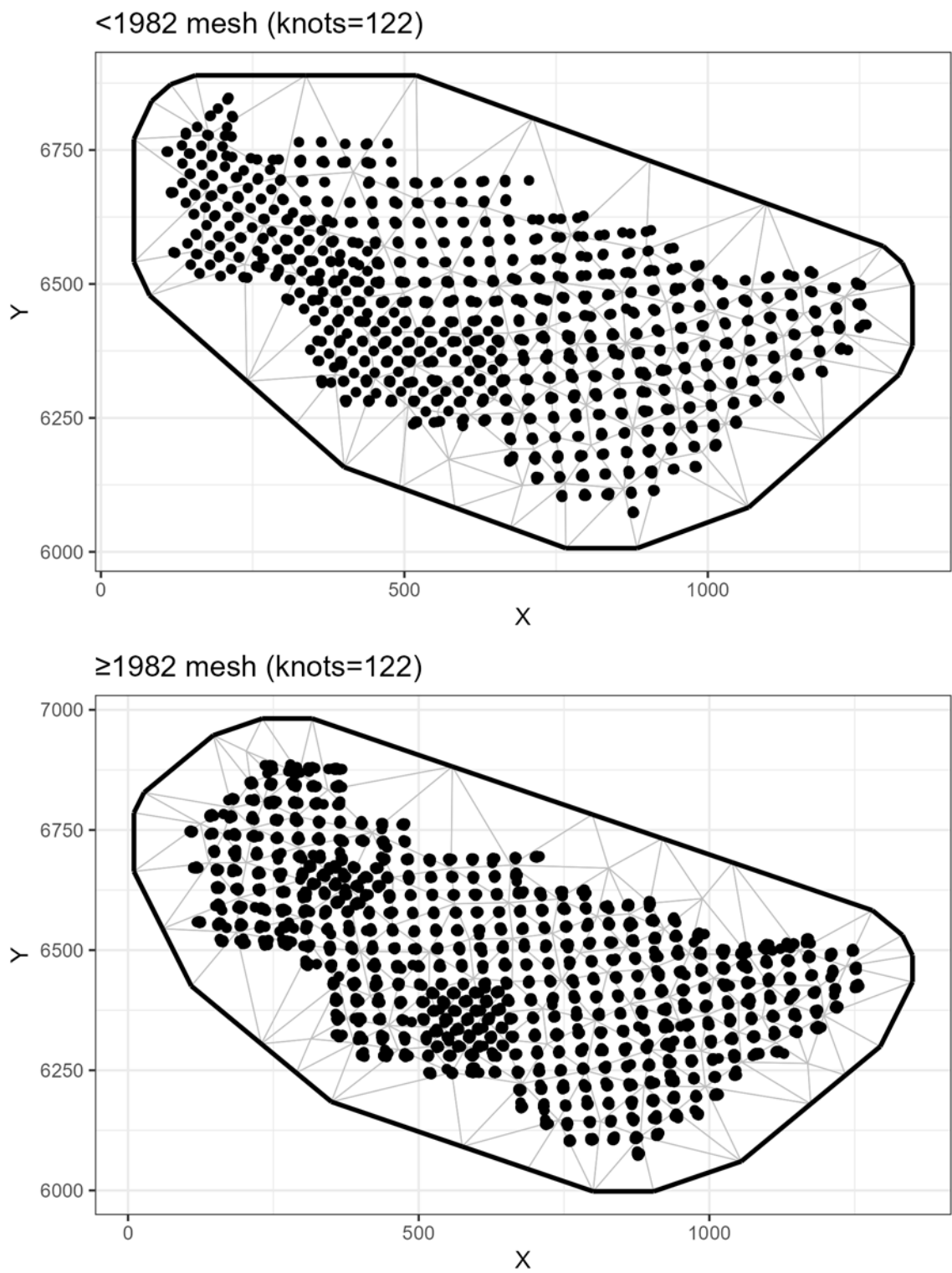
Figure 3: Spatial mesh with 90 knots used for fitting Tanner crab spatial models. Points represent observations and vertices represent knot locations. The title denotes the realized number of knots after mesh generation.
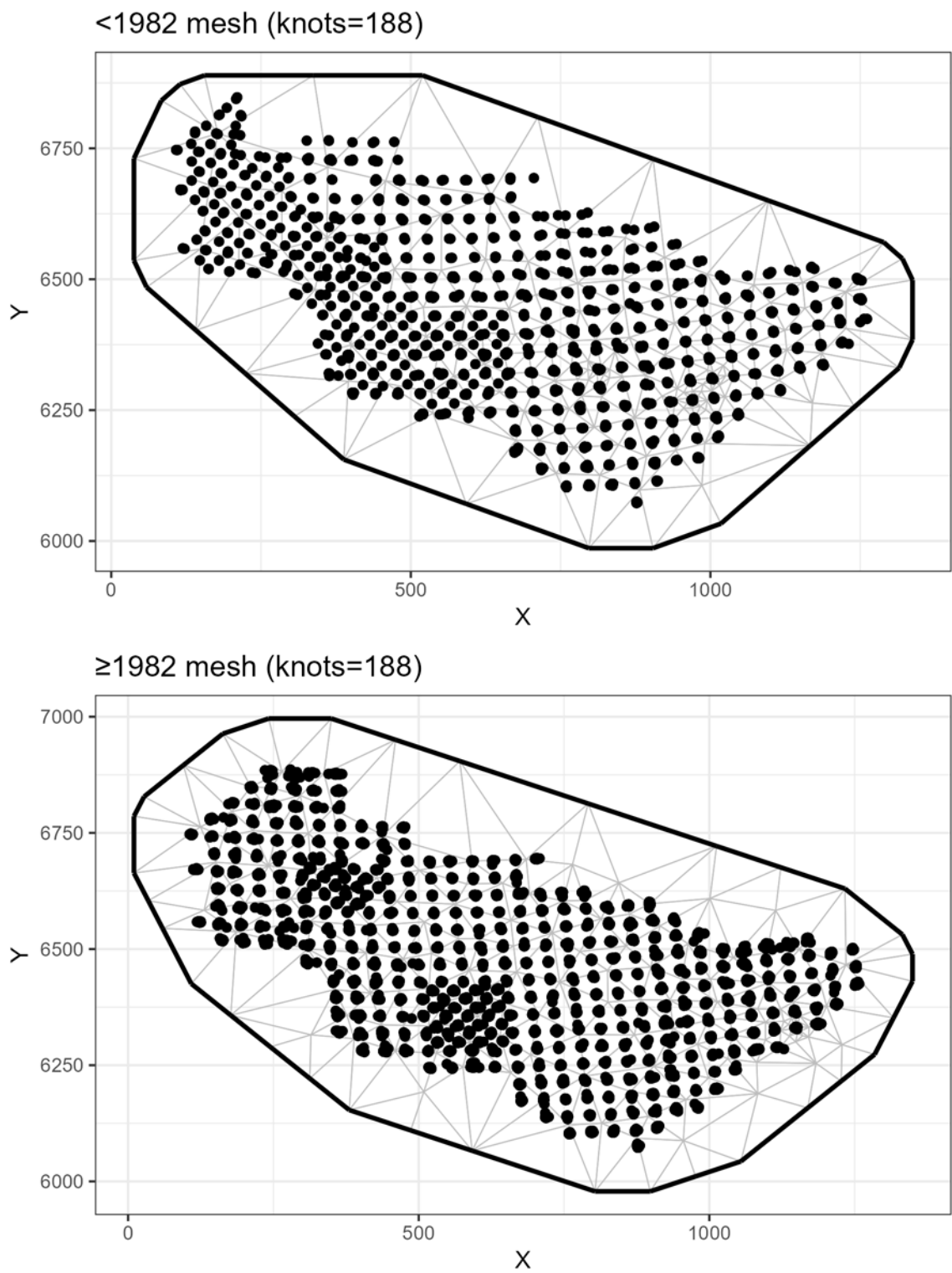
Figure 4: Spatial mesh with 120 knots used for fitting Tanner crab spatial models. Points represent observations and vertices represent knot locations. The title denotes the realized number of knots after mesh generation.
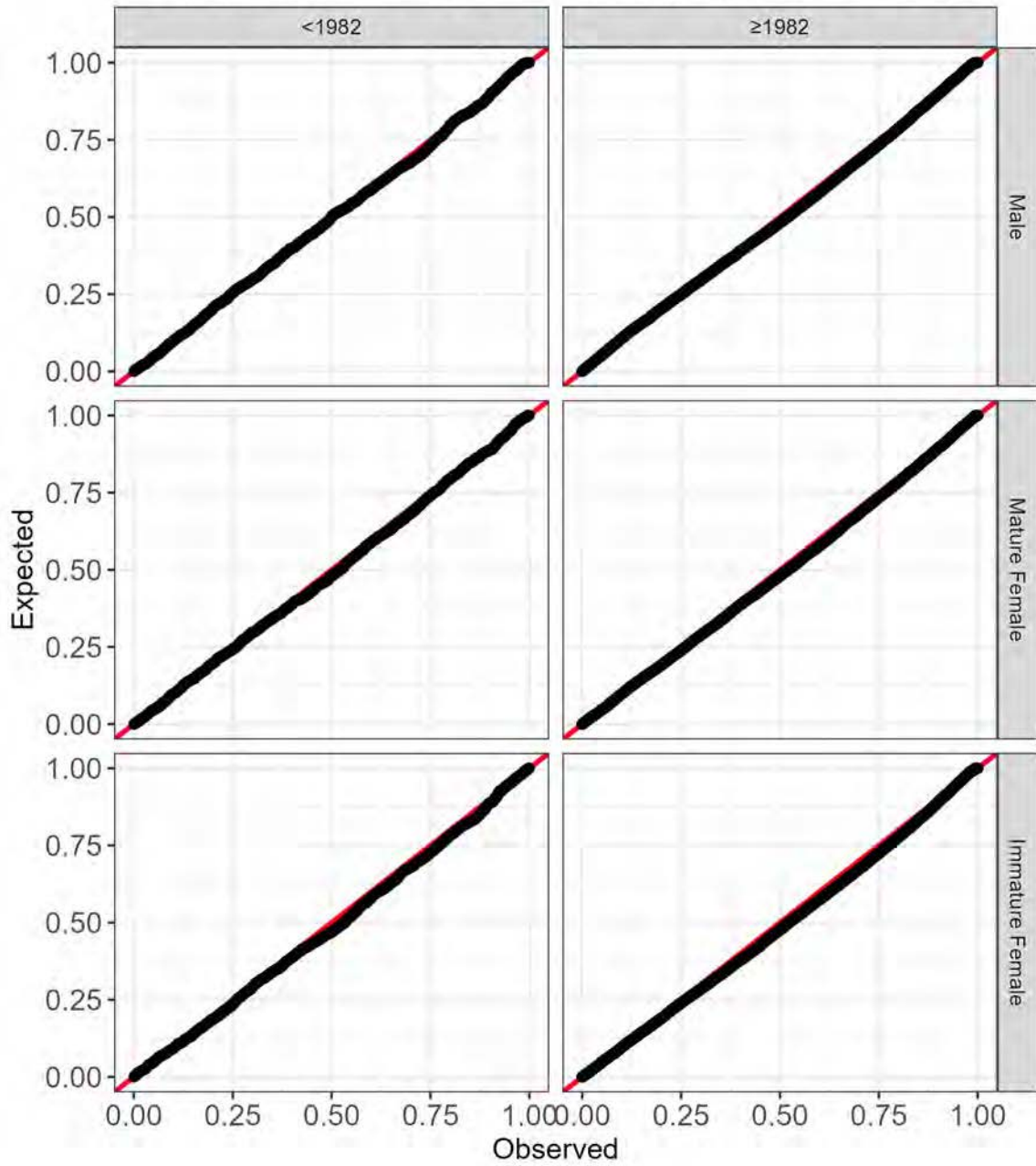
Figure 5: Q-Q plot of DHARMa residuals for abundance models fit with NMFS summer bottom trawl survey data before 1982 (left) and 1982 onward (right) using a delta-gamma model family and 50 knots in the model mesh.
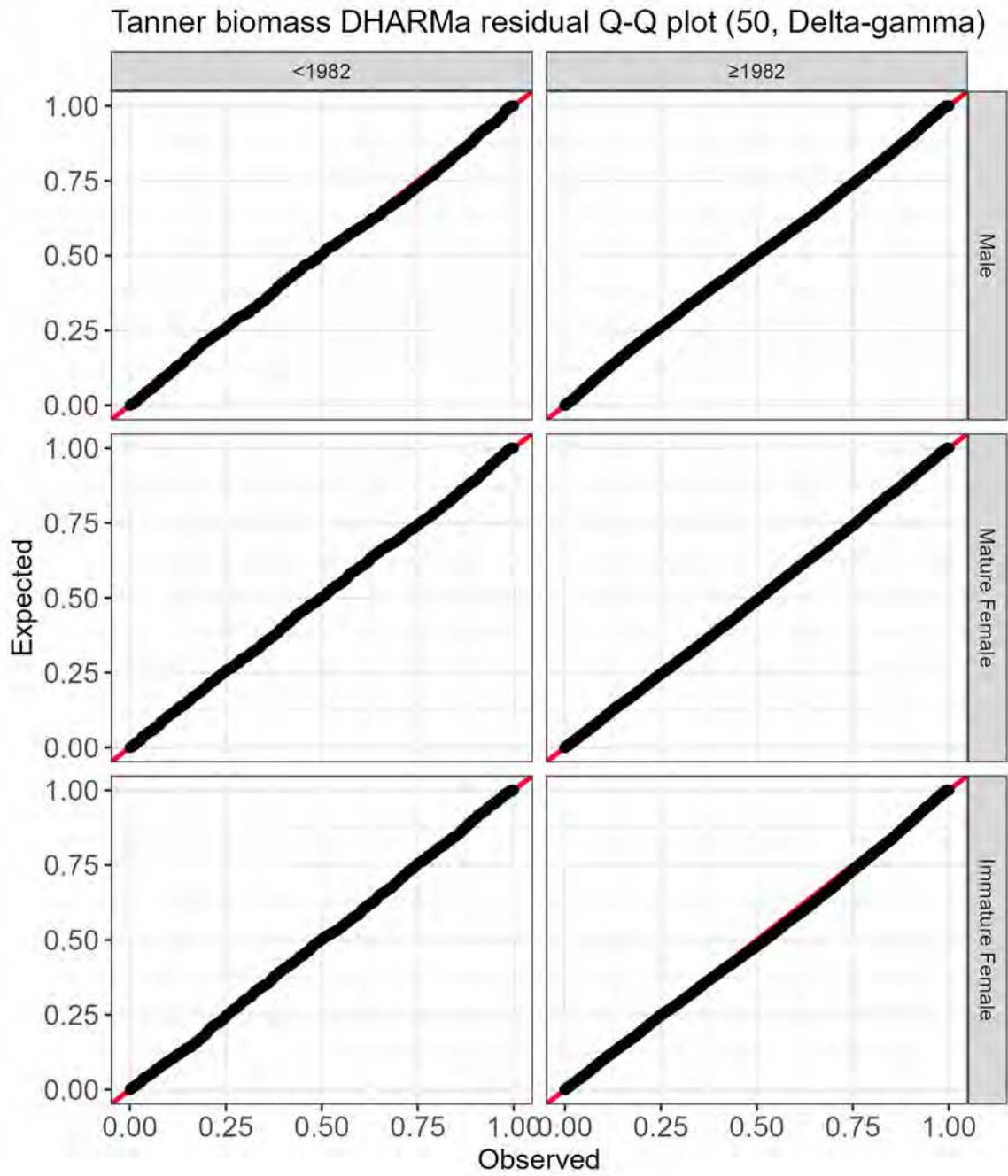
Figure 6: Q-Q plot of DHARMa residuals for biomass models fit with NMFS summer bottom trawl survey data before 1982 (left) and 1982 onward (right) using a delta-gamma model family and 50 knots in the model mesh.
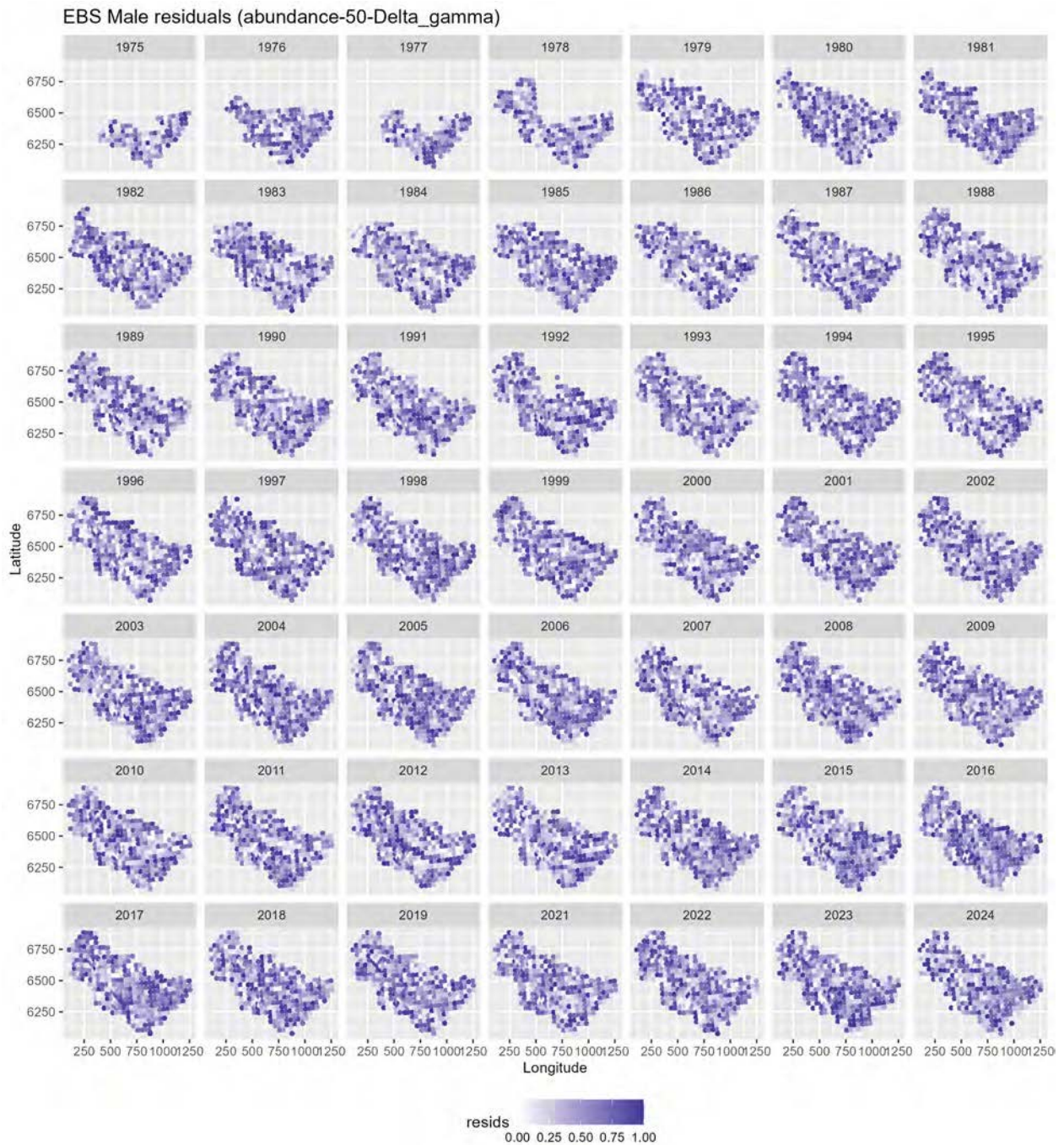
Figure 7: Spatial plot of DHARMa residuals for male abundance models fit using NMFS summer bottom trawl survey data before 1982 and 1982 onward with a 50-knot mesh and a delta-gamma model family. Predictions from both of these periods/models are combined in this figure.
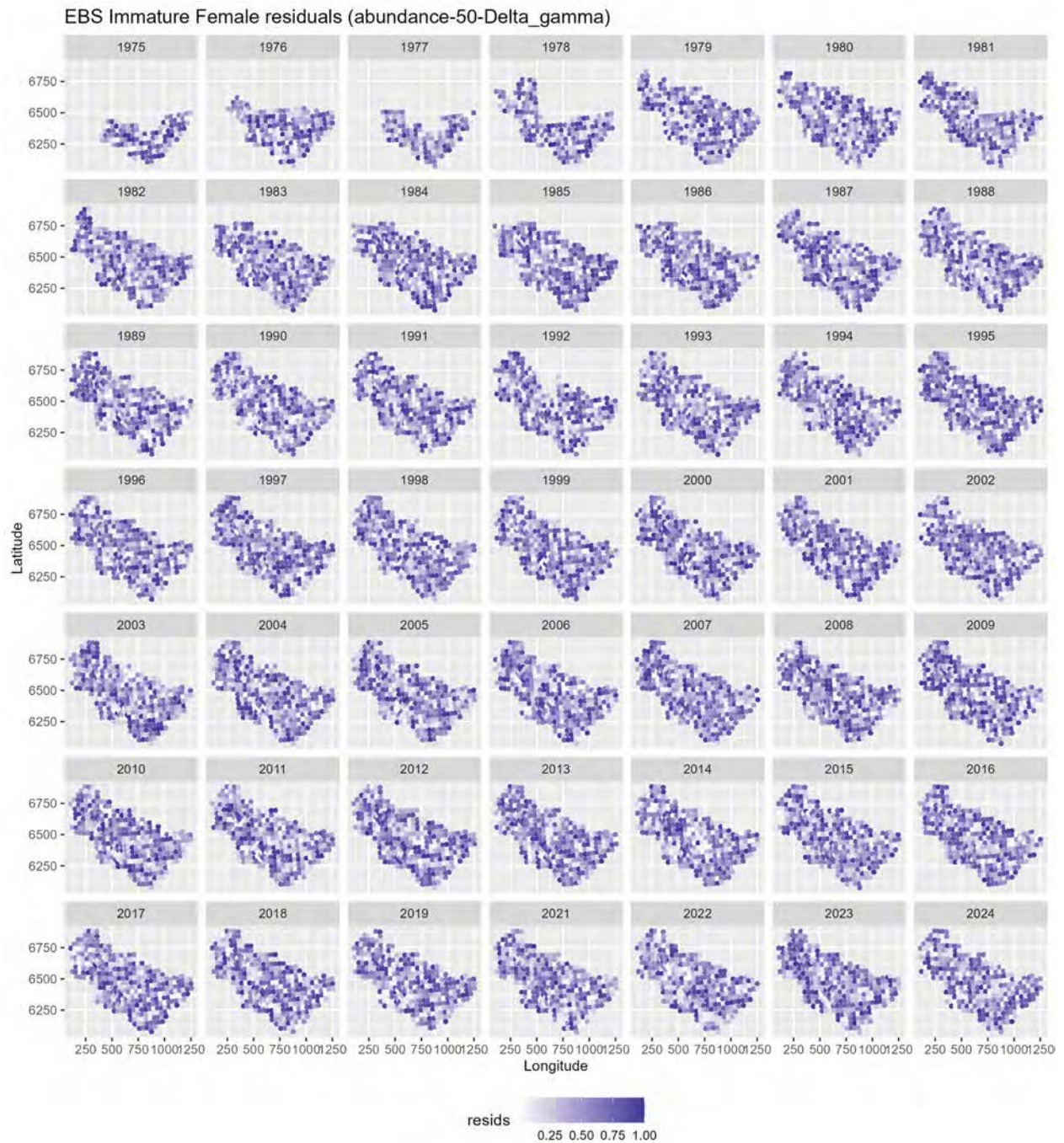
Figure 8: Spatial plot of DHARMa residuals for immature female abundance models fit using NMFS summer bottom trawl survey data before 1982 and 1982 onward with a 50-knot mesh and a delta-gamma model family. Predictions from both of these periods/models are combined in this figure.
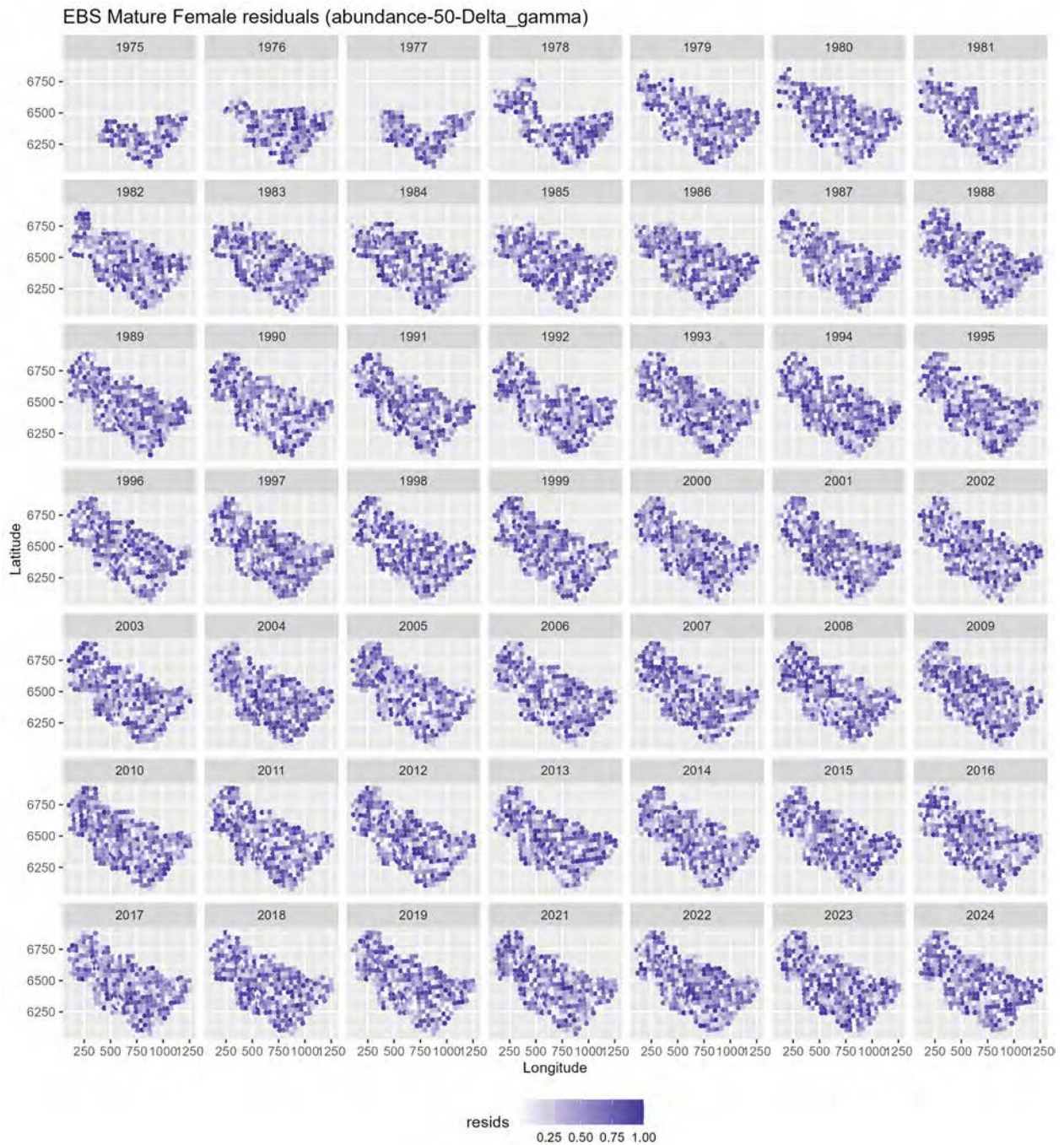
Figure 9: Spatial plot of DHARMa residuals for mature female abundance models fit using NMFS summer bottom trawl survey data before 1982 and 1982 onward with a 50-knot mesh and a delta-gamma model family. Predictions from both of these periods/models are combined in this figure.
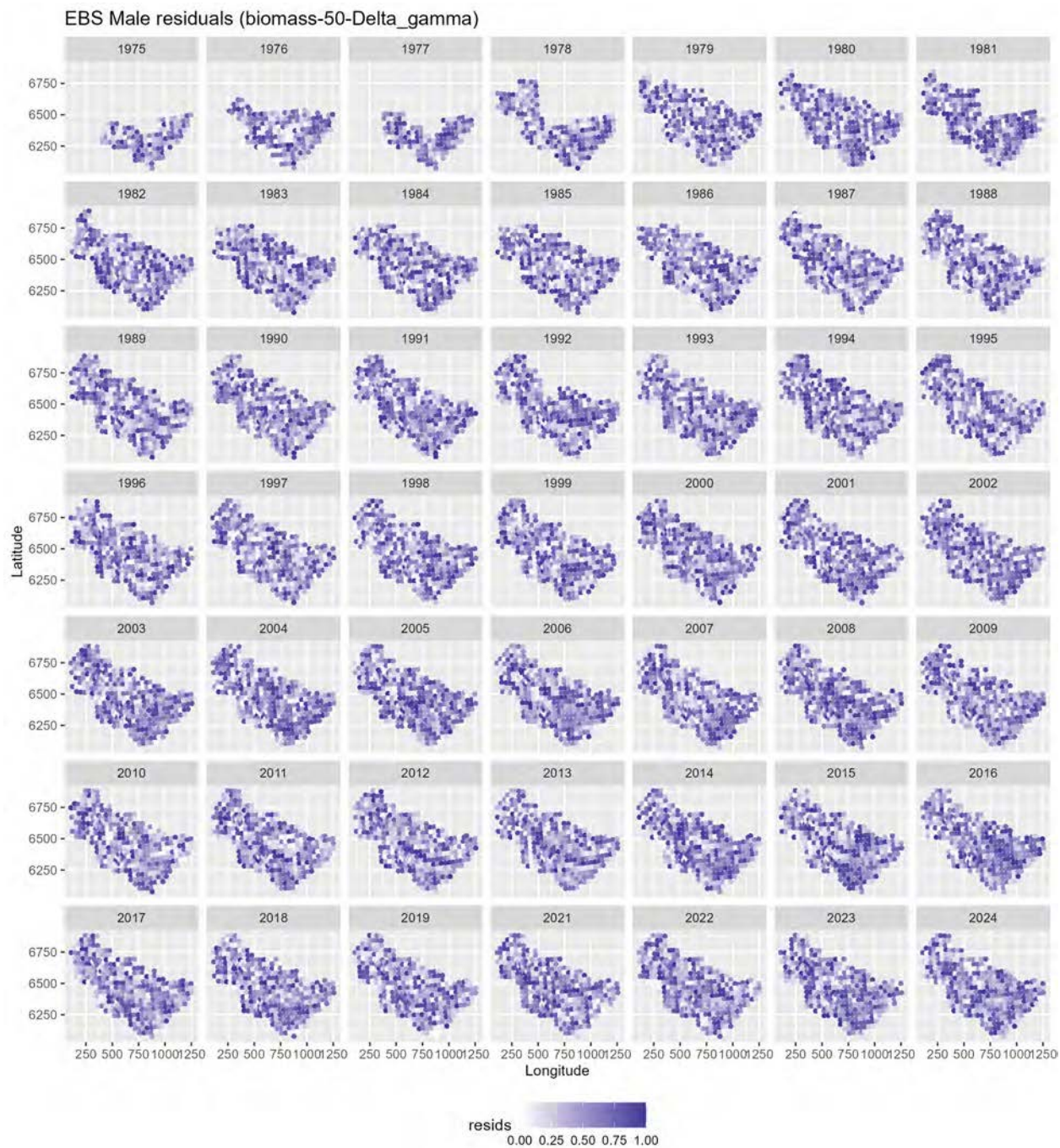
Figure 10: Spatial plot of DHARMa residuals for male biomass models fit using NMFS summer bottom trawl survey data before 1982 and 1982 onward with a 50-knot mesh and a delta-gamma model family. Predictions from both of these periods/models are combined in this figure.
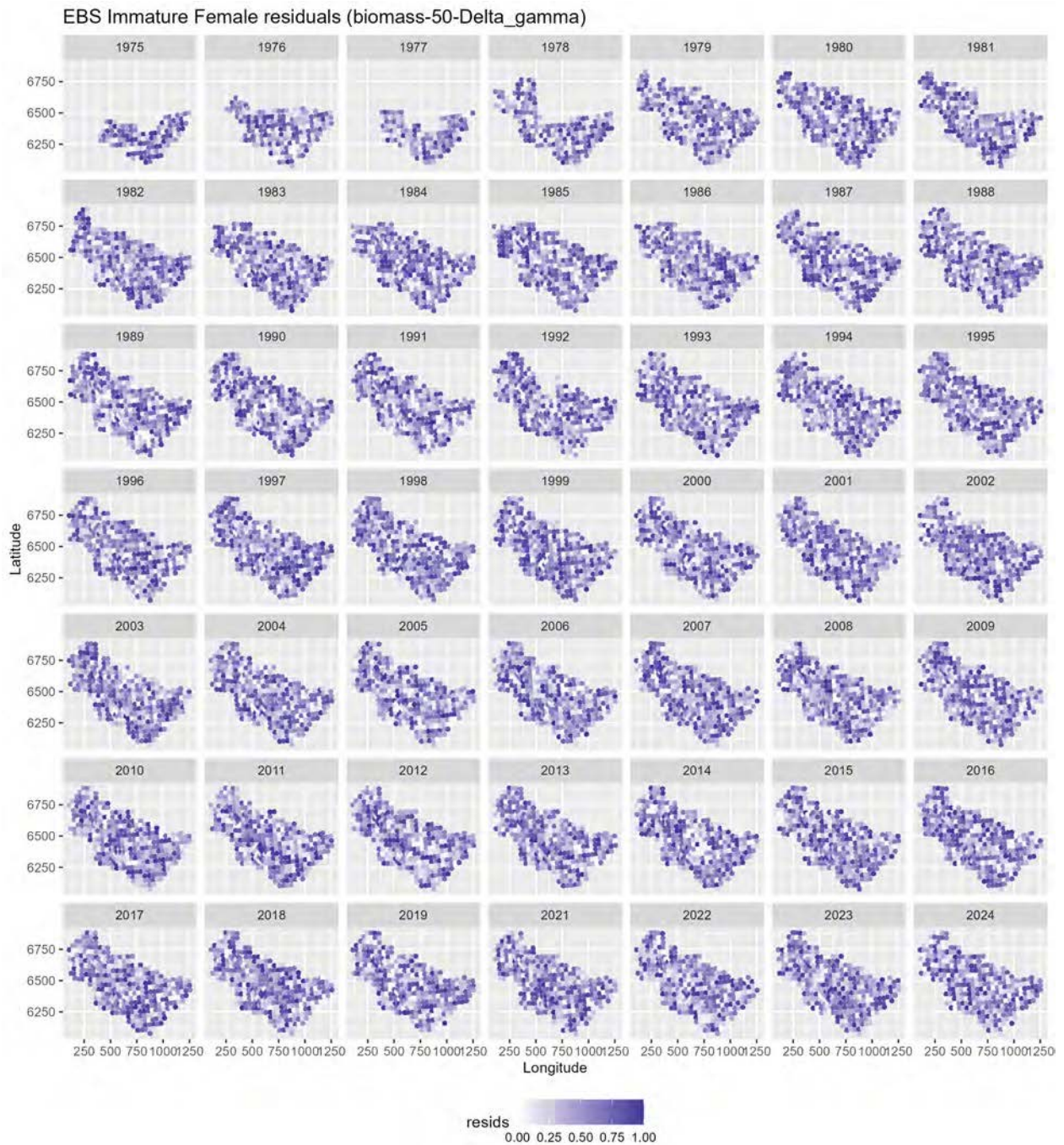
Figure 11: Spatial plot of DHARMa residuals for immature female biomass models fit using NMFS summer bottom trawl survey data before 1982 and 1982 onward with a 50-knot mesh and a delta-gamma model family. Predictions from both of these periods/models are combined in this figure.

Figure 12: Spatial plot of DHARMa residuals for mature female biomass models fit using NMFS summer bottom trawl survey data before 1982 and 1982 onward with a 50-knot mesh and a delta-gamma model family. Predictions from both of these periods/models are combined in this figure.

EBS predicted male abundance
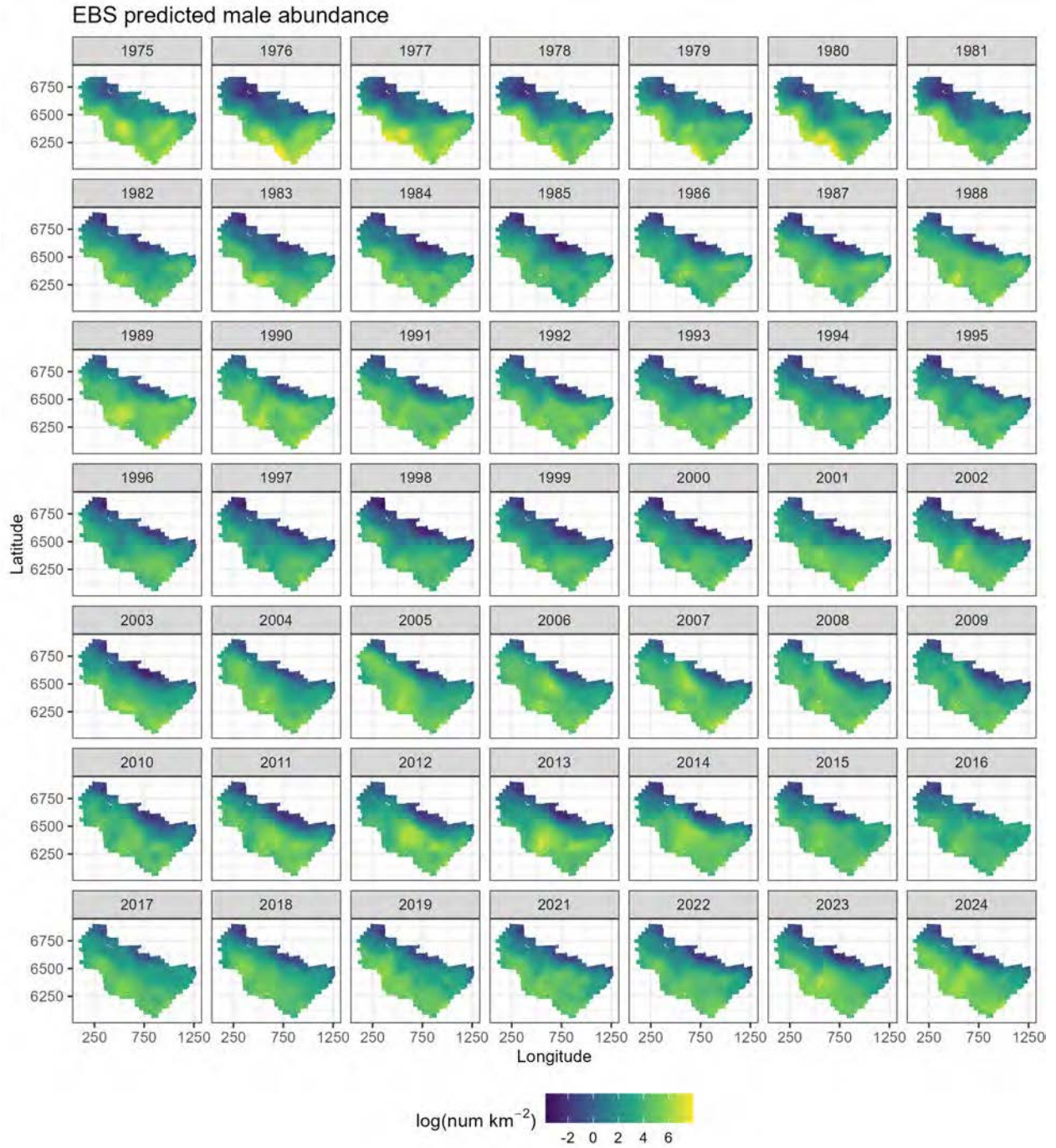
Figure 13: Spatial predictions of male abundance across the Eastern Bering Sea using NMFS summer bottom trawl survey data before 1982 and 1982 onward with a 50-knot mesh and a delta-gamma model family. Predictions from both of these periods/models are combined in this figure.

26
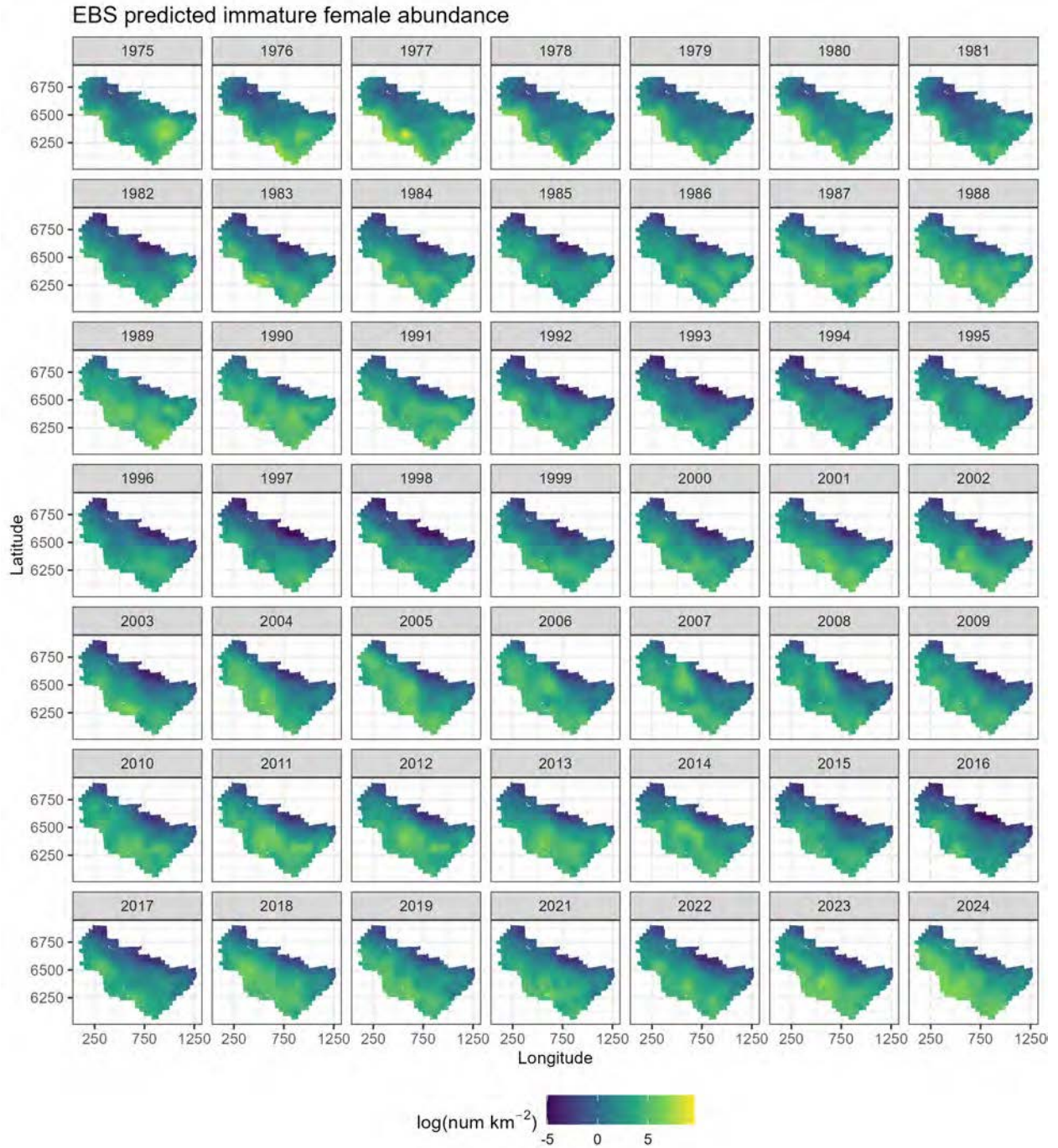
Figure 14: Spatial predictions of immature female abundance across the Eastern Bering Sea using NMFS summer bottom trawl survey data before 1982 and 1982 onward with a 50-knot mesh and a delta-gamma model family. Predictions from both of these periods/models are combined in this figure.
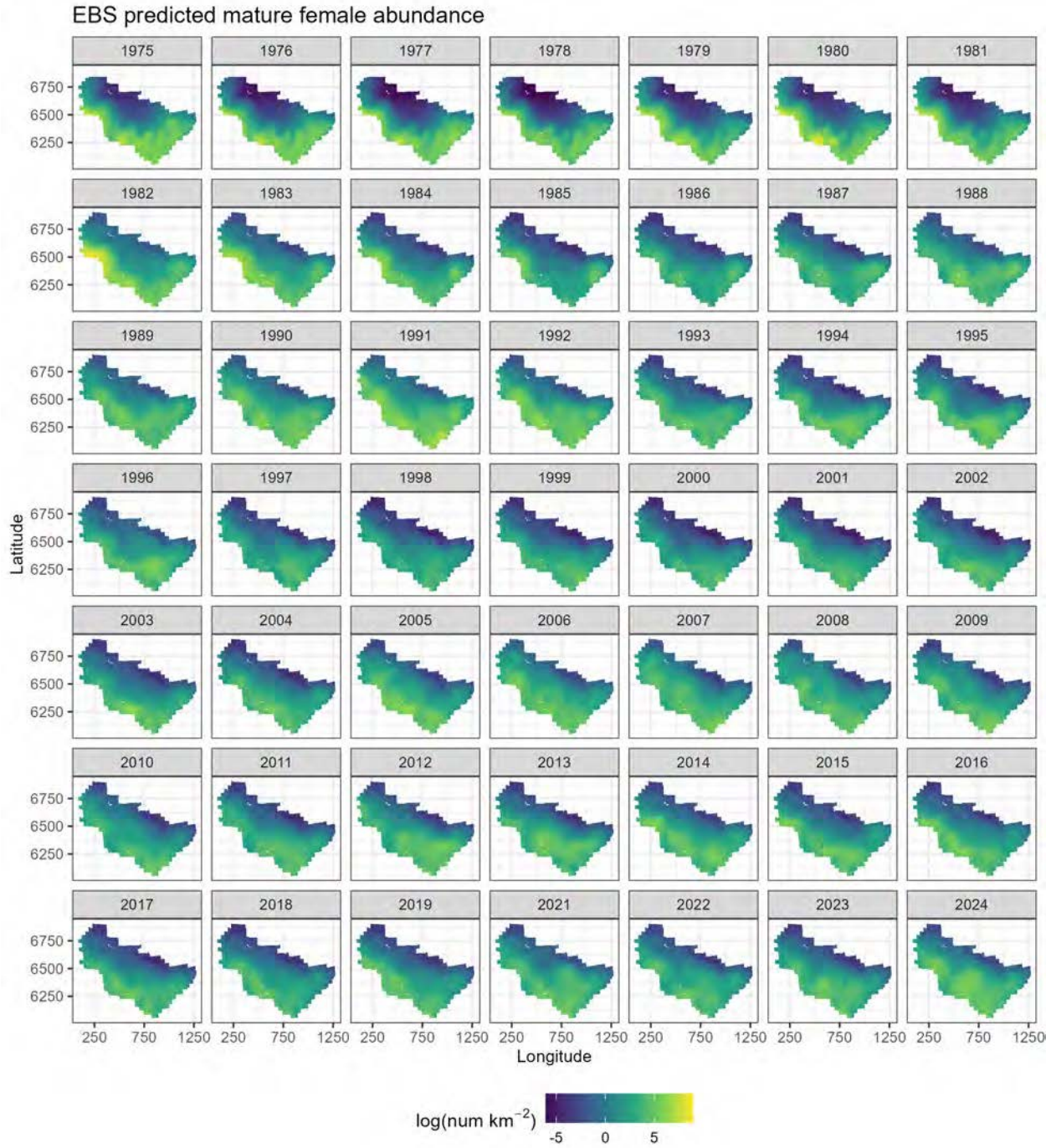
Figure 15: Spatial predictions of mature female abundance across the Eastern Bering Sea using NMFS summer bottom trawl survey data before 1982 and 1982 onward with a 50-knot mesh and a delta-gamma model family. Predictions from both of these periods/models are combined in this figure.
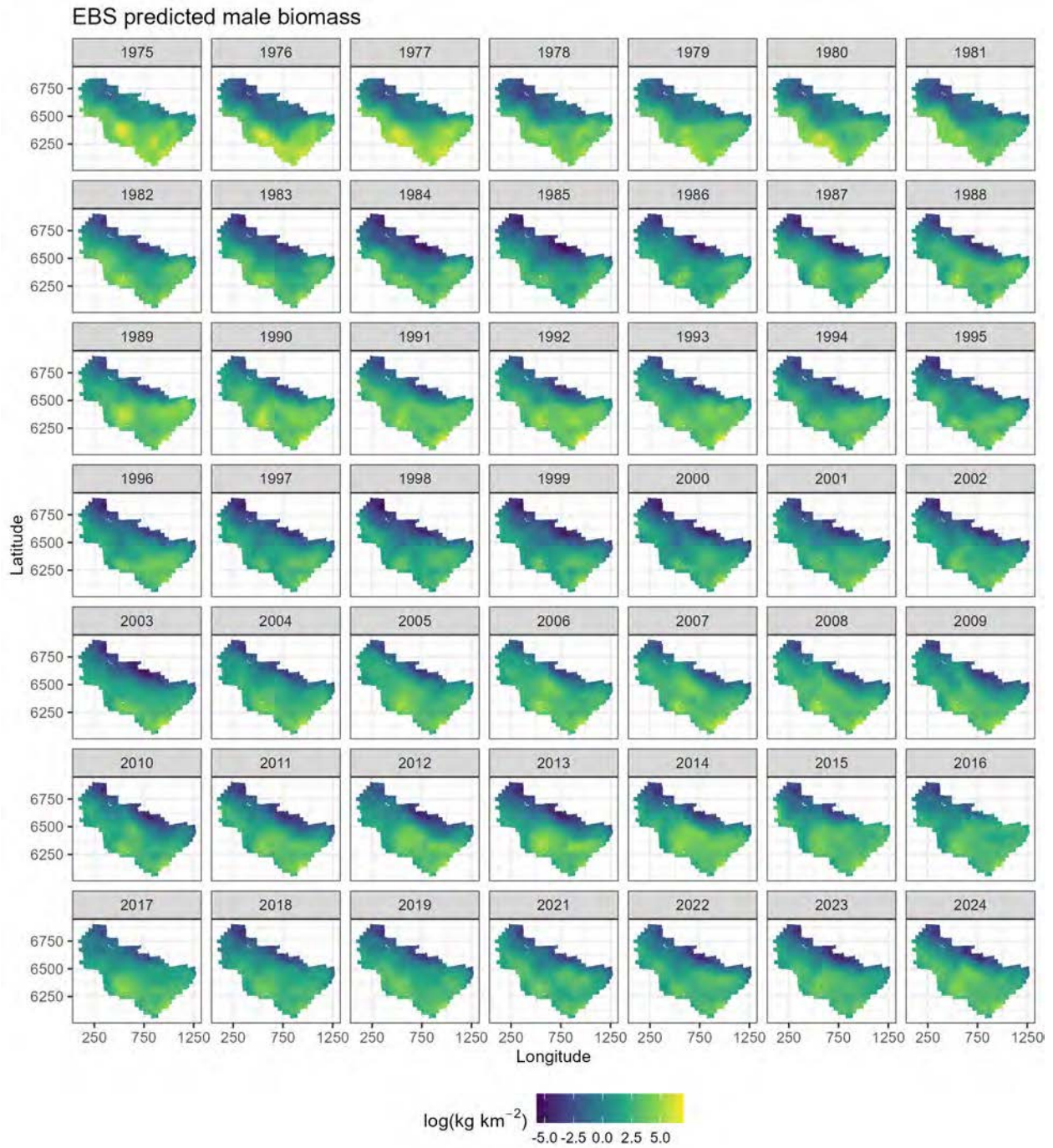
Figure 16: Spatial predictions of male biomass across the Eastern Bering Sea using NMFS summer bottom trawl survey data before 1982 and 1982 onward with a 50-knot mesh and a delta-gamma model family. Predictions from both of these periods/models are combined in this figure.
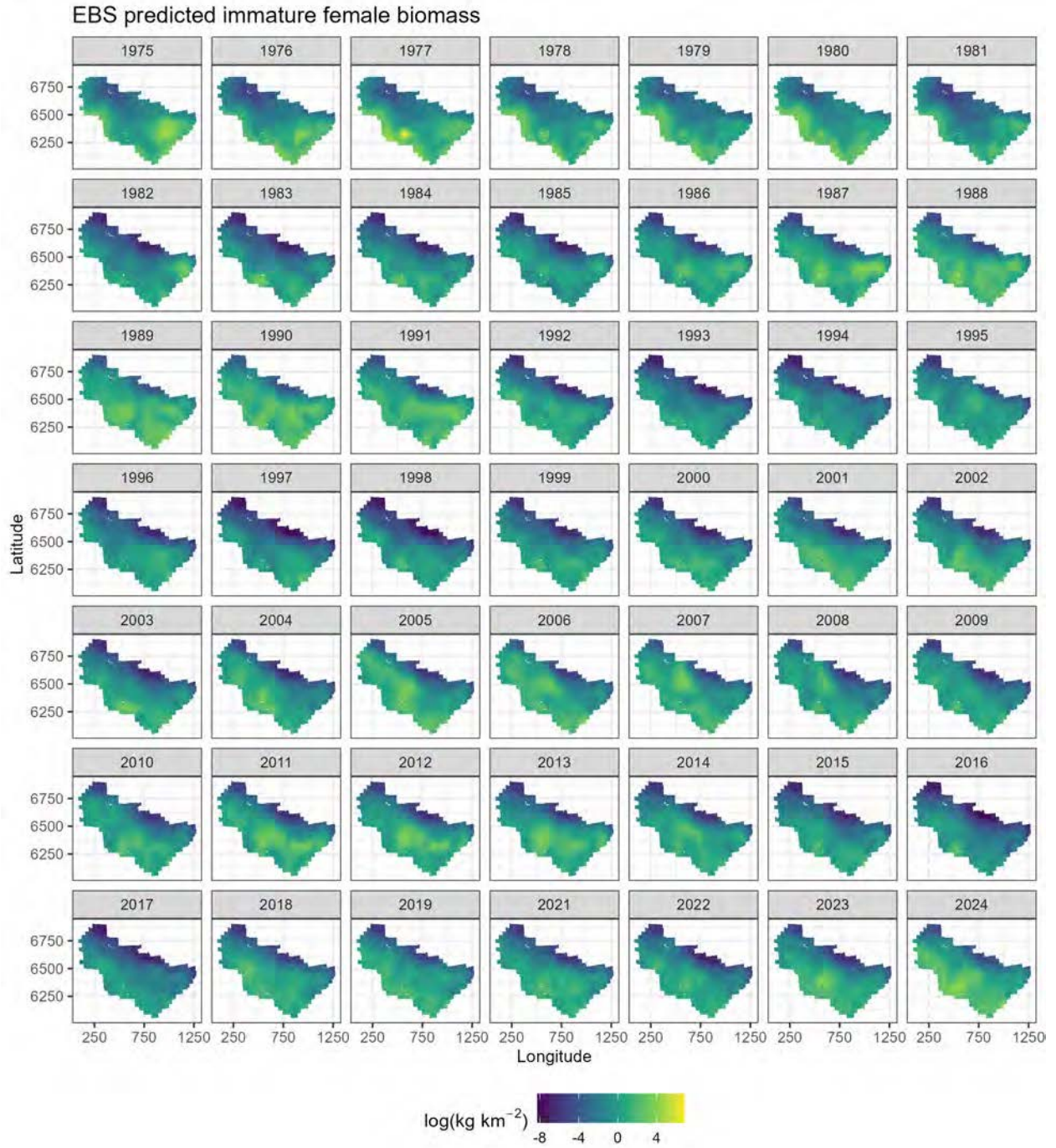
Figure 17: Spatial predictions of immature female biomass across the Eastern Bering Sea using NMFS summer bottom trawl survey data before 1982 and 1982 onward with a 50-knot mesh and a delta-gamma model family. Predictions from both of these periods/models are combined in this figure.
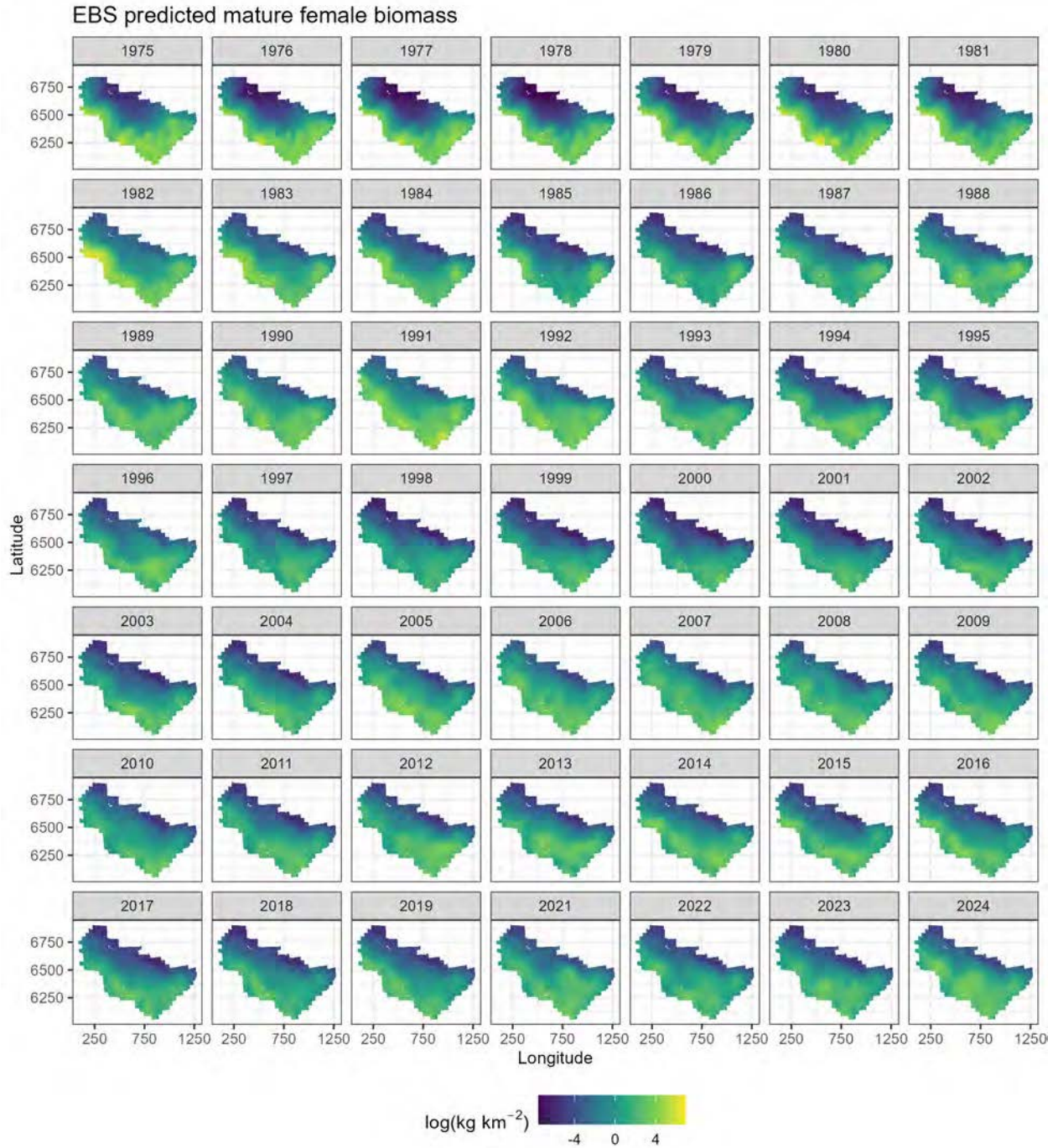
Figure 18: Spatial predictions of mature female biomass across the Eastern Bering Sea using NMFS summer bottom trawl survey data before 1982 and 1982 onward with a 50-knot mesh and a delta-gamma model family. Predictions from both of these periods/models are combined in this figure.
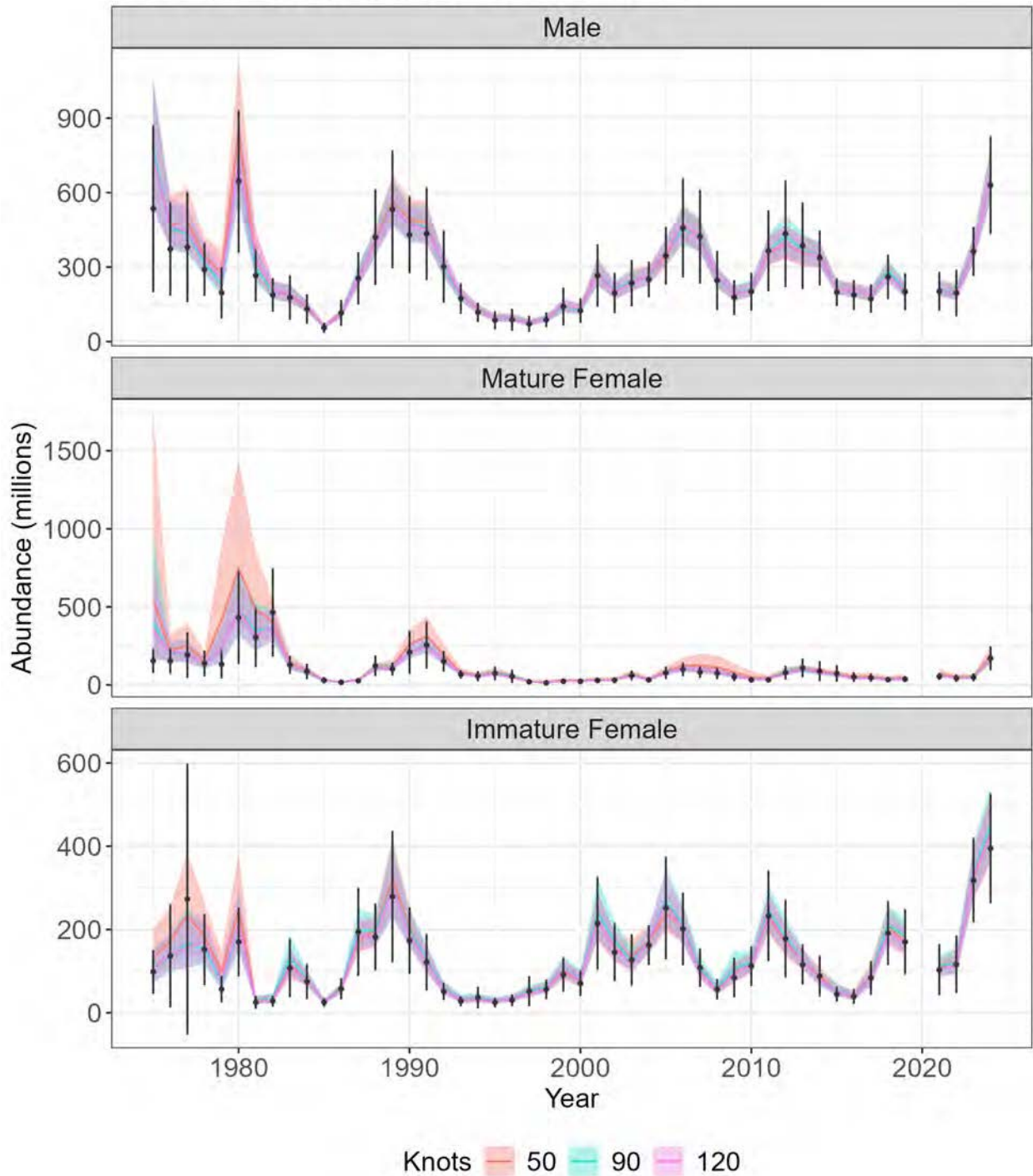
Figure 19: Estimated abundance (millions) for Tanner crab across the Eastern Bering Sea. Colored lines represent abundance (±95% CI) estimated by sdmTMB, with orange, blue, and pink denoting models fit with a 50-, 90-, and 120-knot mesh, respectively. Black points represent abundance (±95% CI) estimated by the NMFS summer bottom trawl survey.
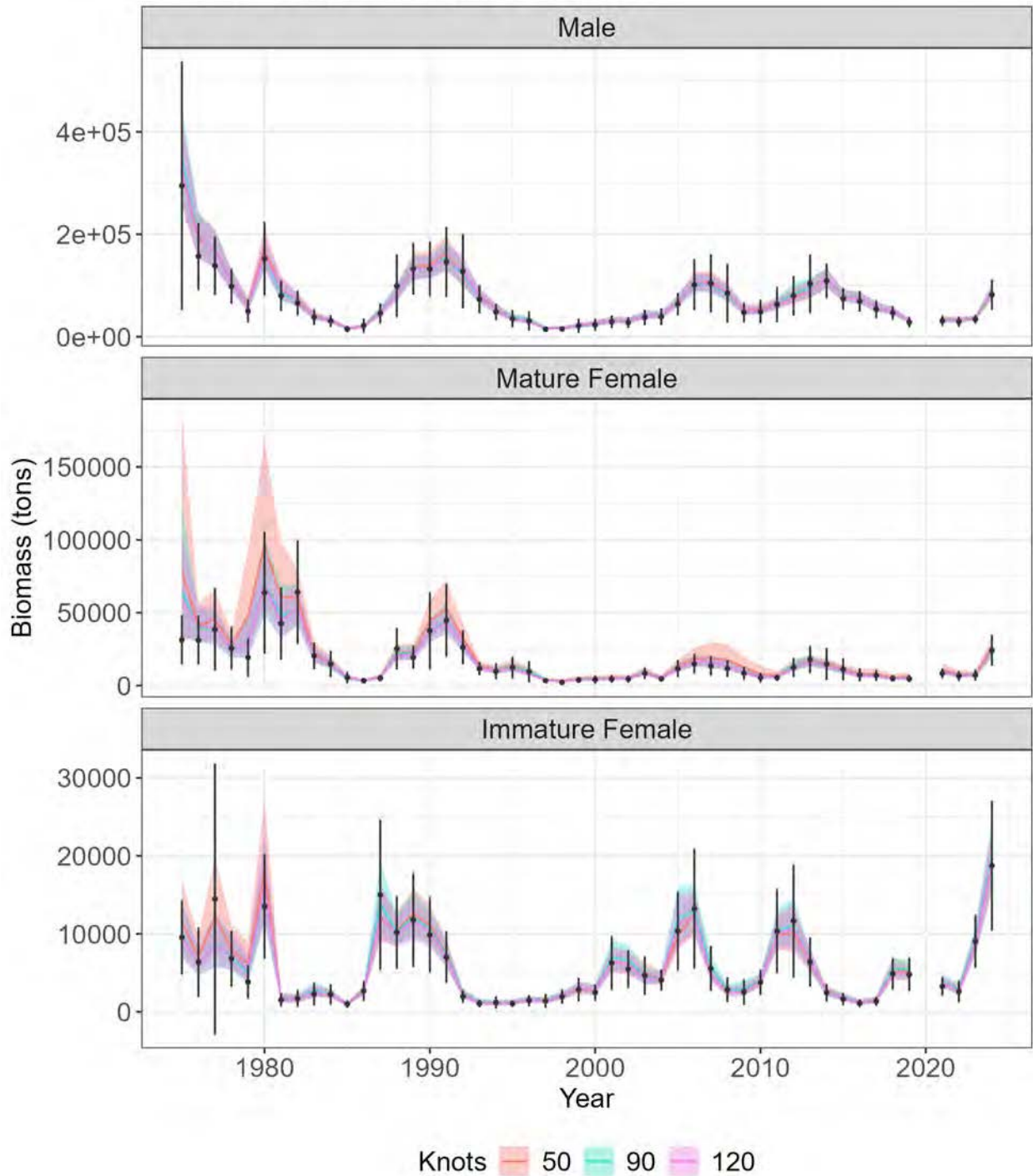
Figure 20: Estimated biomass (tons) for Eastern Bering Sea Tanner crab across the Eastern Bering Sea. Colored lines represent abundance (±95% CI) estimated by sdmTMB, with orange, blue, and pink denoting models fit with a 50-, 90-, and 120-knot mesh, respectively. Black points represent biomass (±95% CI) estimated by the NMFS summer bottom trawl survey.
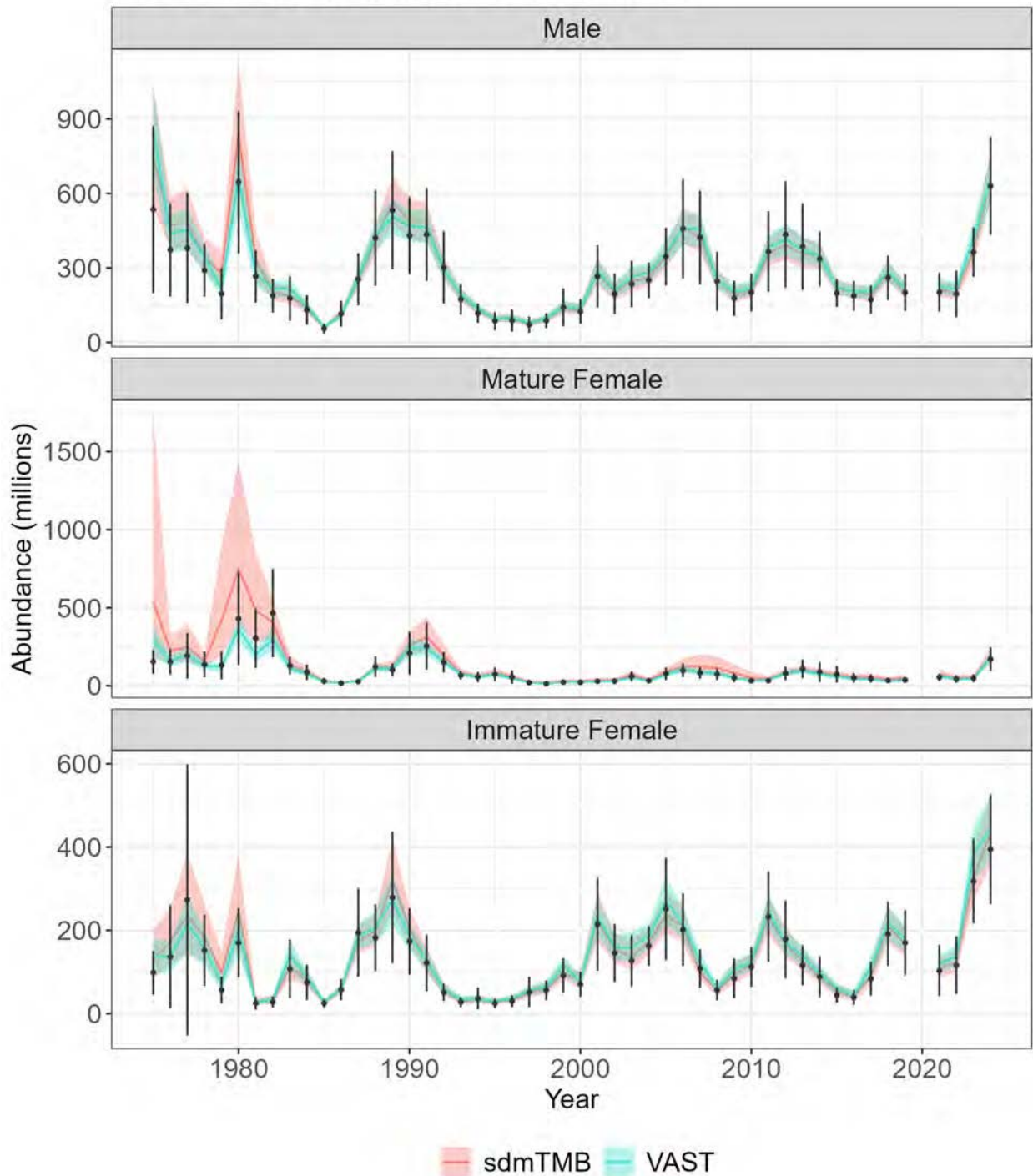
Figure 21: Estimated abundance (millions; ±95% CI) for Eastern Bering Sea Tanner crab predicted using sdmTMB (pink) and VAST (blue). Both algorithms fit models using a delta-gamma family at 50 knots. Black points represent abundance (±95% CI) estimated by the NMFS summer bottom trawl survey.
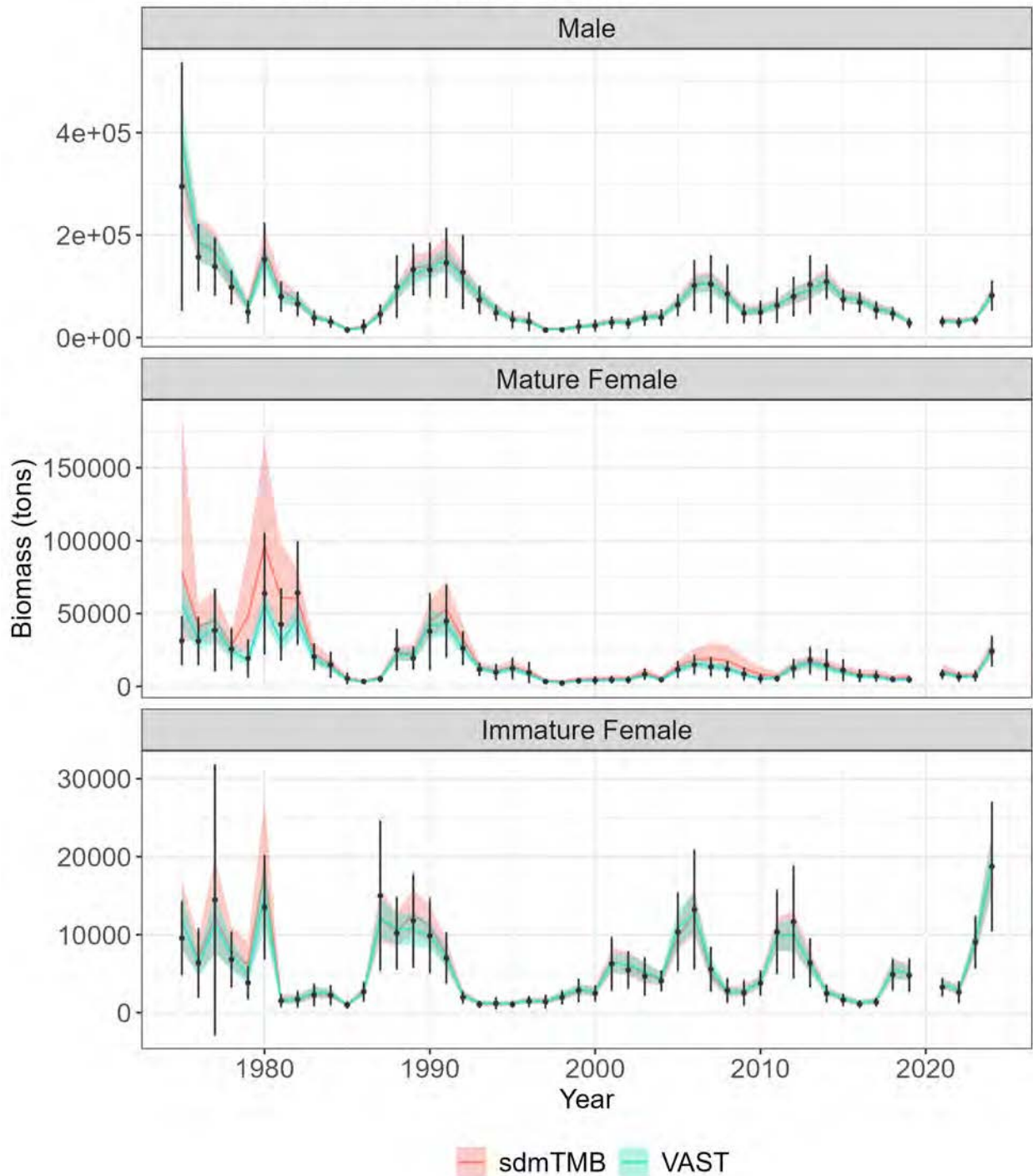
Figure 22: Estimated biomass (tons; ±95% CI) for Eastern Bering Sea Tanner crab predicted using sdmTMB (pink) and VAST (blue). Both algorithms fit models using a delta-gamma family at 50 knots. Black points represent abundance (±95% CI) estimated by the NMFS summer bottom trawl survey.

Figure 23: Spatial mesh with 50 knots used for fitting St. Matthew Island blue king crab spatial models. Points represent observations and vertices represent knot locations.

Figure 24: Spatial mesh with 90 knots used for fitting St. Matthew Island blue king crab spatial models. Points represent observations and vertices represent knot locations.

Figure 25: Spatial mesh with 120 knots used for fitting St. Matthew Island blue king crab spatial models. Points represent observations and vertices represent knot locations.
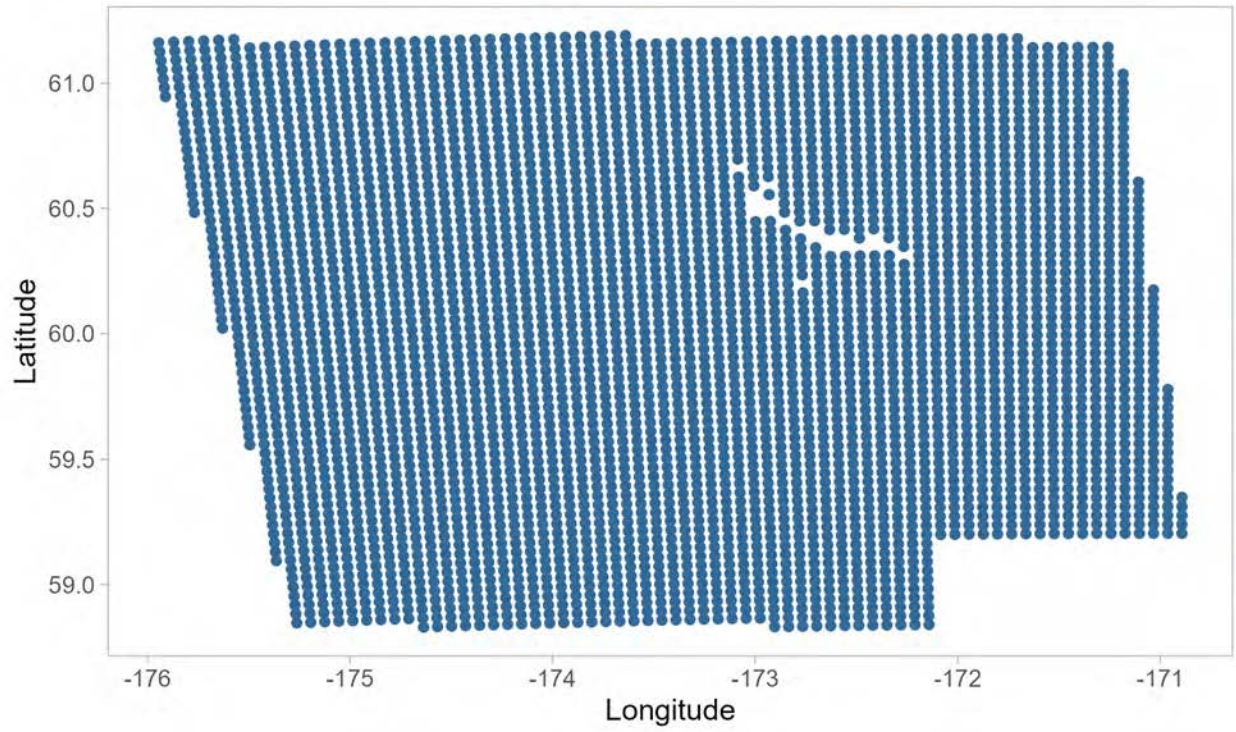
Figure 26: Prediction grid used for St. Matthew Island blue king crab spatial abundance predictions. Spatial resolution is 4 km^2.
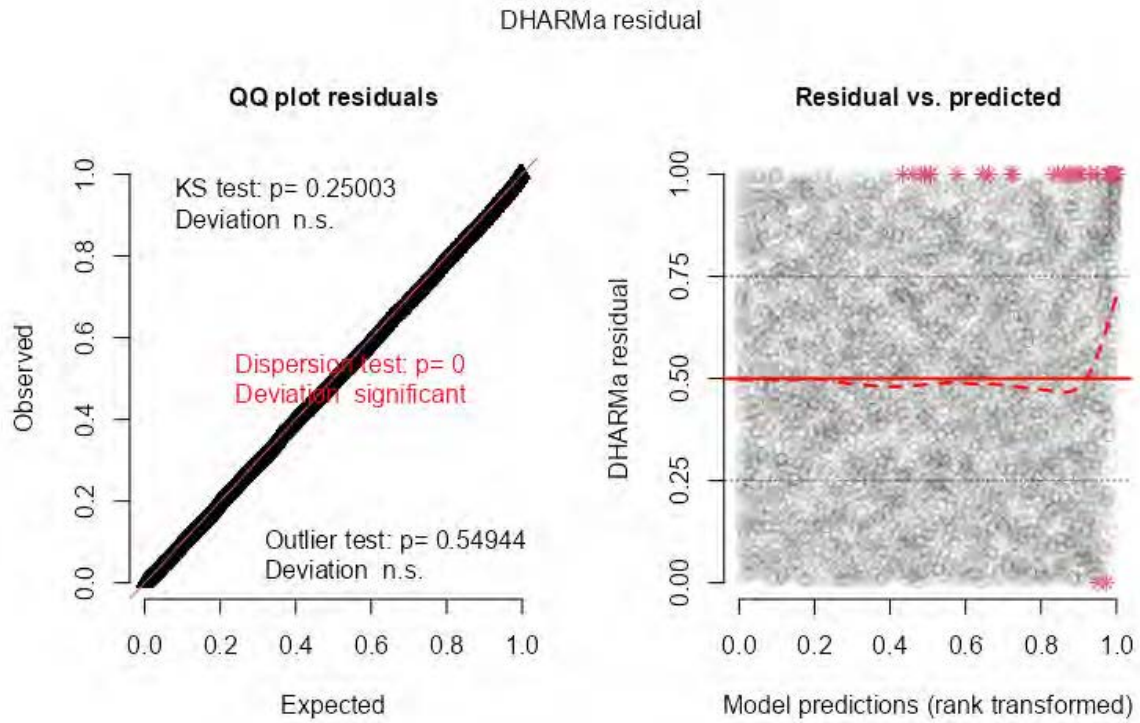
Figure 27: Model diagnostic plots using DHARMa residuals for the SMBKC IID Tweedie model with 120 knots.
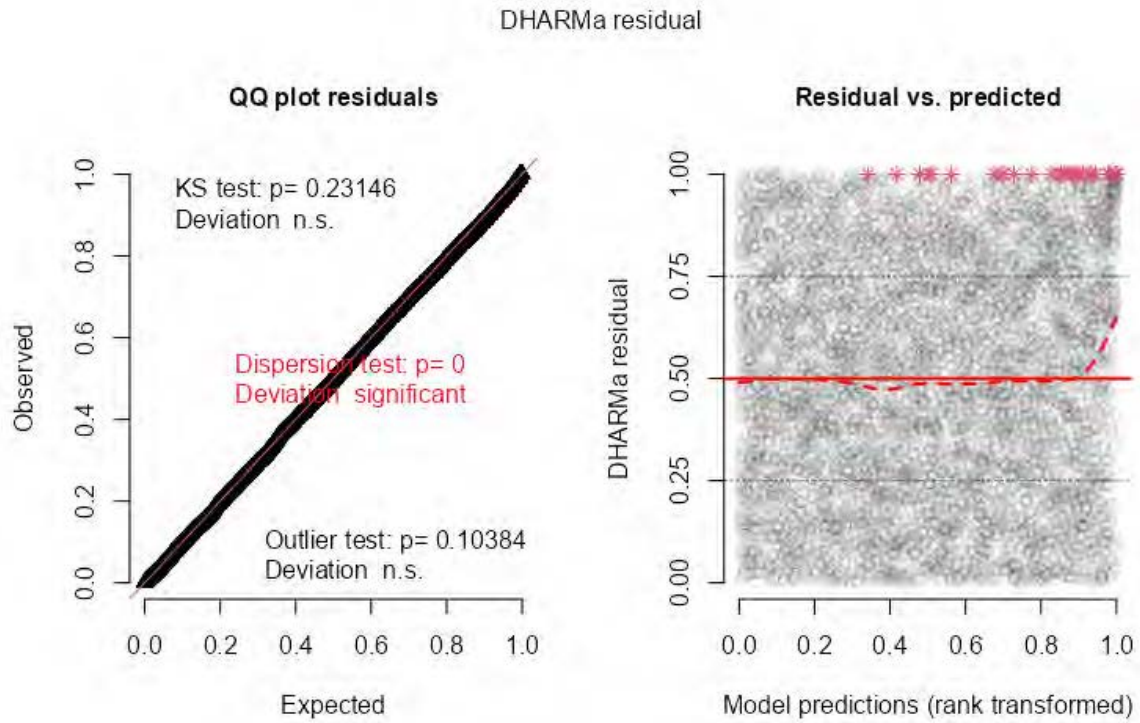
Figure 28: Model diagnostic plots using DHARMa residuals for the SMBKC IID Tweedie model with 90 knots.
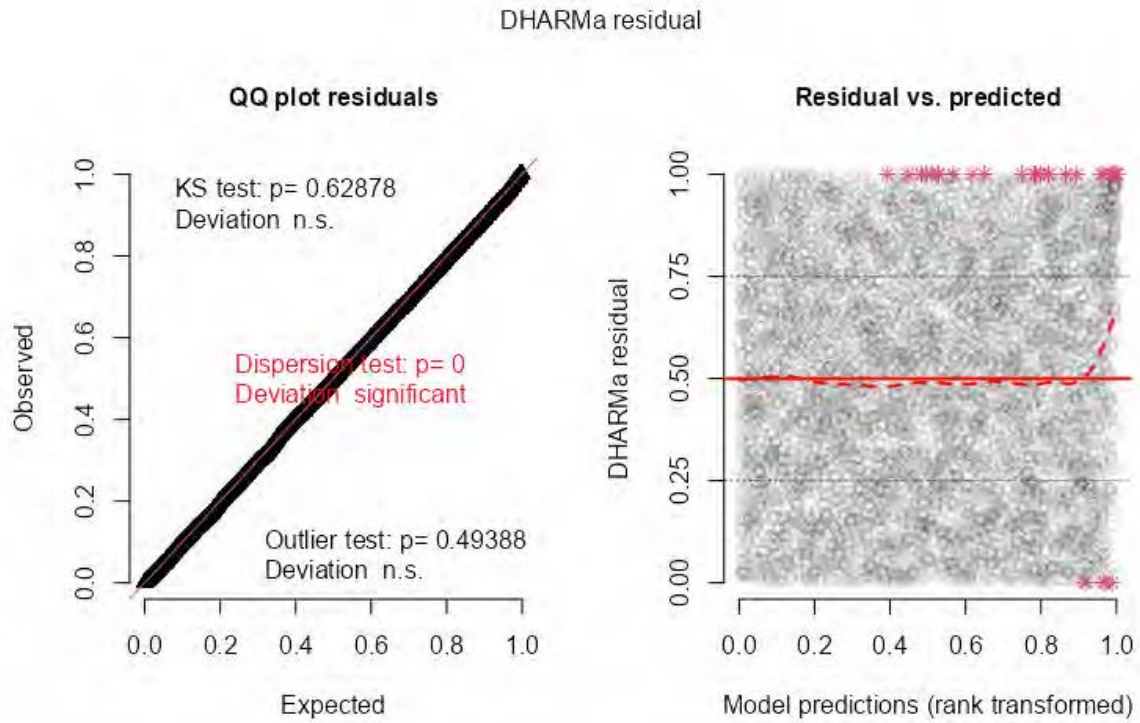
Figure 29: Model diagnostic plots using DHARMa residuals for the SMBKC random walk Tweedie model with 120 knots.
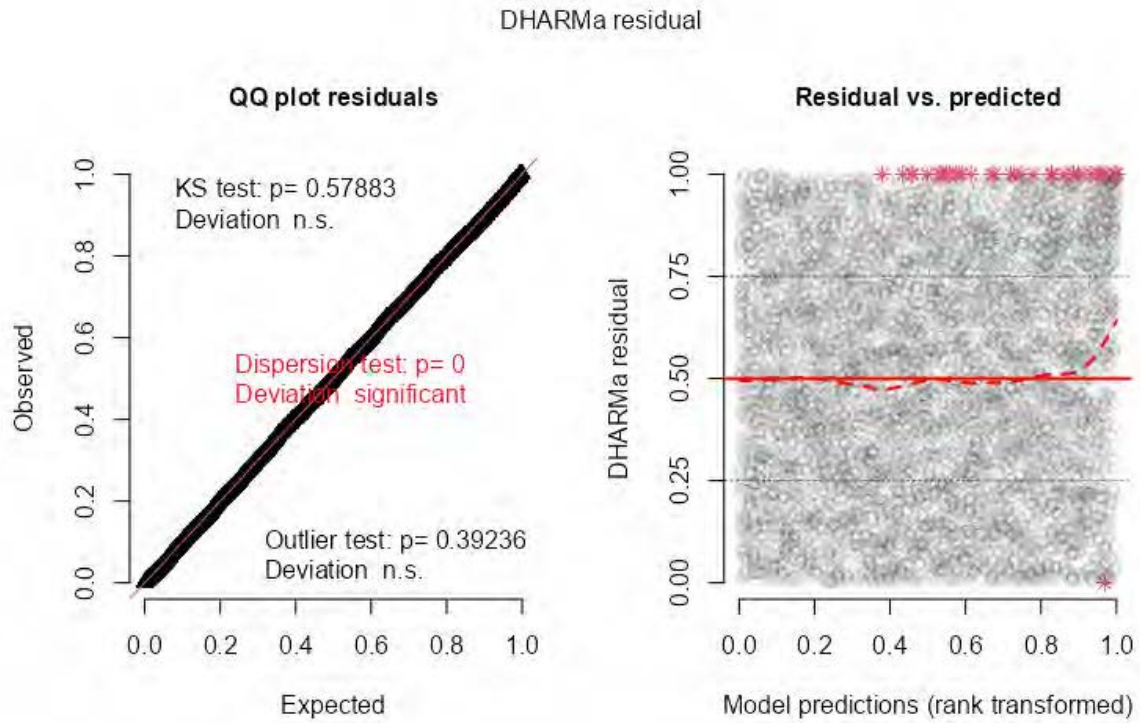
Figure 30: Model diagnostic plots using DHARMa residuals for the SMBKC random walk Tweedie model with 90 knots.
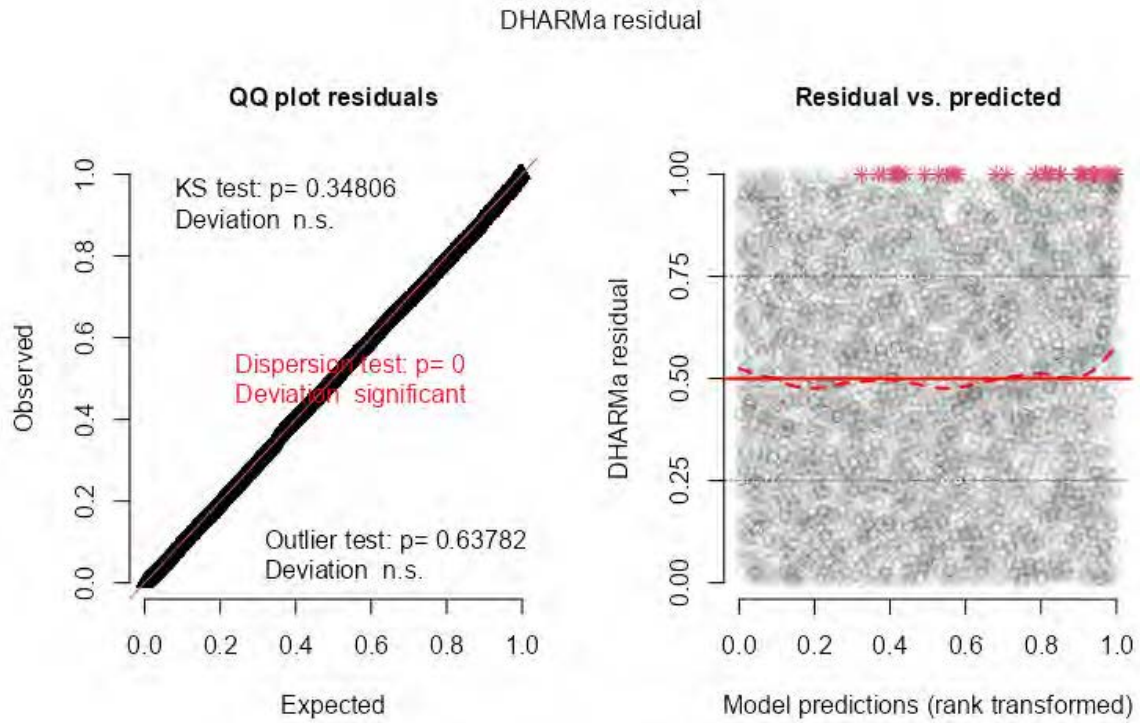
Figure 31: Model diagnostic plots using DHARMa residuals for the SMBKC random walk Tweedie model with 50 knots.
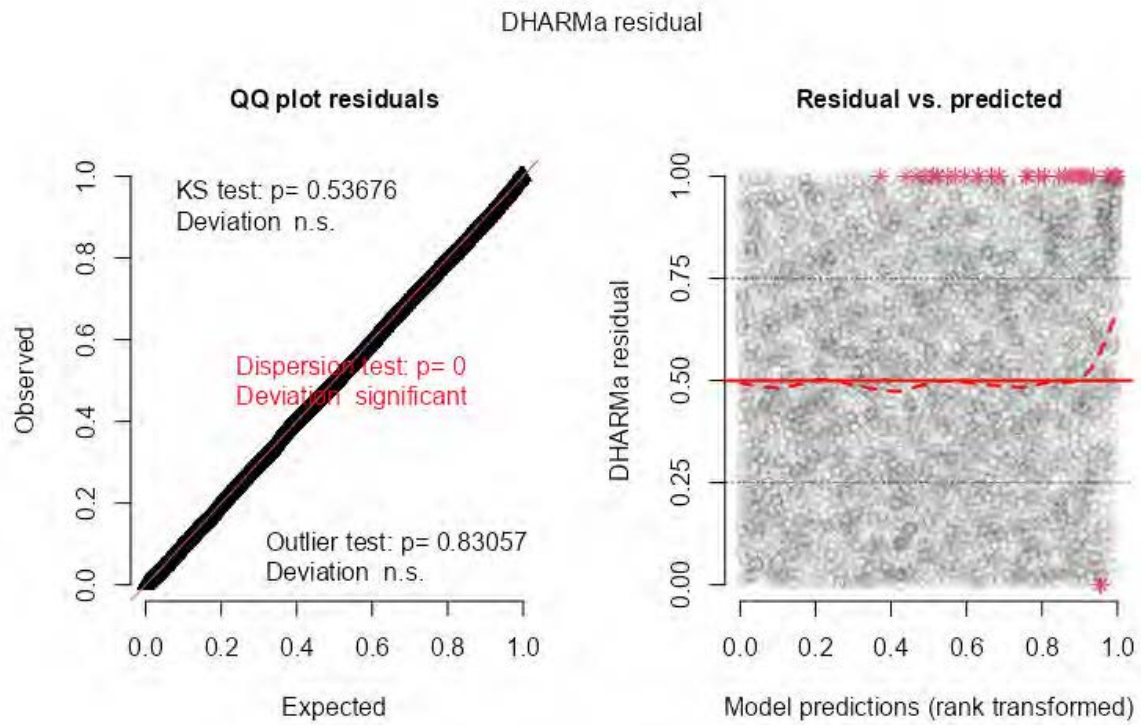
Figure 32: Model diagnostic plots using DHARMa residuals for the SMBKC AR1 Tweedie model with 120 knots.
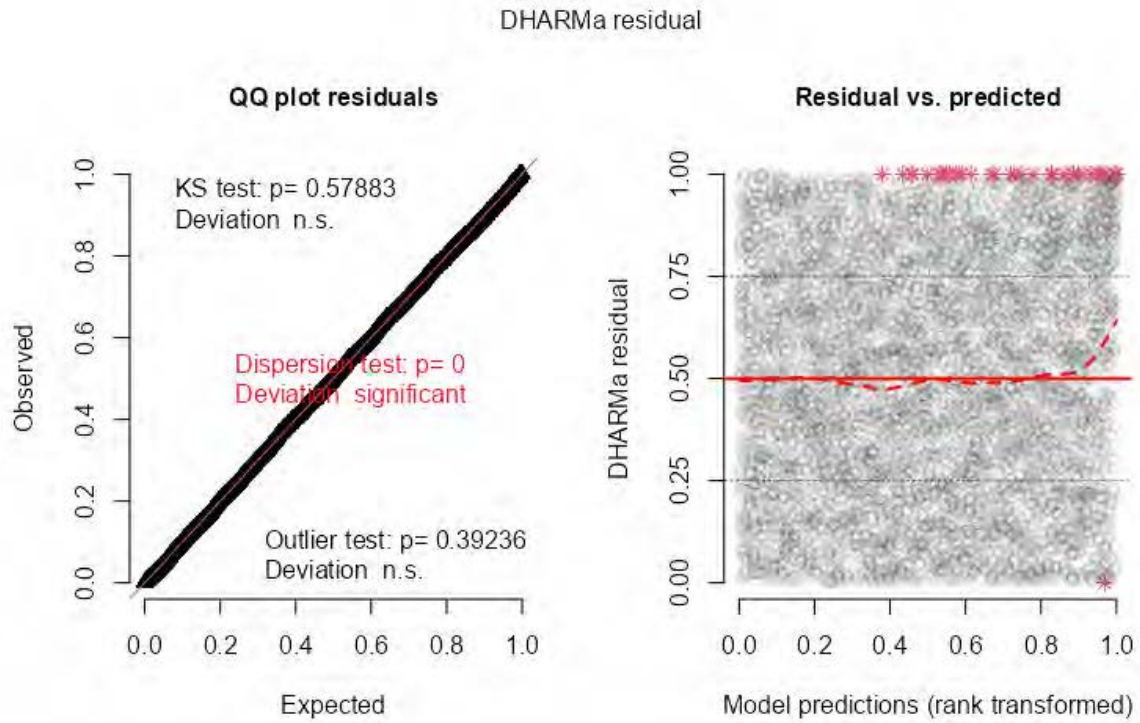
Figure 33: Model diagnostic plots using DHARMa residuals for the SMBKC AR1 Tweedie model with 90 knots.
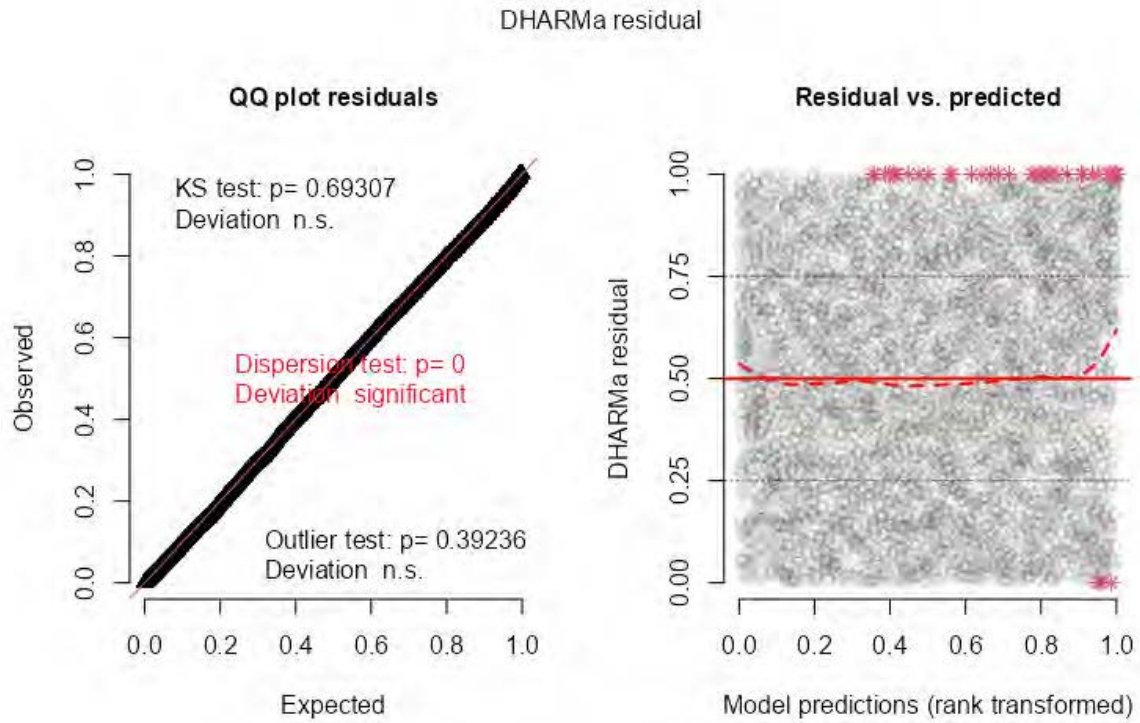
Figure 34: Model diagnostic plots using DHARMa residuals for the SMBKC AR1 Tweedie model with 50 knots.
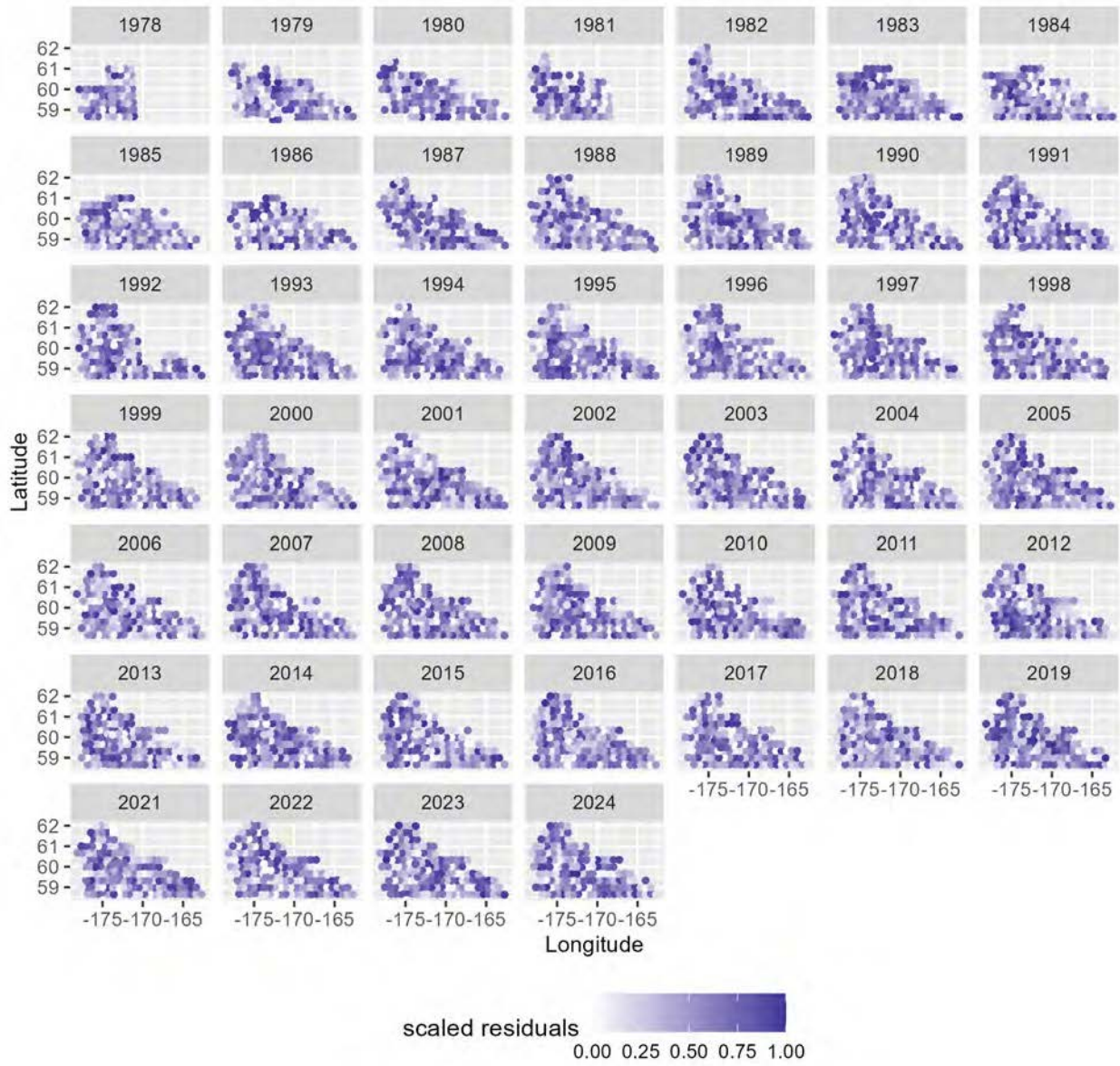
Figure 35: Spatial distribution of DHARMa residuals for the SMBKC IID Tweedie model with 120 knots.
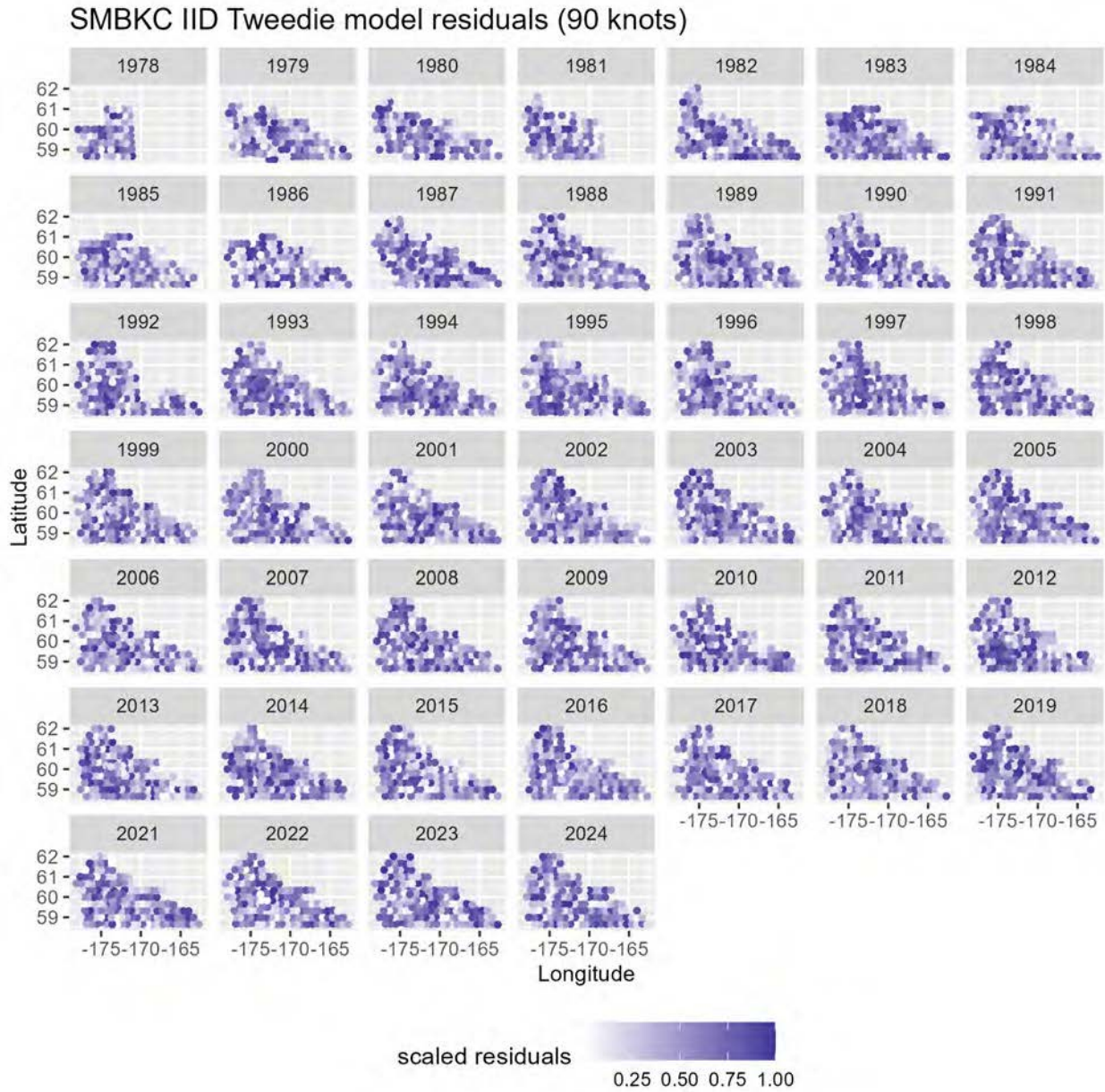
Figure 36: Spatial distribution of DHARMa residuals for the SMBKC IID Tweedie model with 90 knots.
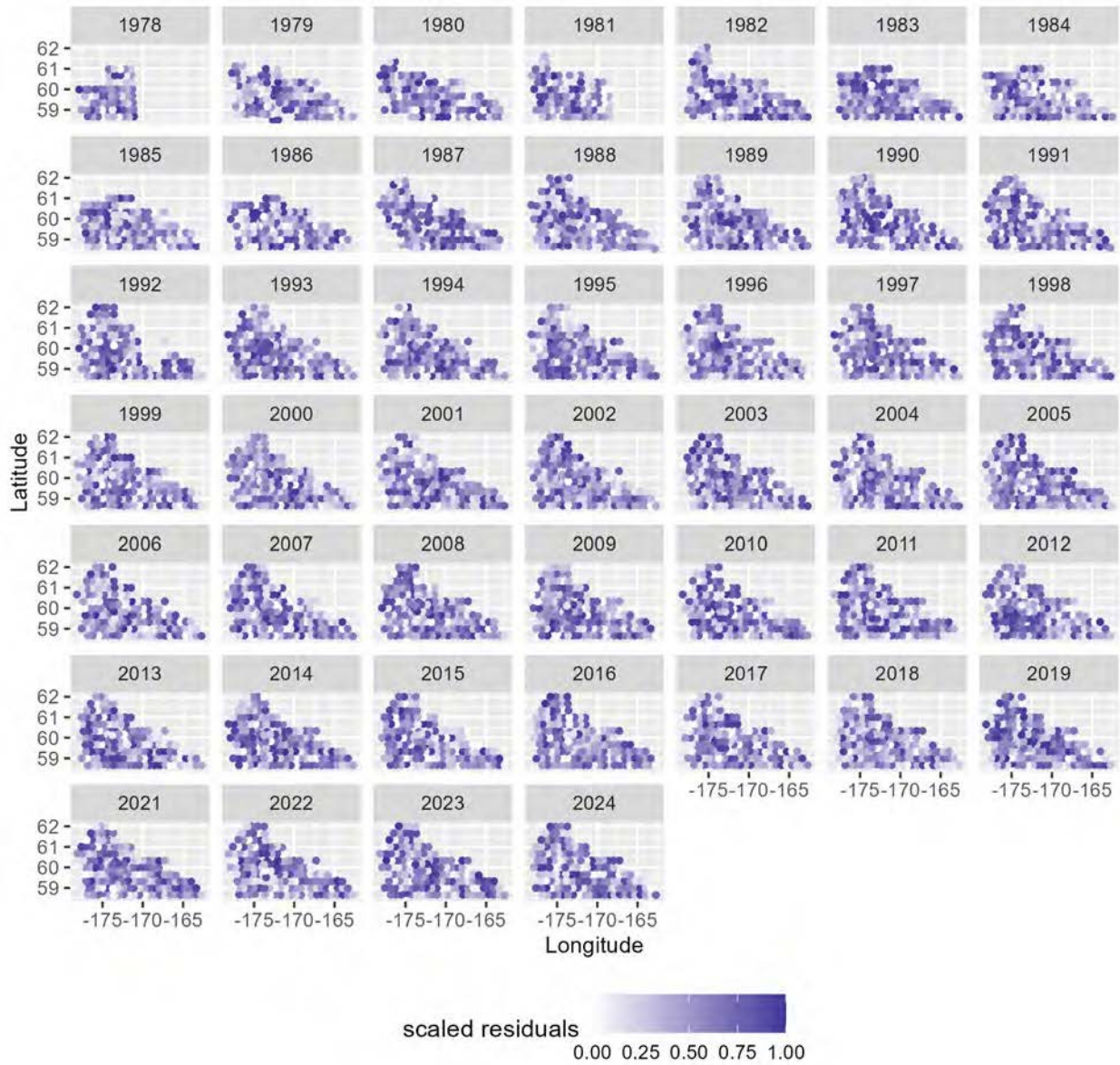
Figure 37: Spatial distribution of DHARMa residuals for the SMBKC random walk Tweedie model with 120 knots.
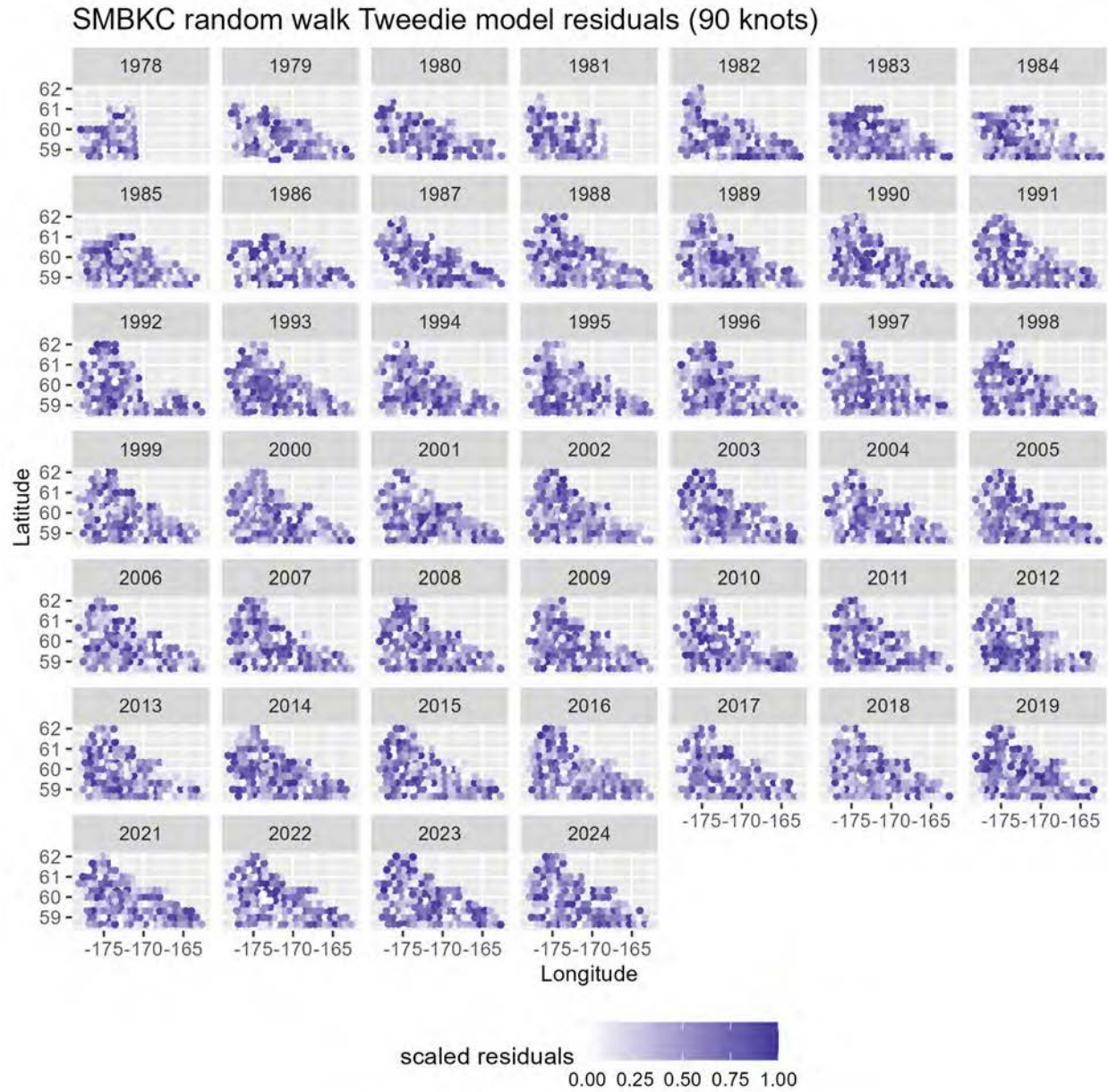
Figure 38: Spatial distribution of DHARMa residuals for the SMBKC random walk Tweedie model with 90 knots.
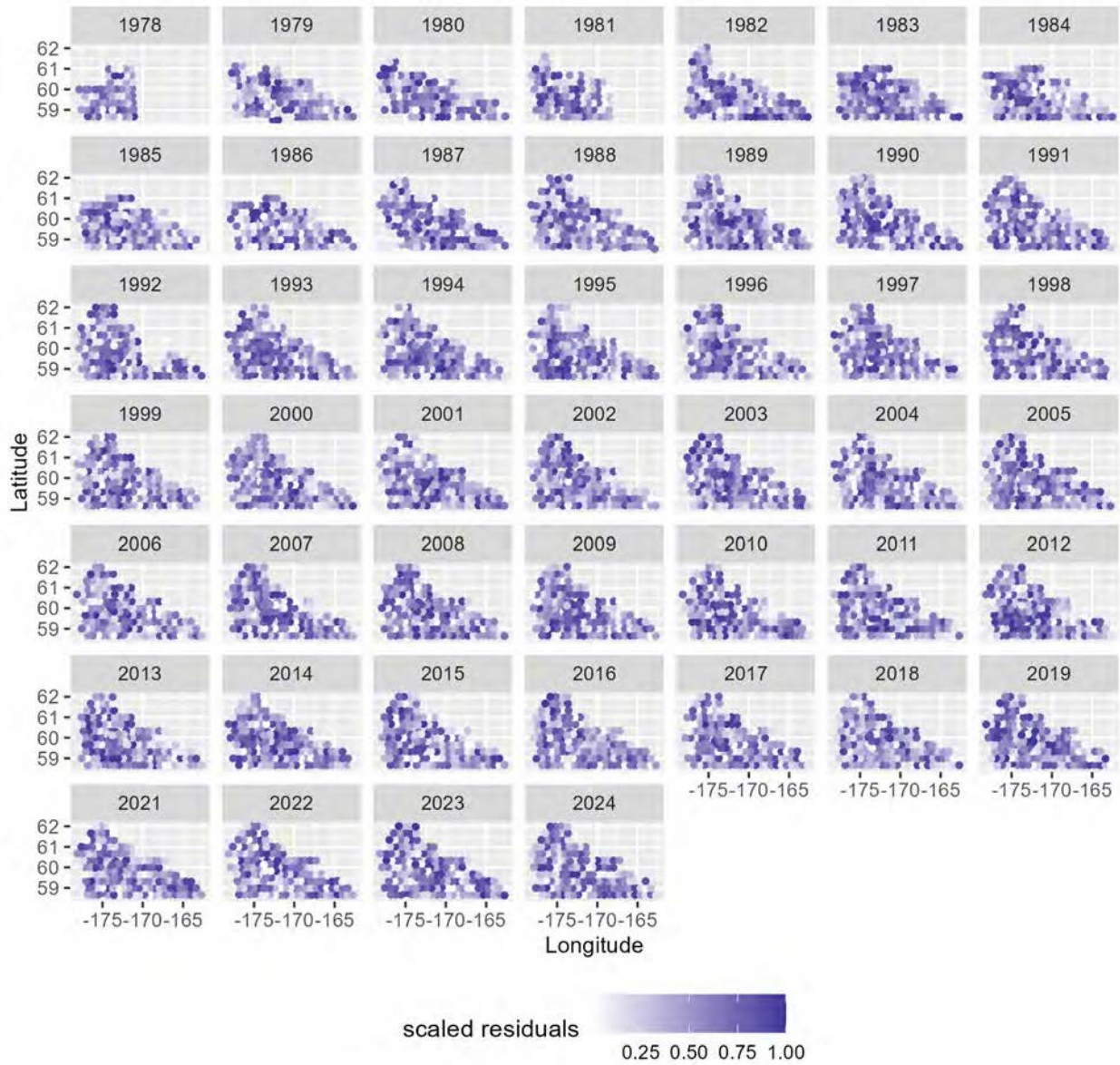
Figure 39: Spatial distribution of DHARMa residuals for the SMBKC random walk Tweedie model with 50 knots.
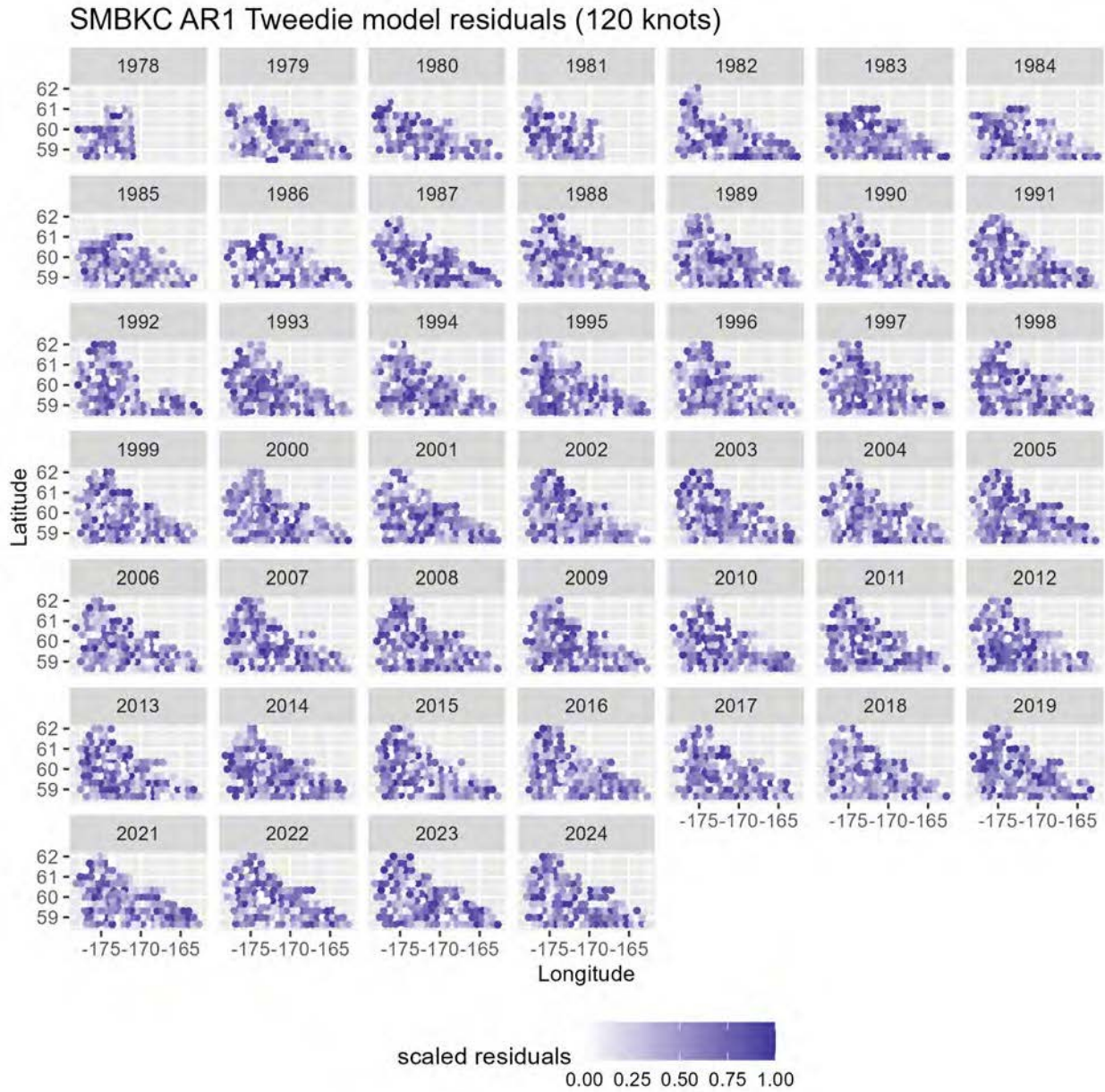
Figure 40: Spatial distribution of DHARMa residuals for the SMBKC AR1 Tweedie model with 120 knots.
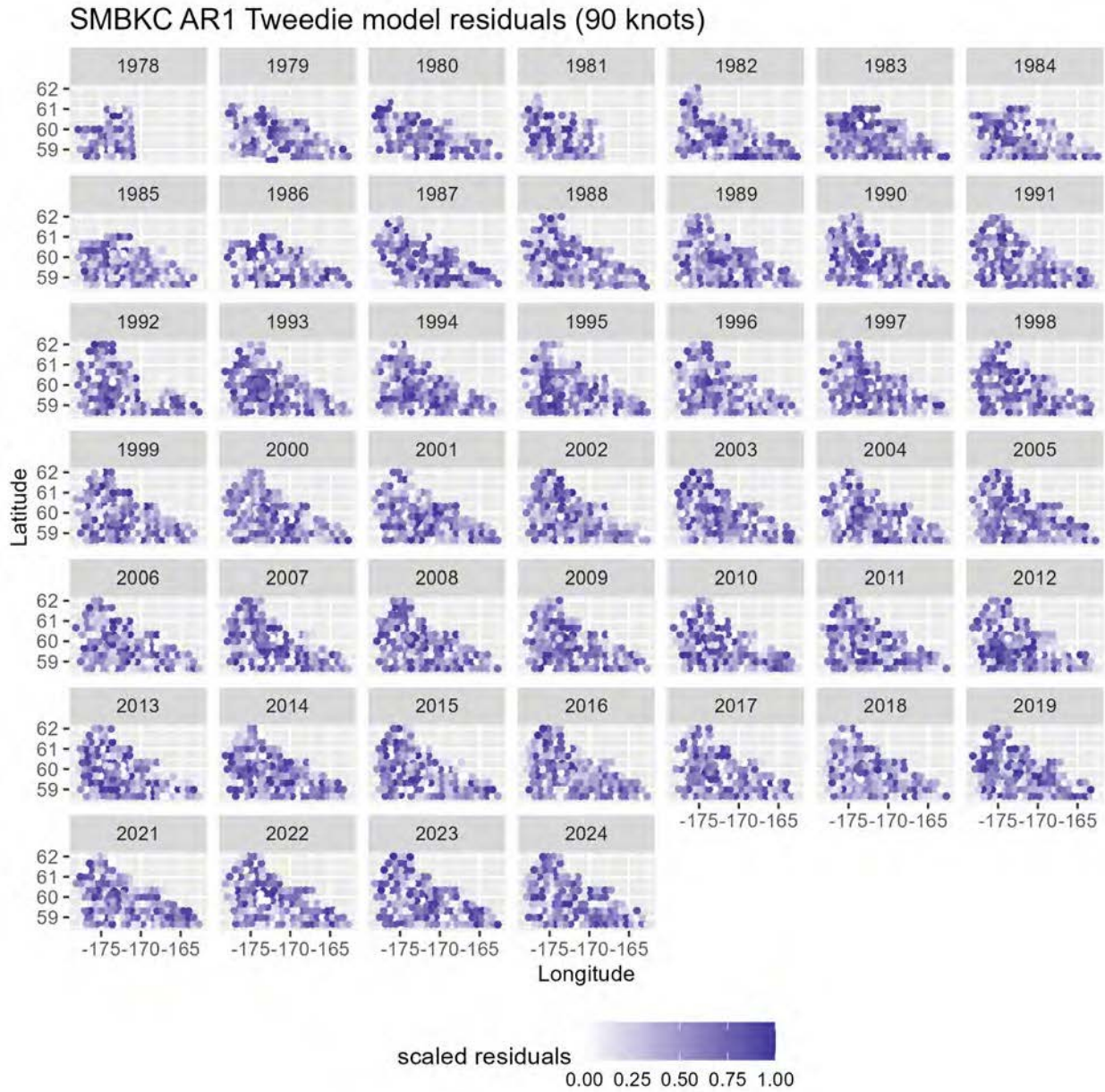
Figure 41: Spatial distribution of DHARMa residuals for the SMBKC AR1 Tweedie model with 90 knots.
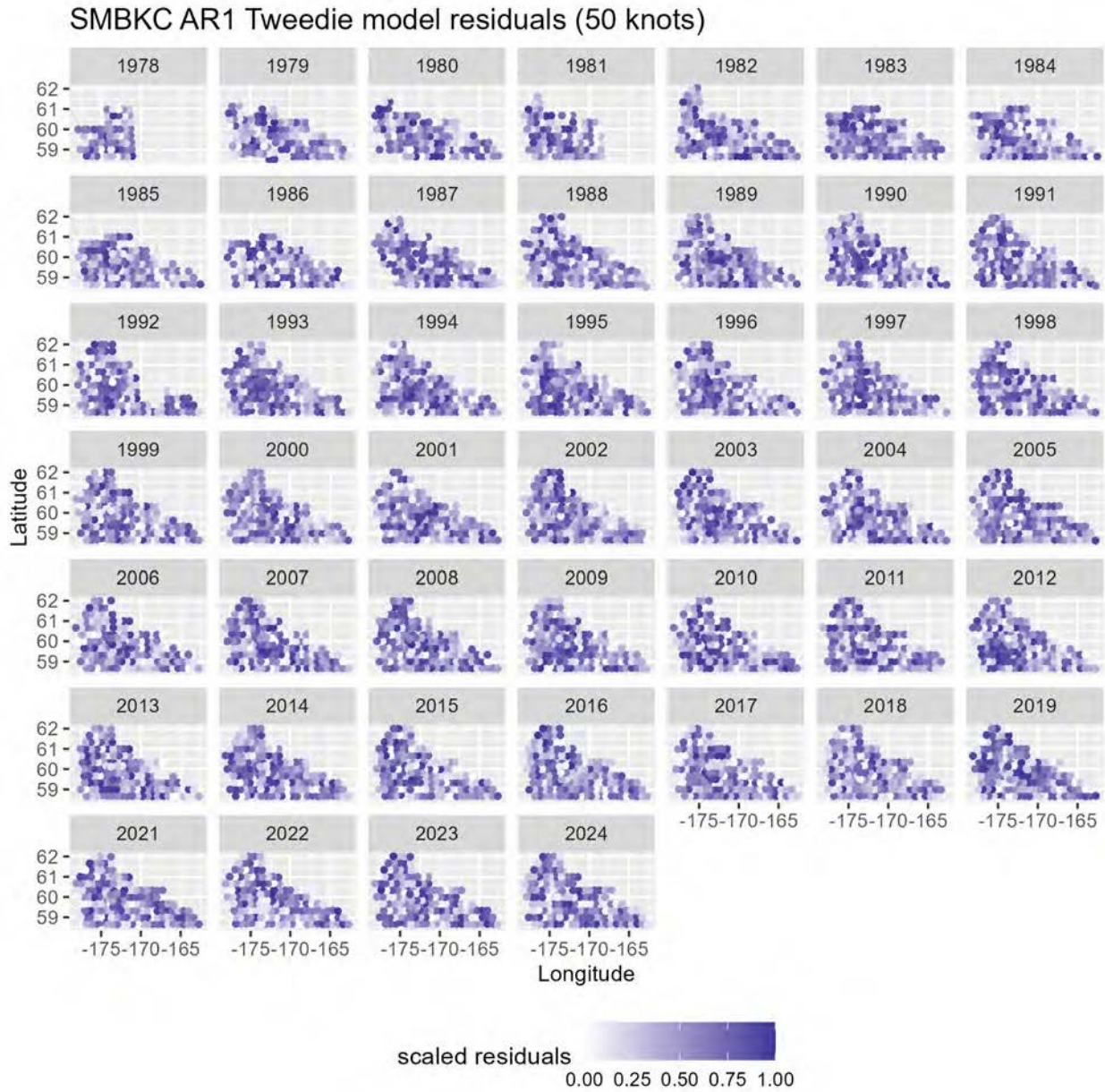
Figure 42: Spatial distribution of DHARMa residuals for the SMBKC AR1 Tweedie model with 50 knots.
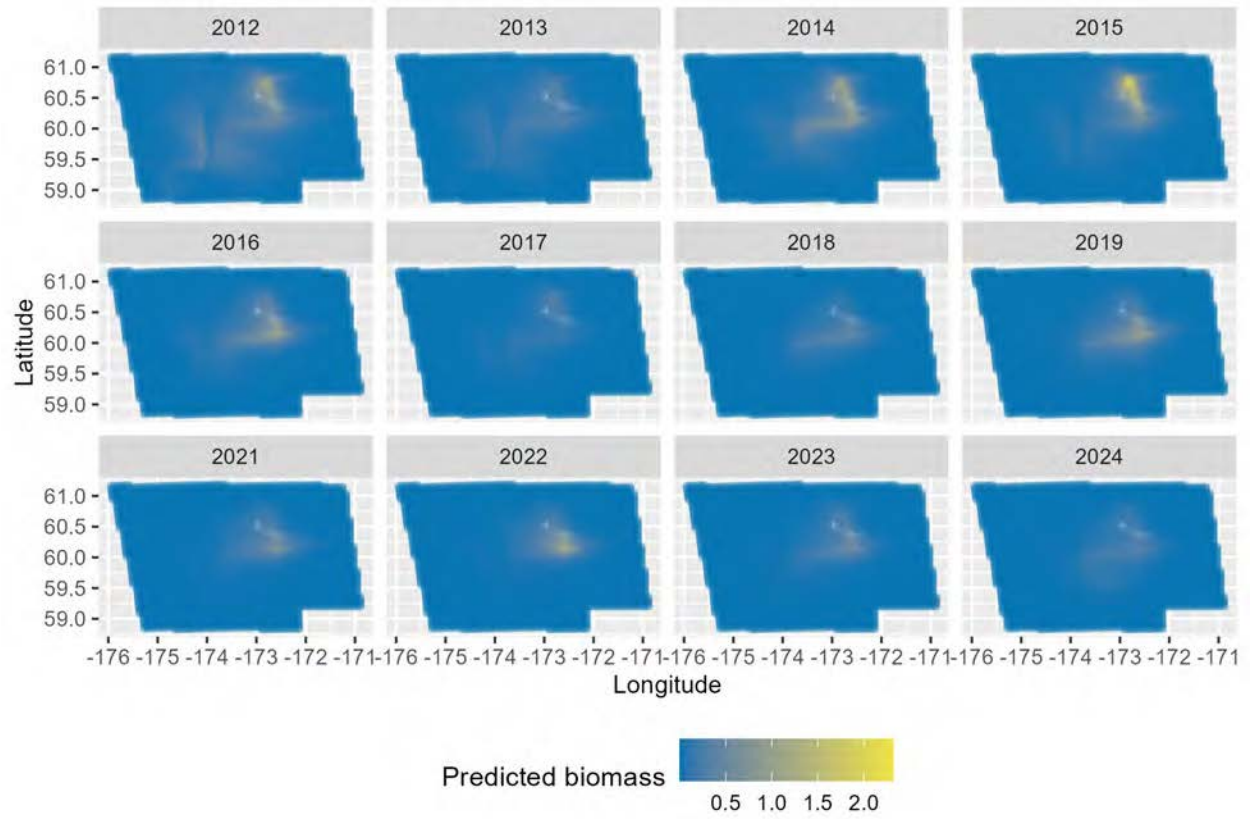
Figure 43: Heat map of St. Matthew Island blue king crab predicted abundance from the IID Tweedie model with 50 knots.
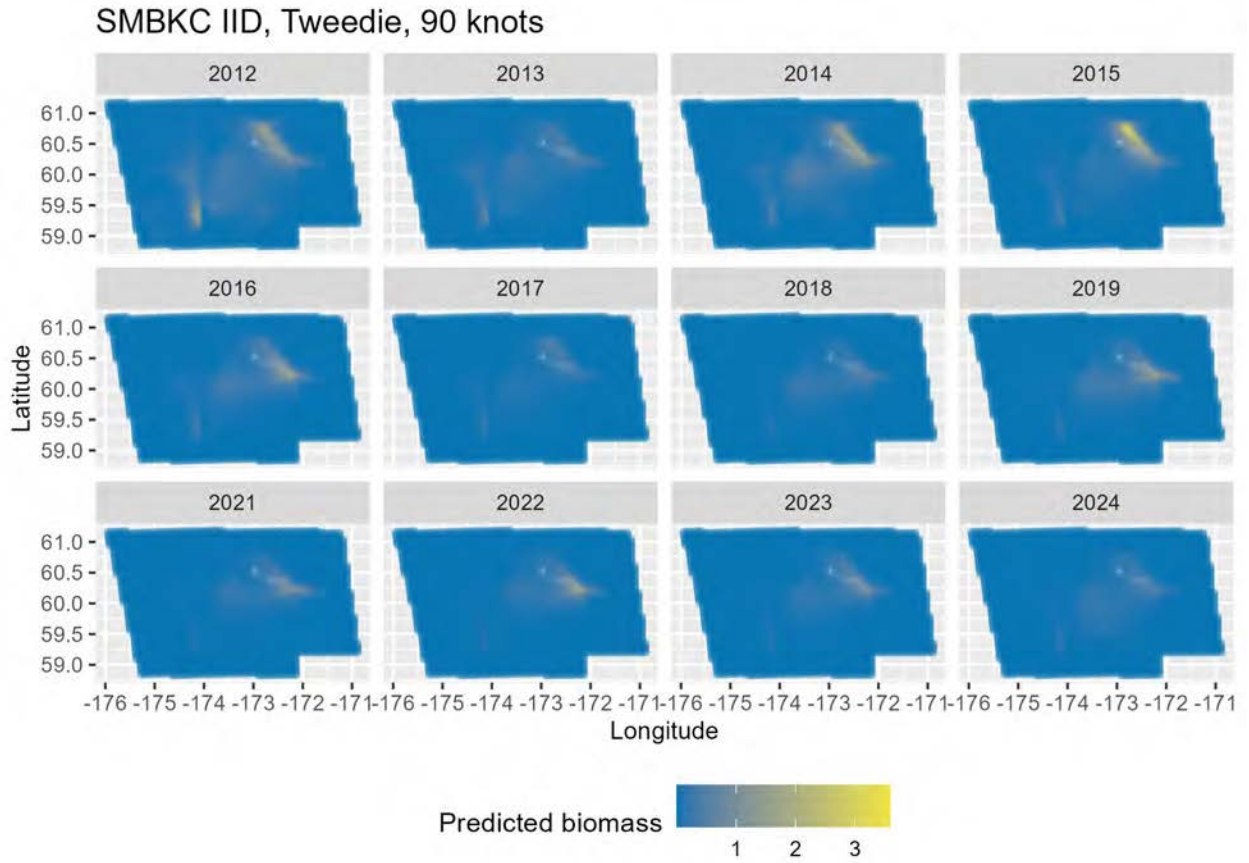
Figure 44: Heat map of St. Matthew Island blue king crab predicted abundance from the IID Tweedie model with 90 knots.
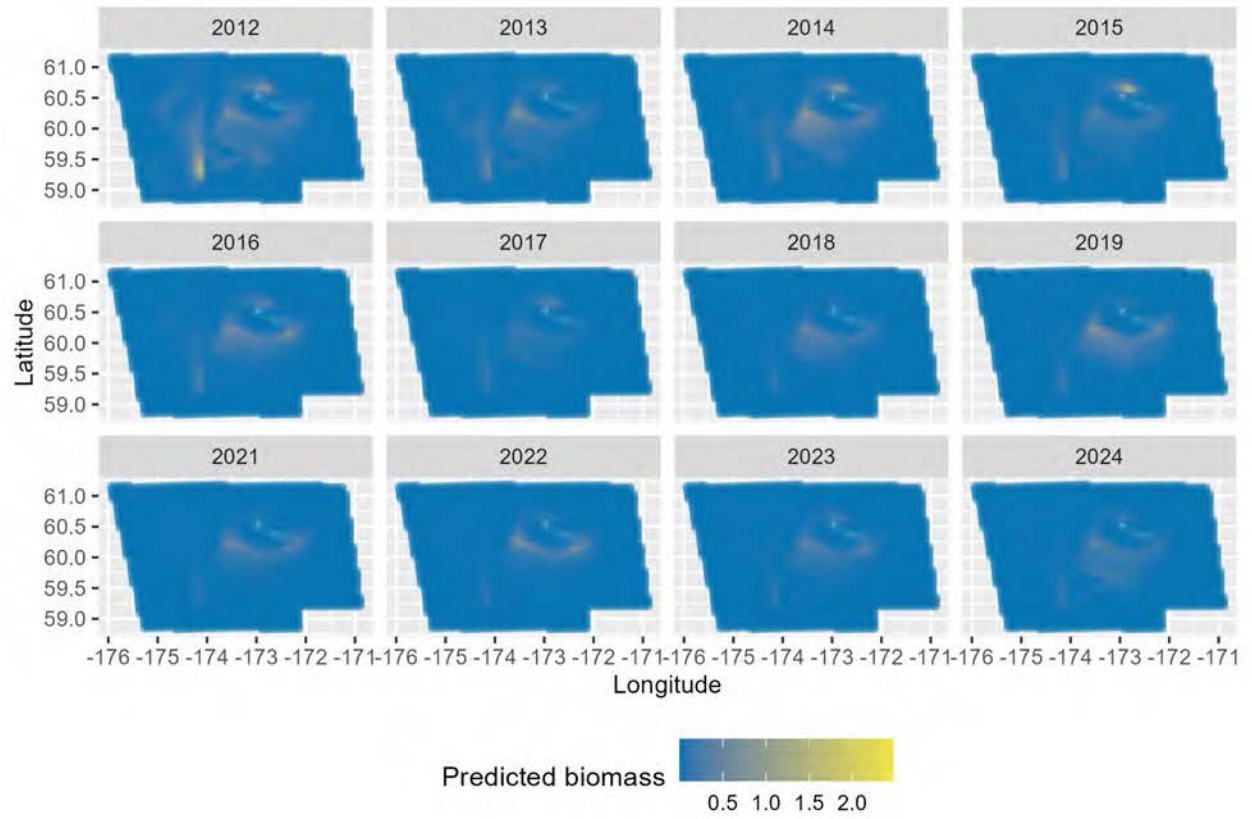
Figure 45: Heat map of St. Matthew Island blue king crab predicted abundance from the IID Tweedie model with 120 knots.
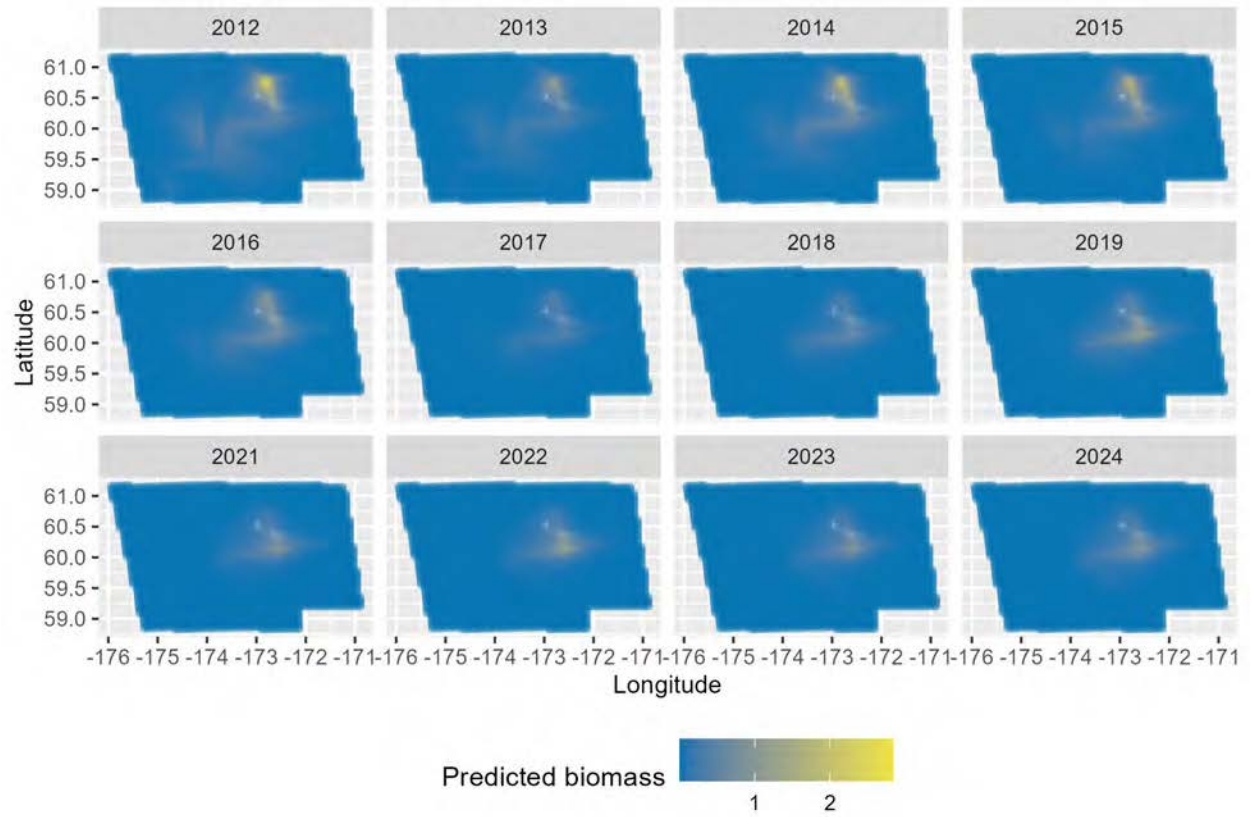
Figure 46: Heat map of St. Matthew Island blue king crab predicted abundance from the random walk Tweedie model with 50 knots.
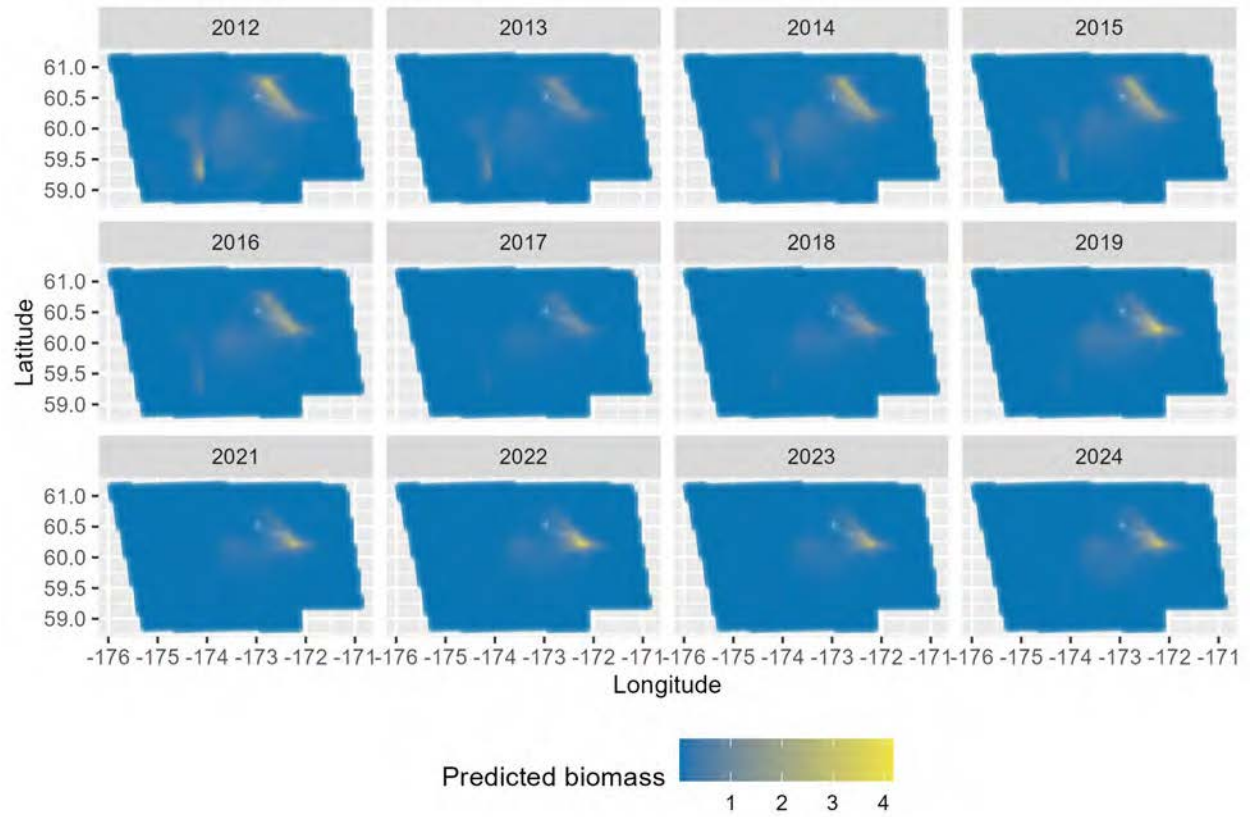
Figure 47: Heat map of St. Matthew Island blue king crab predicted abundance from the random walk Tweedie model with 90 knots.
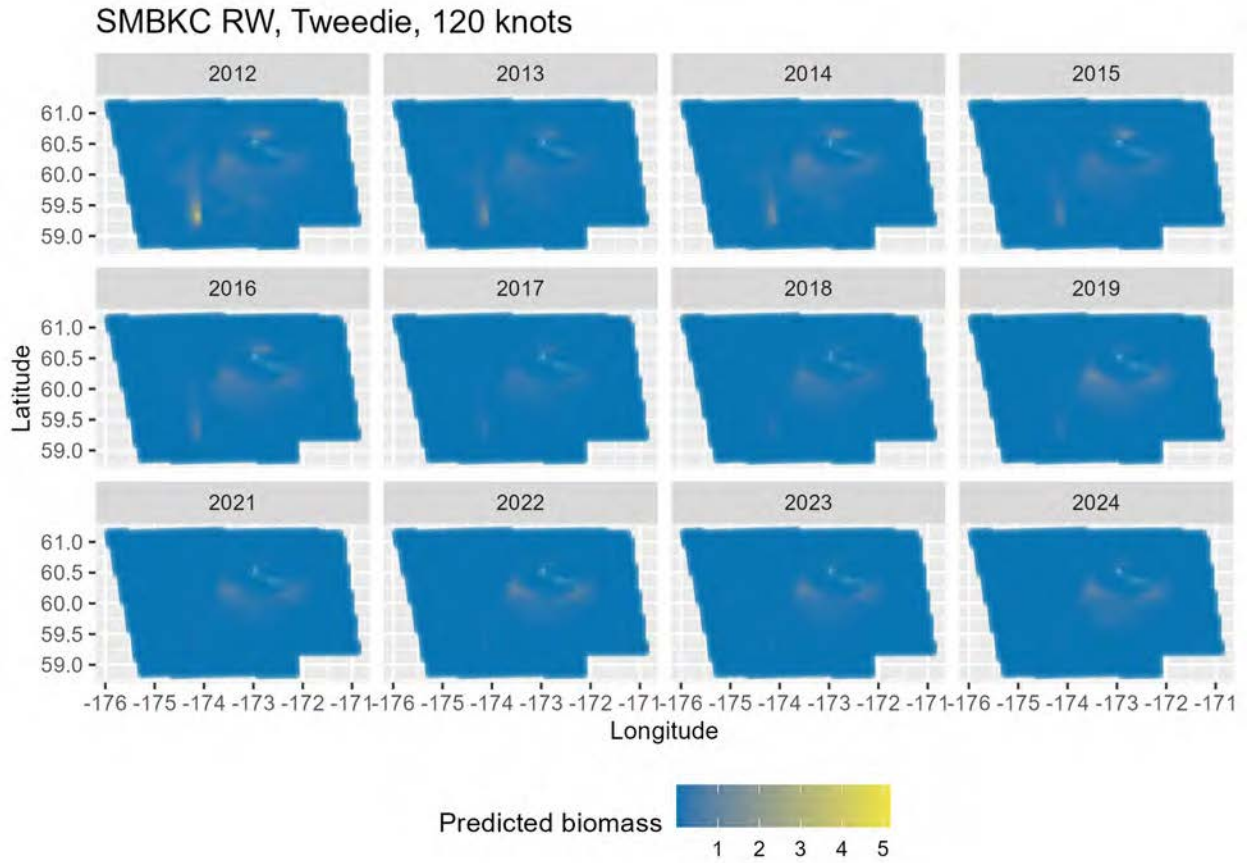
Figure 48: Heat map of St. Matthew Island blue king crab predicted abundance from the random walk Tweedie model with 120 knots.
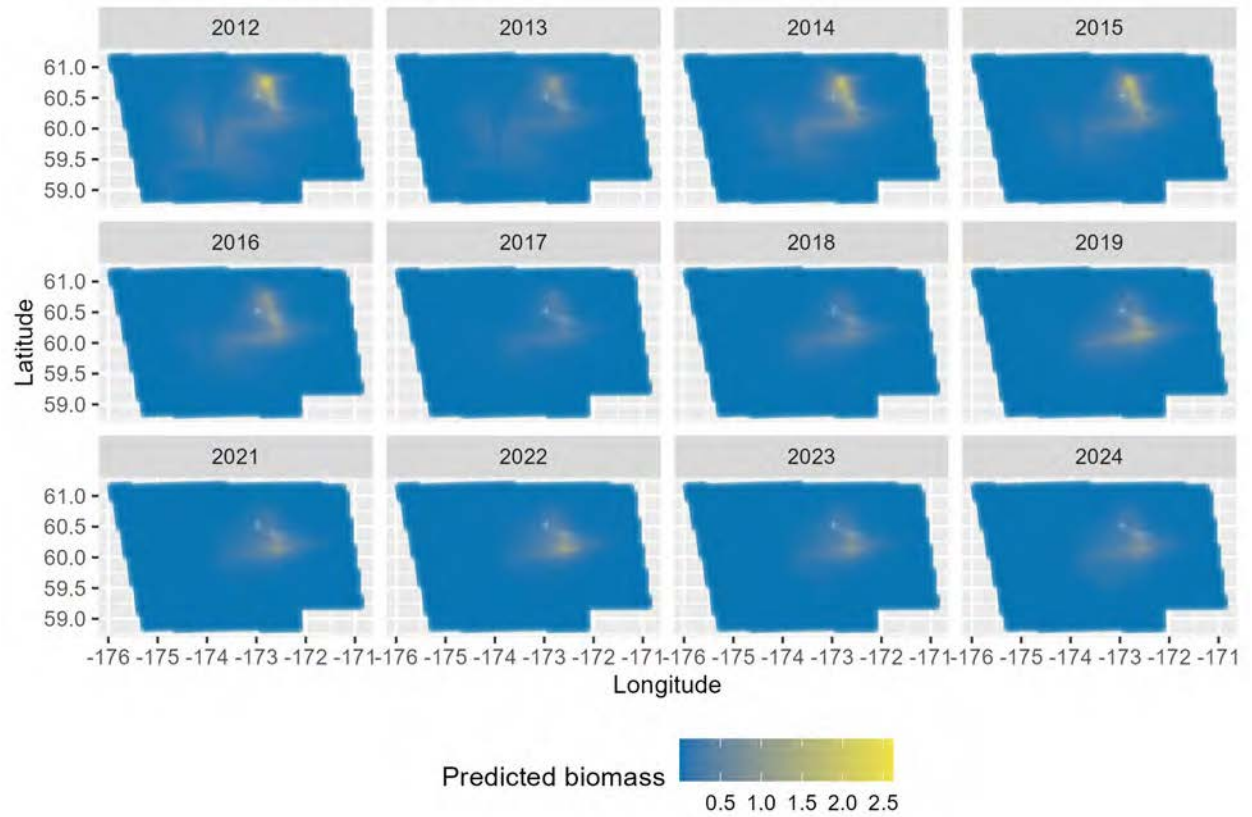
Figure 49: Heat map of St. Matthew Island blue king crab predicted abundance from the AR1 Tweedie model with 50 knots.
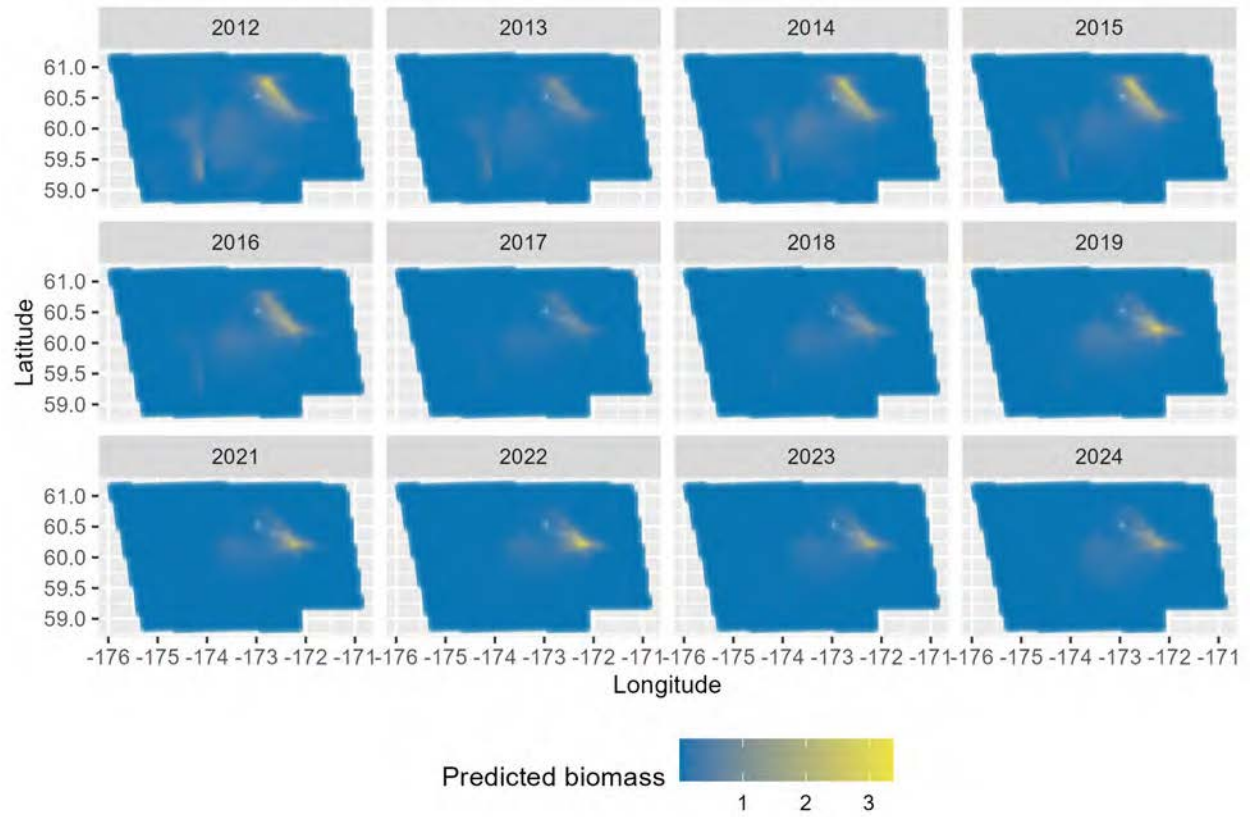
Figure 50: Heat map of St. Matthew Island blue king crab predicted abundance from the AR1 Tweedie model with 90 knots.
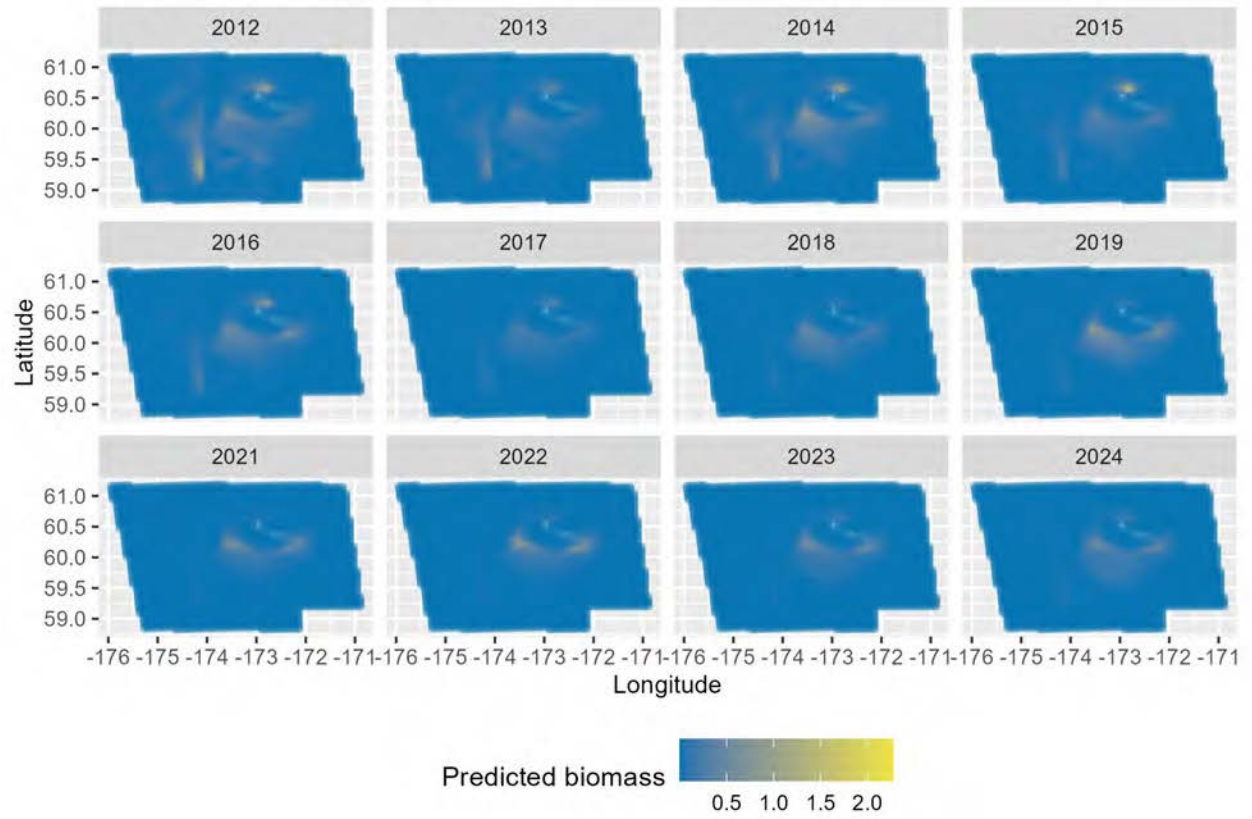
Figure 51: Heat map of St. Matthew Island blue king crab predicted abundance from the AR1 Tweedie model with 120 knots.
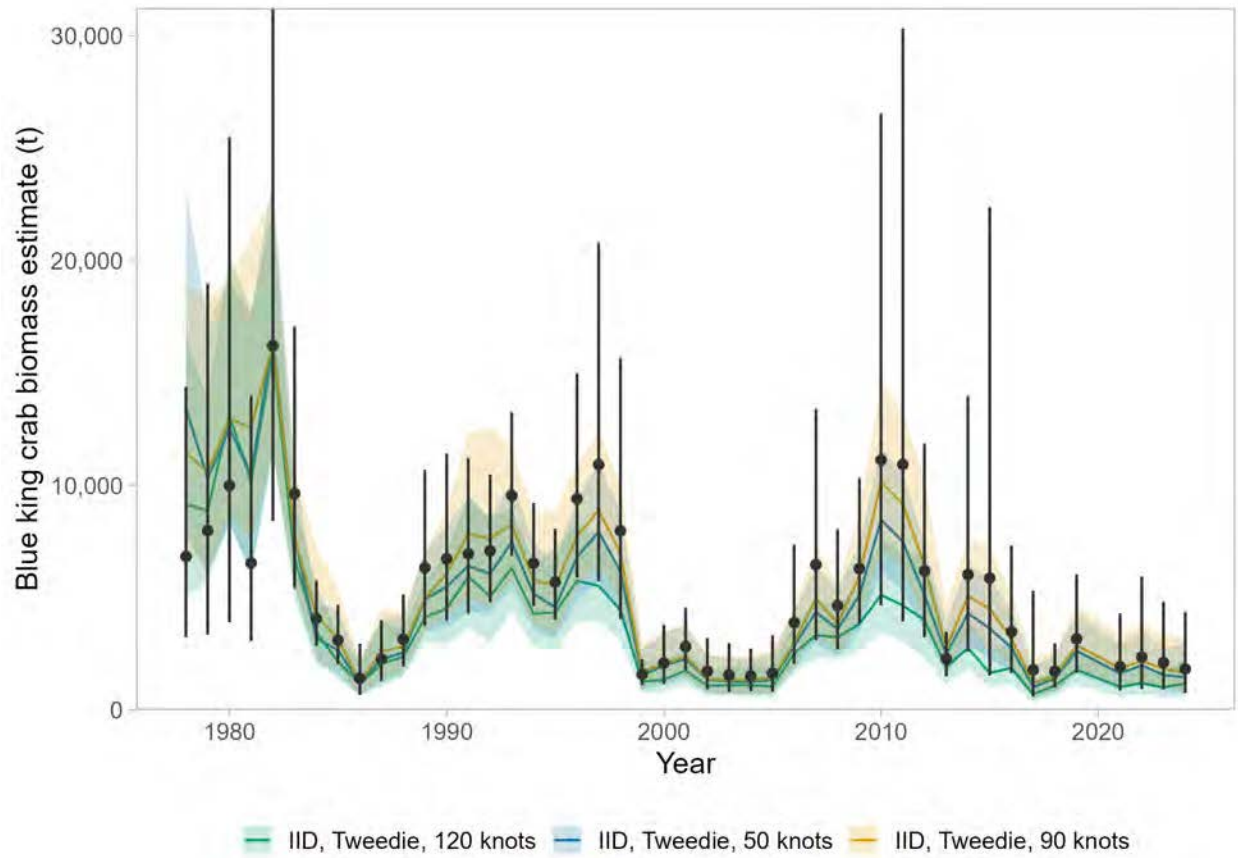
Figure 52: Estimated biomass (t) for St. Matthew Island blue king crab. Colored lines represent biomass (±95% CI) estimated using sdmTMB with spatial random fields estimated as independent and identically distributed (IID). Black points represent biomass (±95% CI) estimated by the NMFS EBS bottom trawl survey.
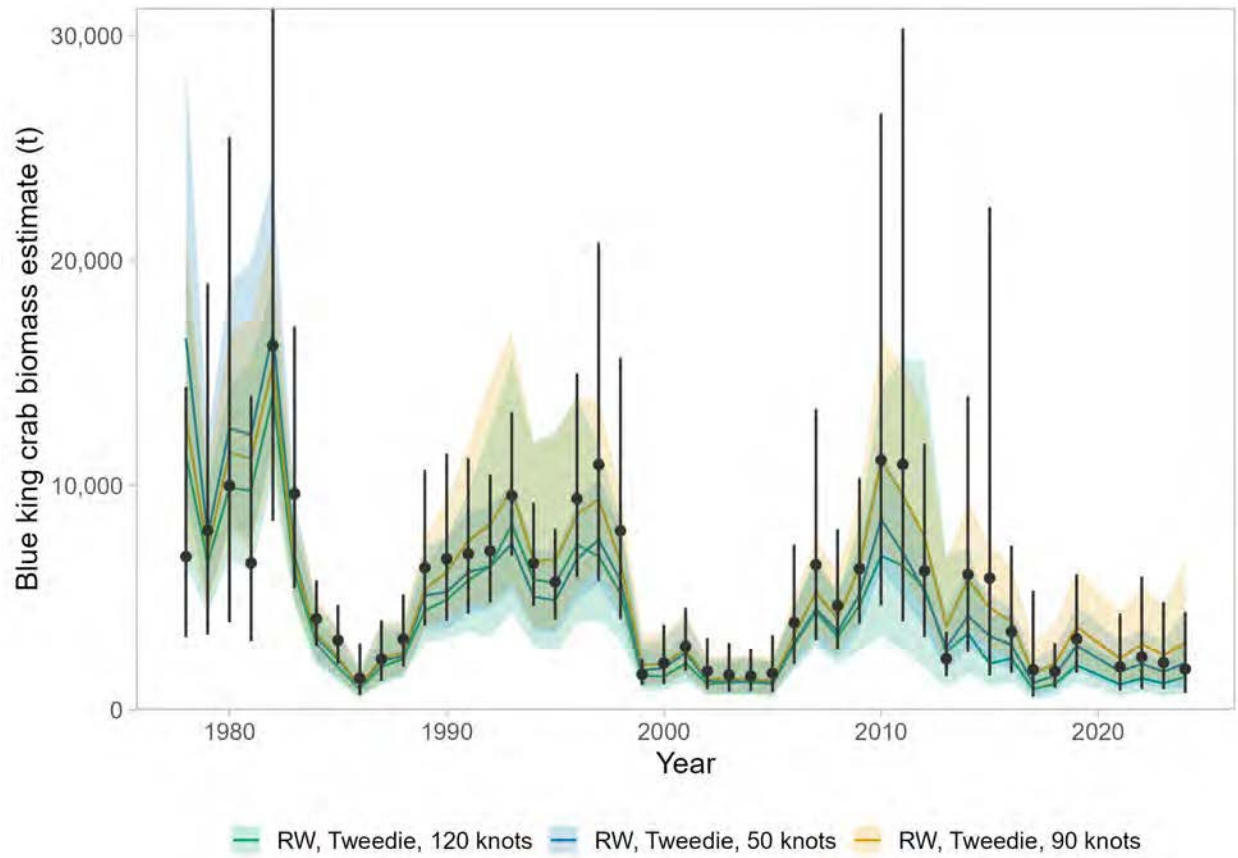
Figure 53: Estimated biomass (t) for St. Matthew Island blue king crab. Colored lines represent biomass (±95% CI) estimated using sdmTMB with spatial random fields estimated using a random walk. Black points represent biomass (±95% CI) estimated by the NMFS EBS bottom trawl survey.
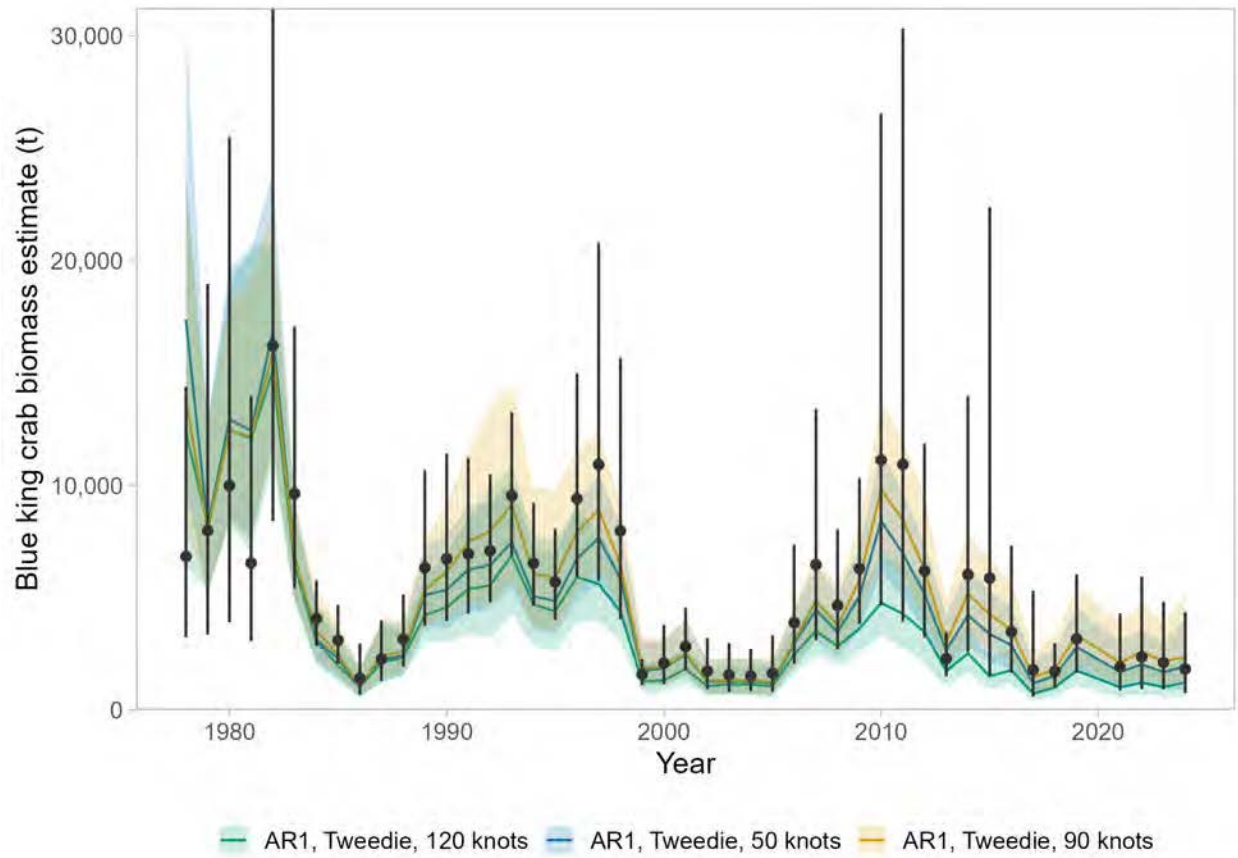
Figure 54: Estimated biomass (t) for St. Matthew Island blue king crab. Colored lines represent biomass (±95% CI) estimated using sdmTMB with spatial random fields estimated as first-order autoregressive (AR1). Black points represent biomass (±95% CI) estimated by the NMFS EBS bottom trawl survey.
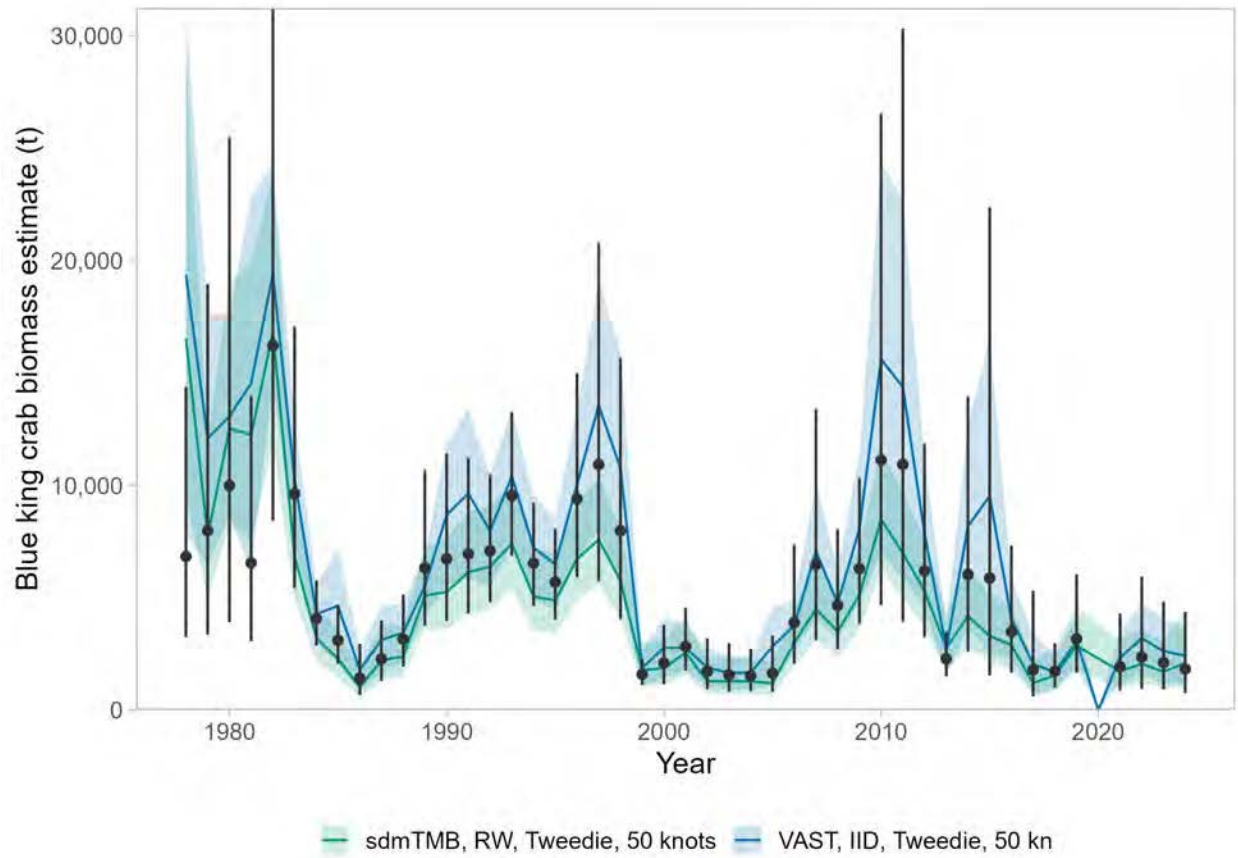
Figure 55: Estimated biomass (t) for St. Matthew Island blue king crab. Colored lines represent biomass (±95% CI) estimated using sdmTMB or VAST. Black points represent biomass (±95% CI) estimated by the NMFS EBS bottom trawl survey.
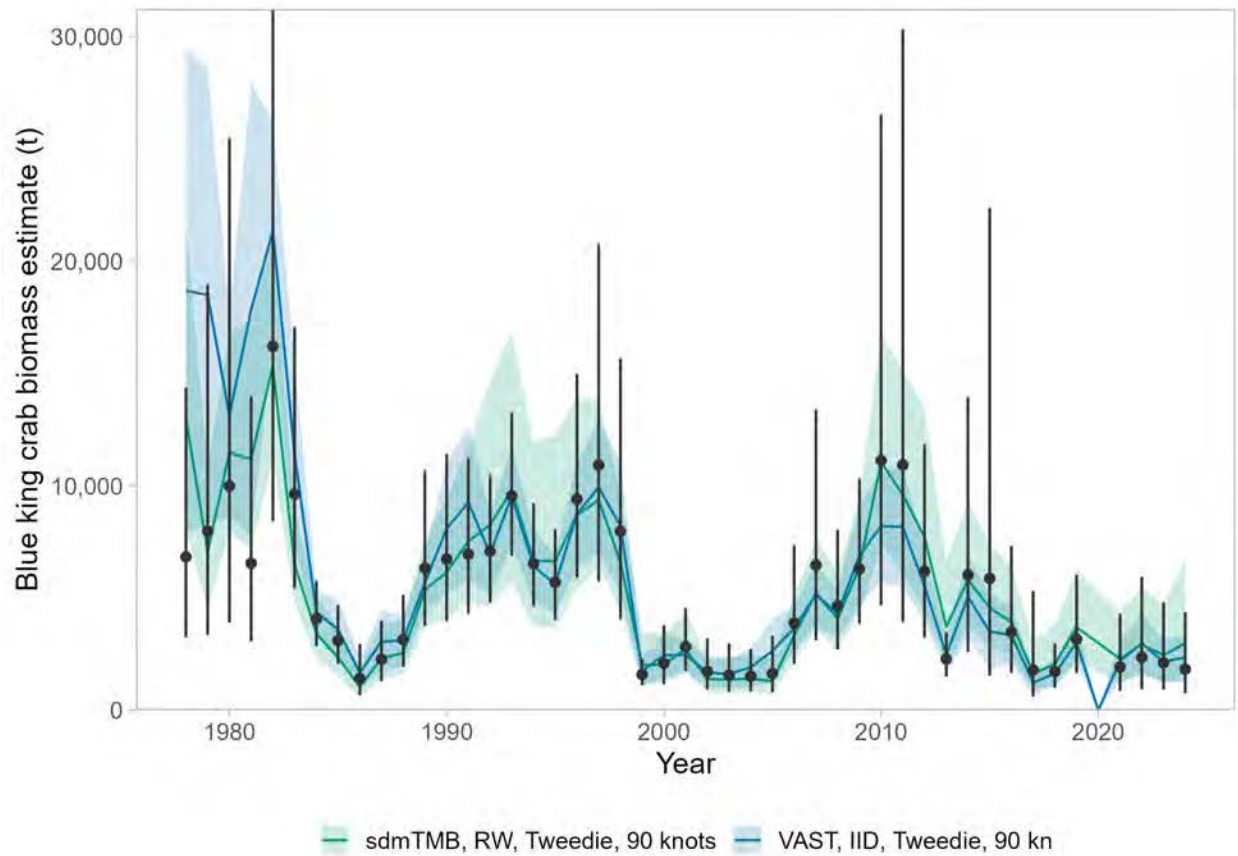
Figure 56: Estimated biomass (t) for St. Matthew Island blue king crab. Colored lines represent biomass (±95% CI) estimated using sdmTMB or VAST. Black points represent biomass (±95% CI) estimated by the NMFS EBS bottom trawl survey.
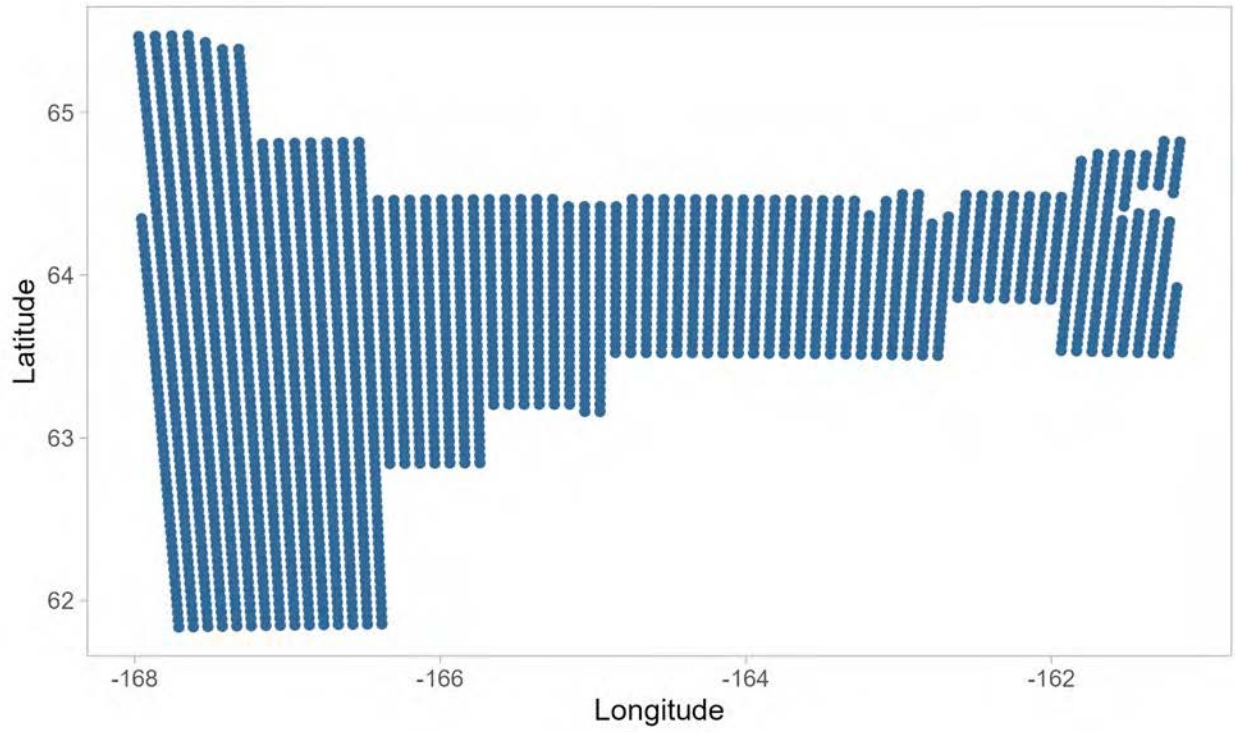
Figure 57: Prediction grid used for Norton Sound red king crab spatial abundance predictions. Spatial resolution is 5 km^2.
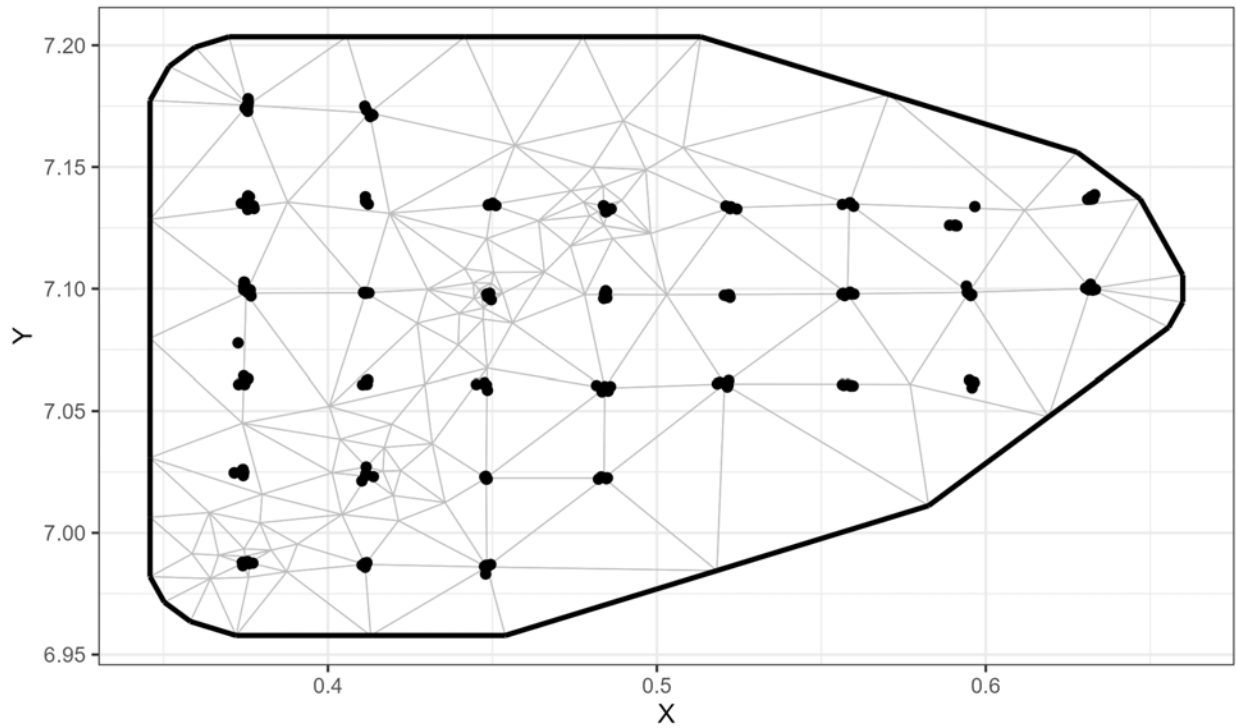
Figure 58: Spatial mesh with 30 knots used for fitting Norton Sound red king crab spatial models. Points represent observations and vertices represent knot locations.
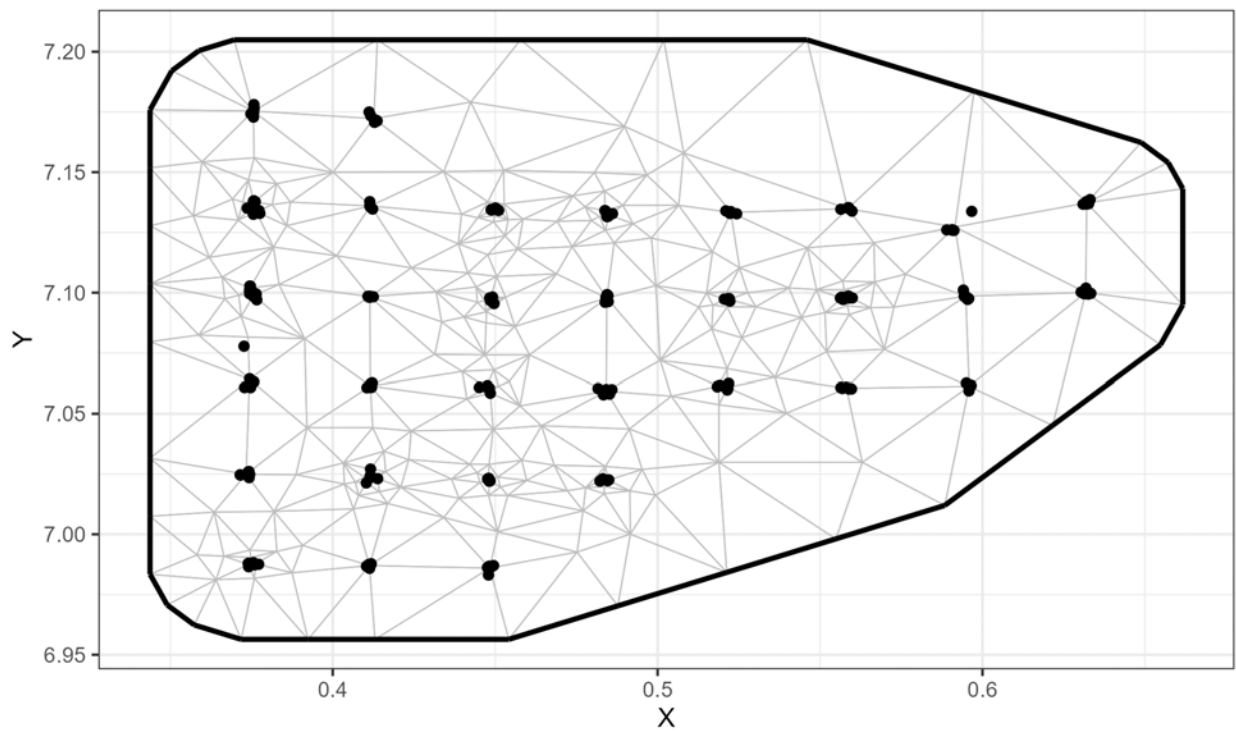
Figure 59: Spatial mesh with 50 knots used for fitting Norton Sound red king crab spatial models. Points represent observations and vertices represent knot locations.
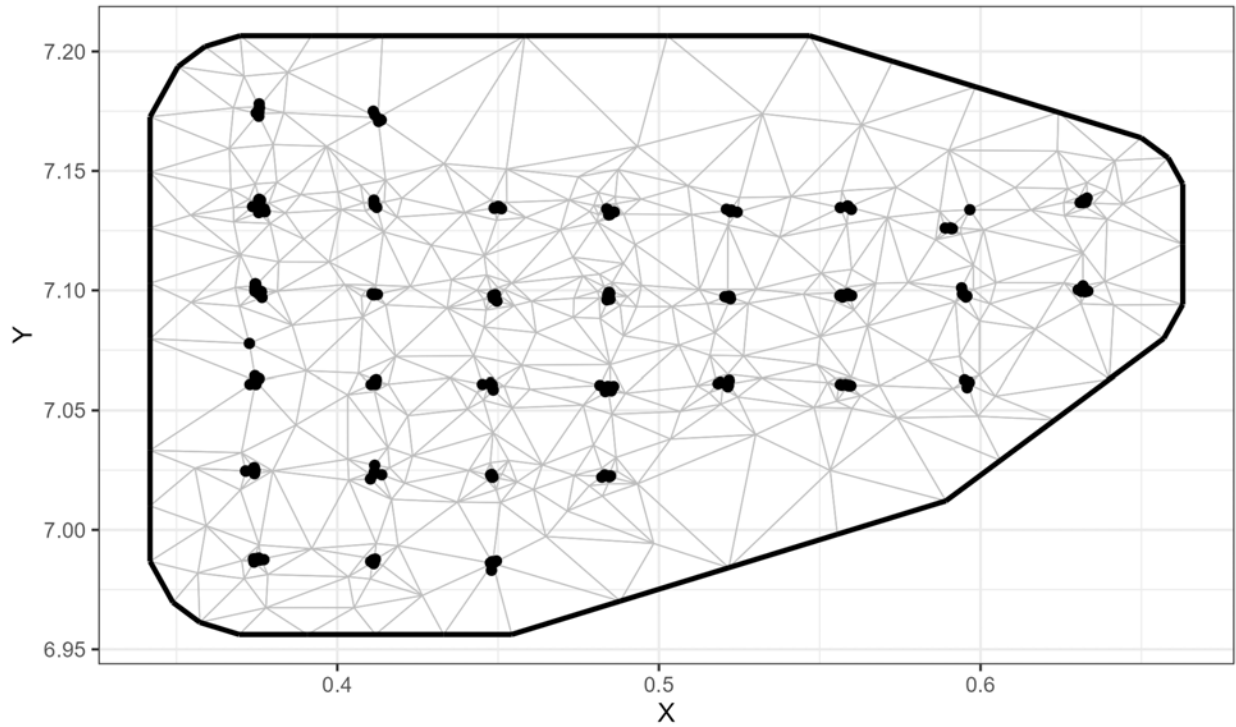
Figure 60: Spatial mesh with 100 knots used for fitting Norton Sound red king crab spatial models. Points represent observations and vertices represent knot locations.
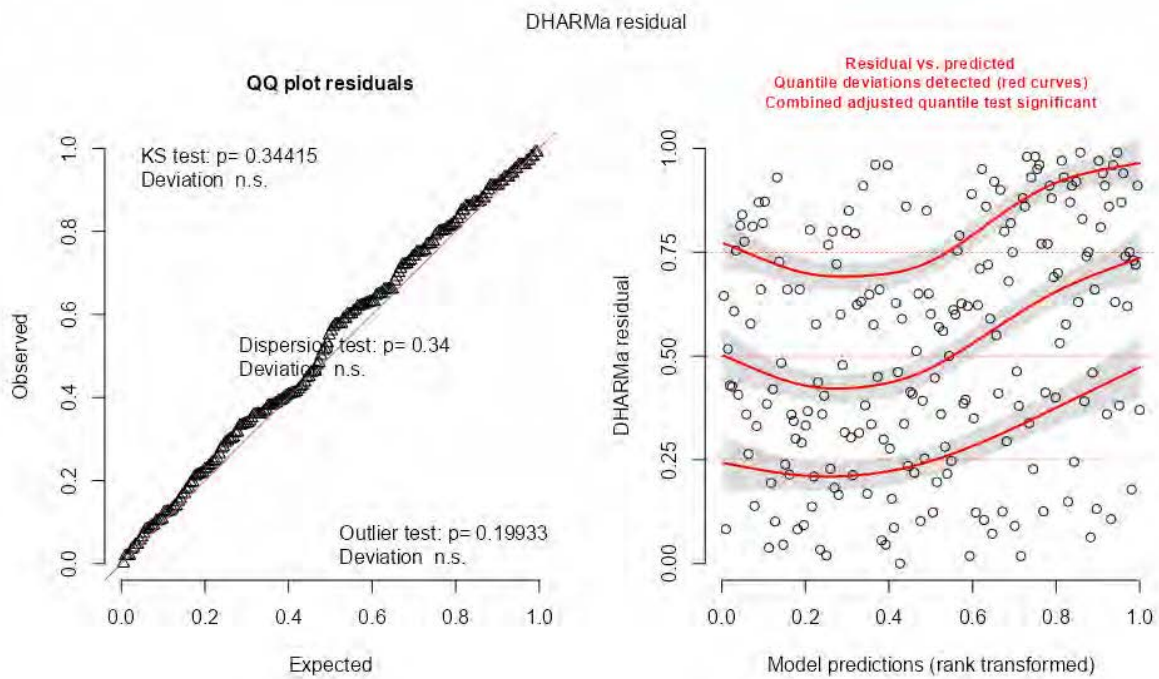
Figure 61: Model diagnostic plots using DHARMa residuals for the Norton Sound red king crab model (random walk, Tweedie, 30 knots).
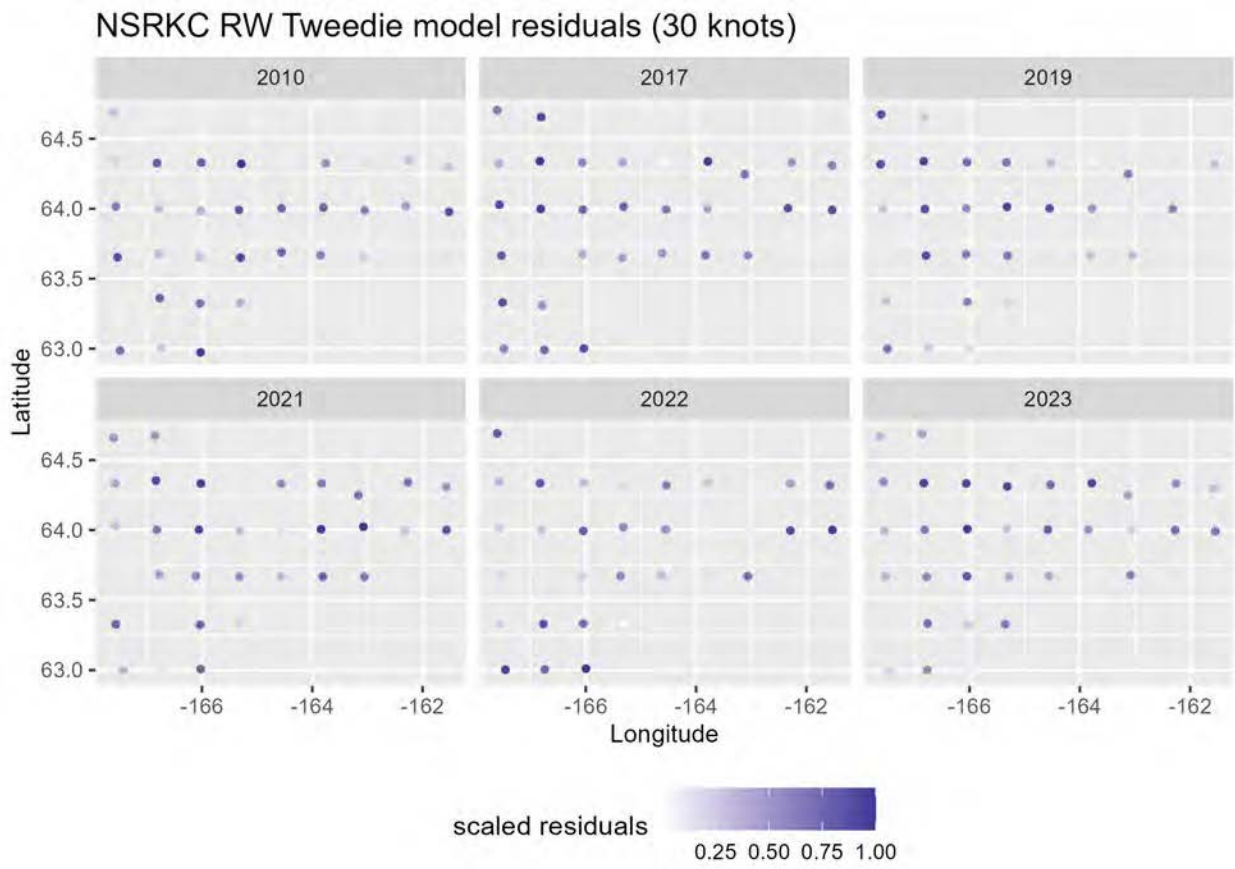
Figure 62: Spatial distribution of DHARMa residuals for the NSRKC RW Tweedie model with 30 knots.
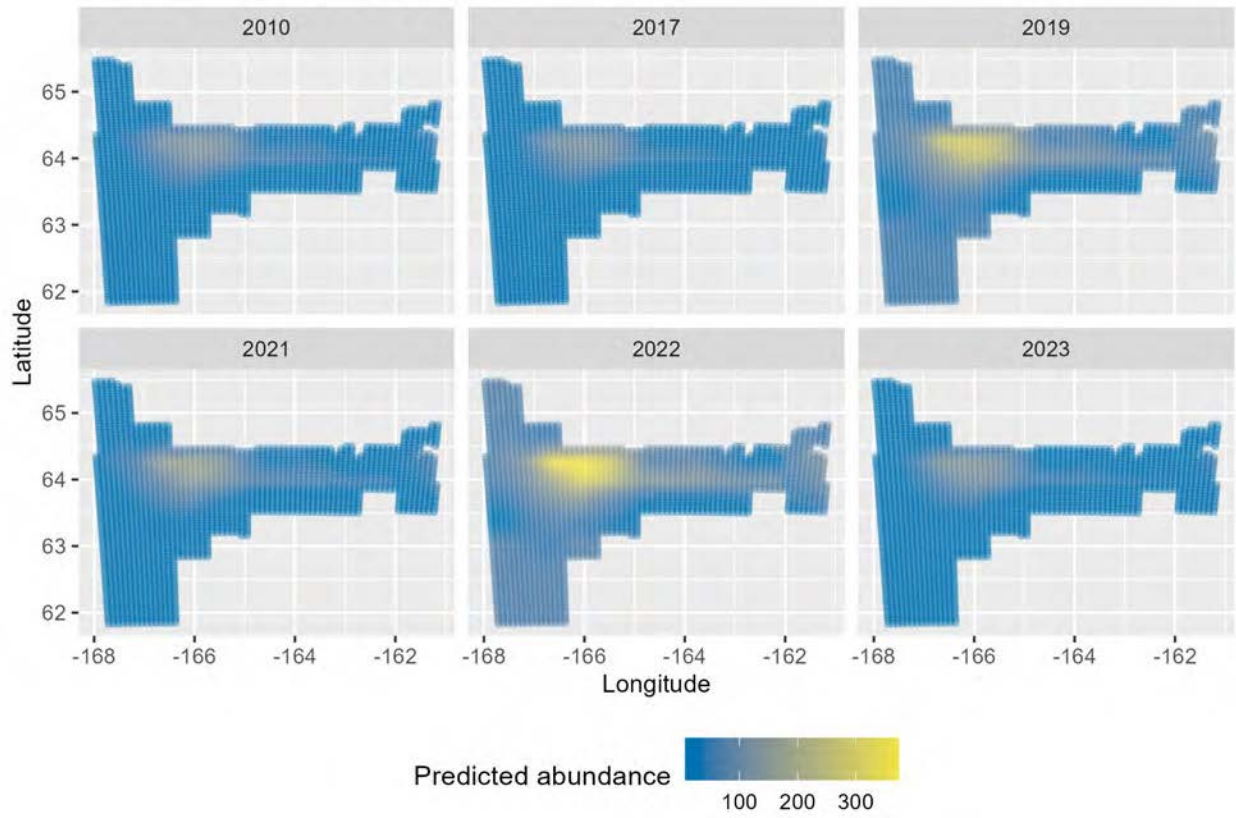
Figure 63: Heat map of Norton Sound red king crab predicted abundance generated using the model (random walk, Tweedie, 30 knots).
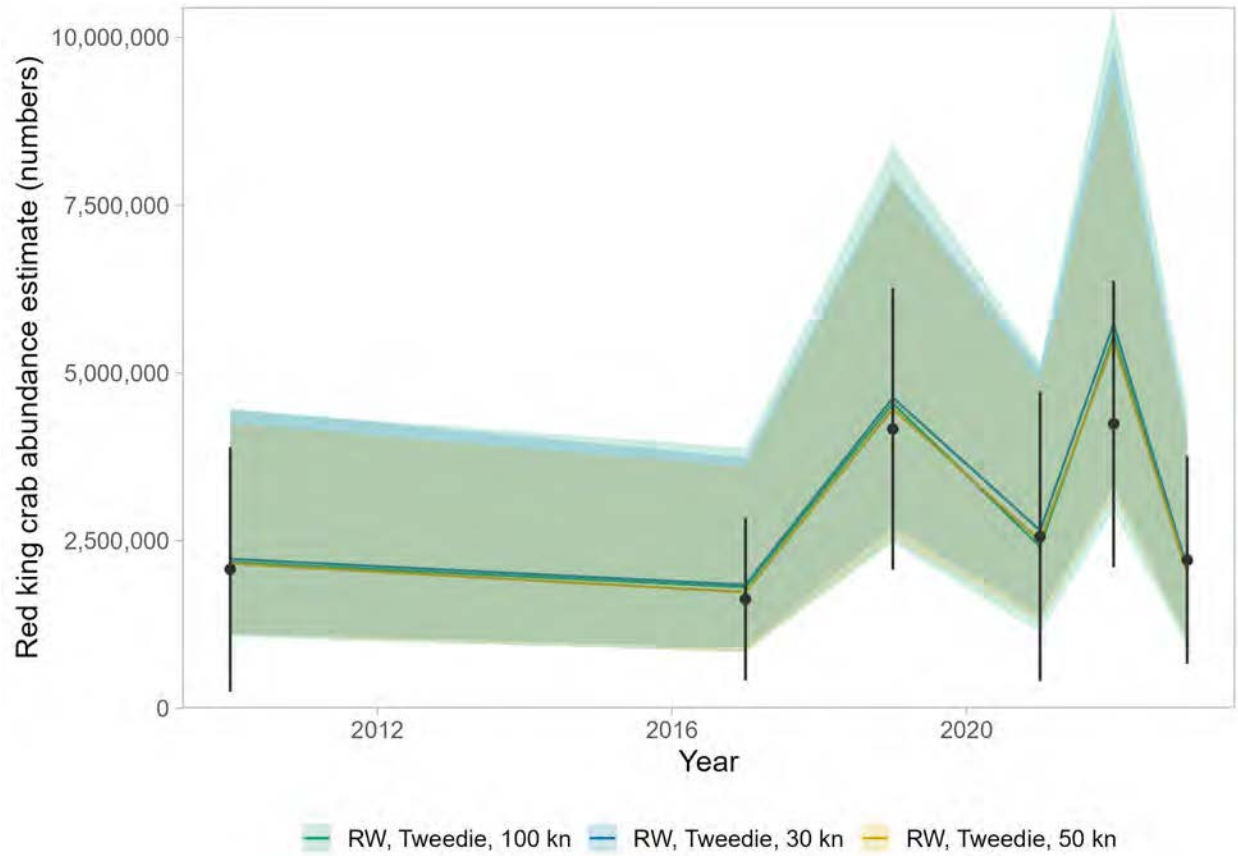
Figure 64: Estimated abundance in number of crab for Norton Sound red king crab. Colored lines represent abundance (±95% CI) estimated using sdmTMB. Black points represent abundance (±95% CI) estimated by the trawl surveys.
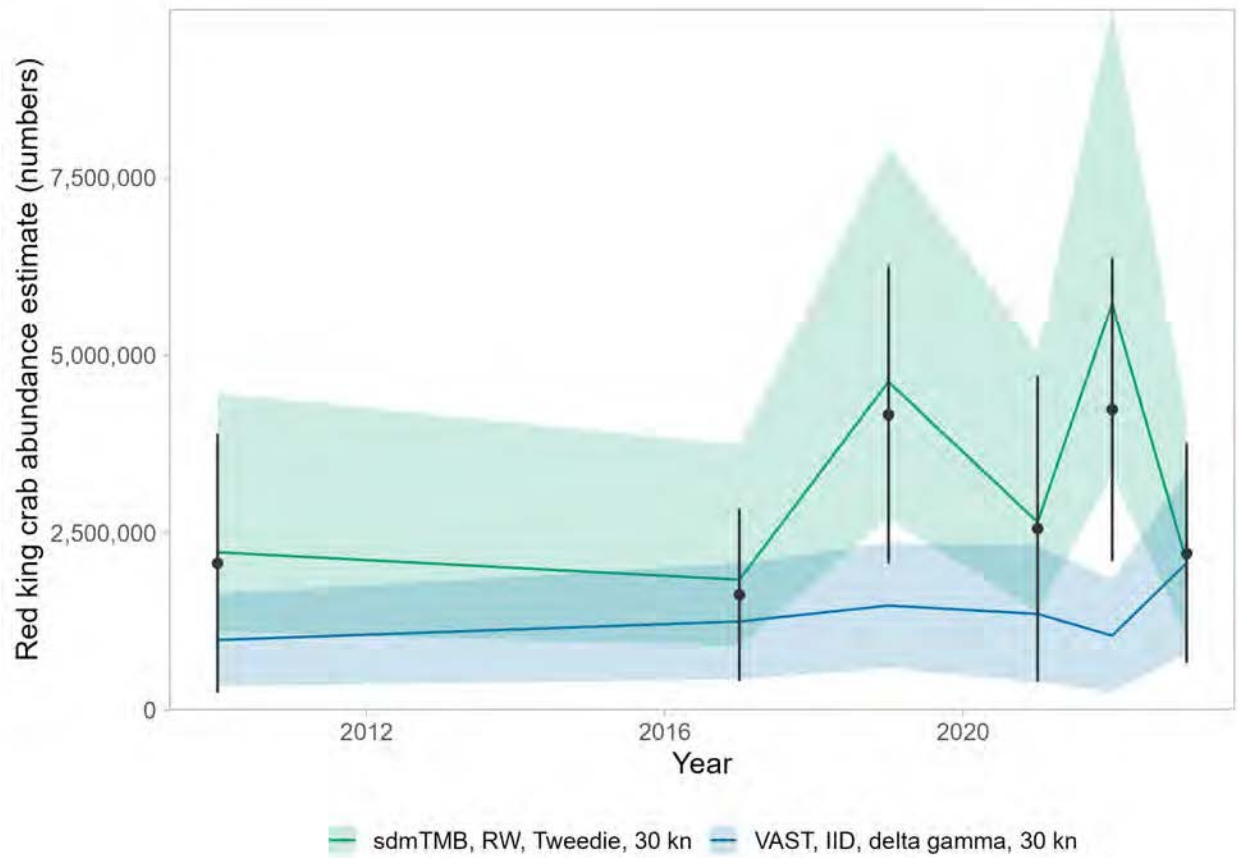
Figure 65: Estimated abundance in number of crab for Norton Sound red king crab,. Colored lines represent abundance (±95% CI) estimated using sdmTMB or VAST. Black points represent abundance (±95% CI) estimated by the trawl surveys.

Appendix
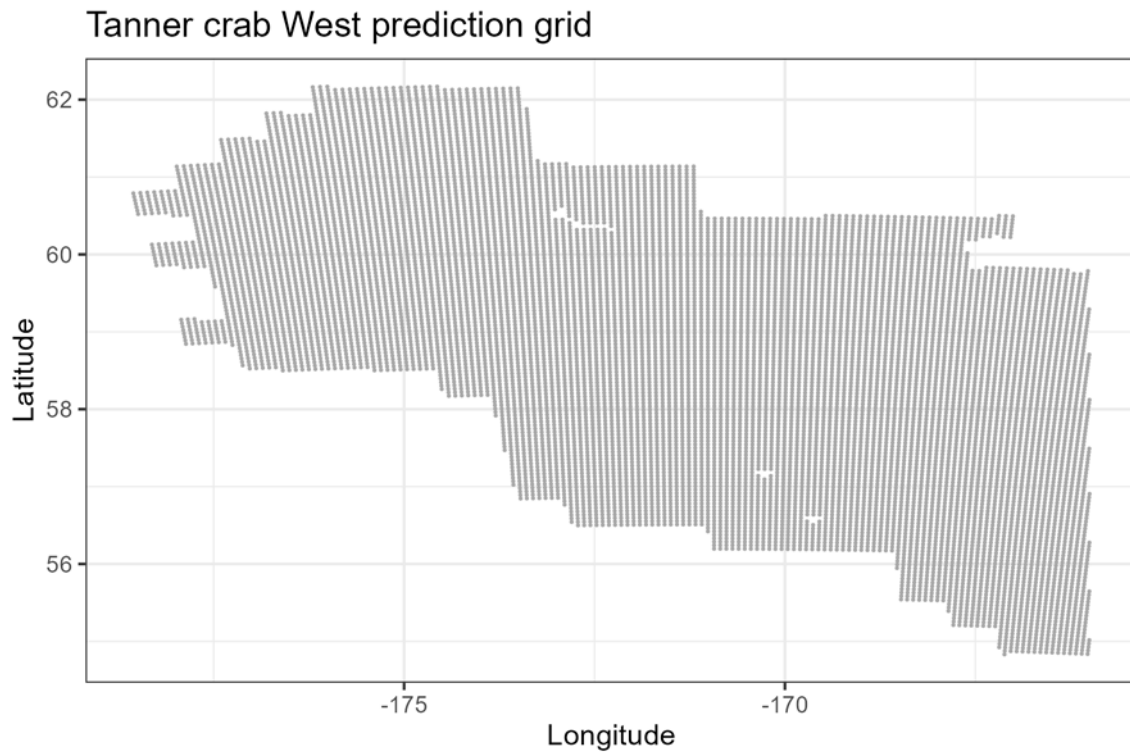
Figure 66: Prediction grid used to predict spatial abundance and biomass for Tanner crab west of 166°. Spatial resolution is 5km^2 and does not include land.
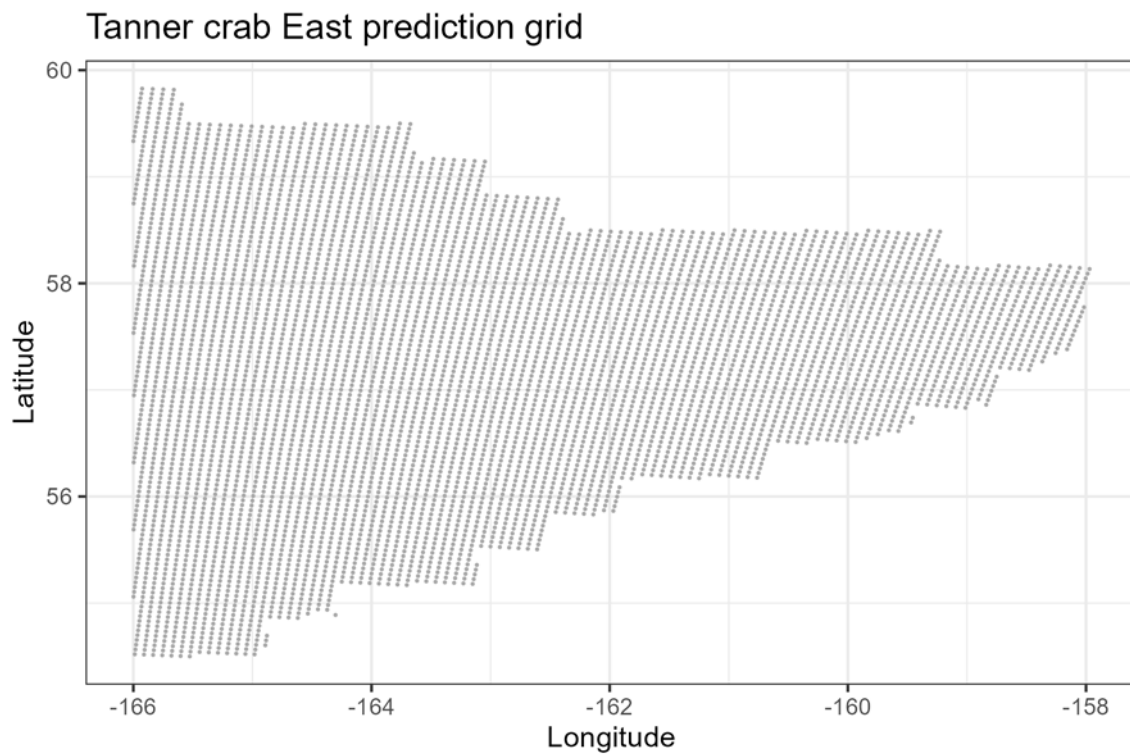
Figure 67: Prediction grid used to predict spatial abundance and biomass for Tanner crab east of 166°. Spatial resolution is 5km^2 and does not include land.
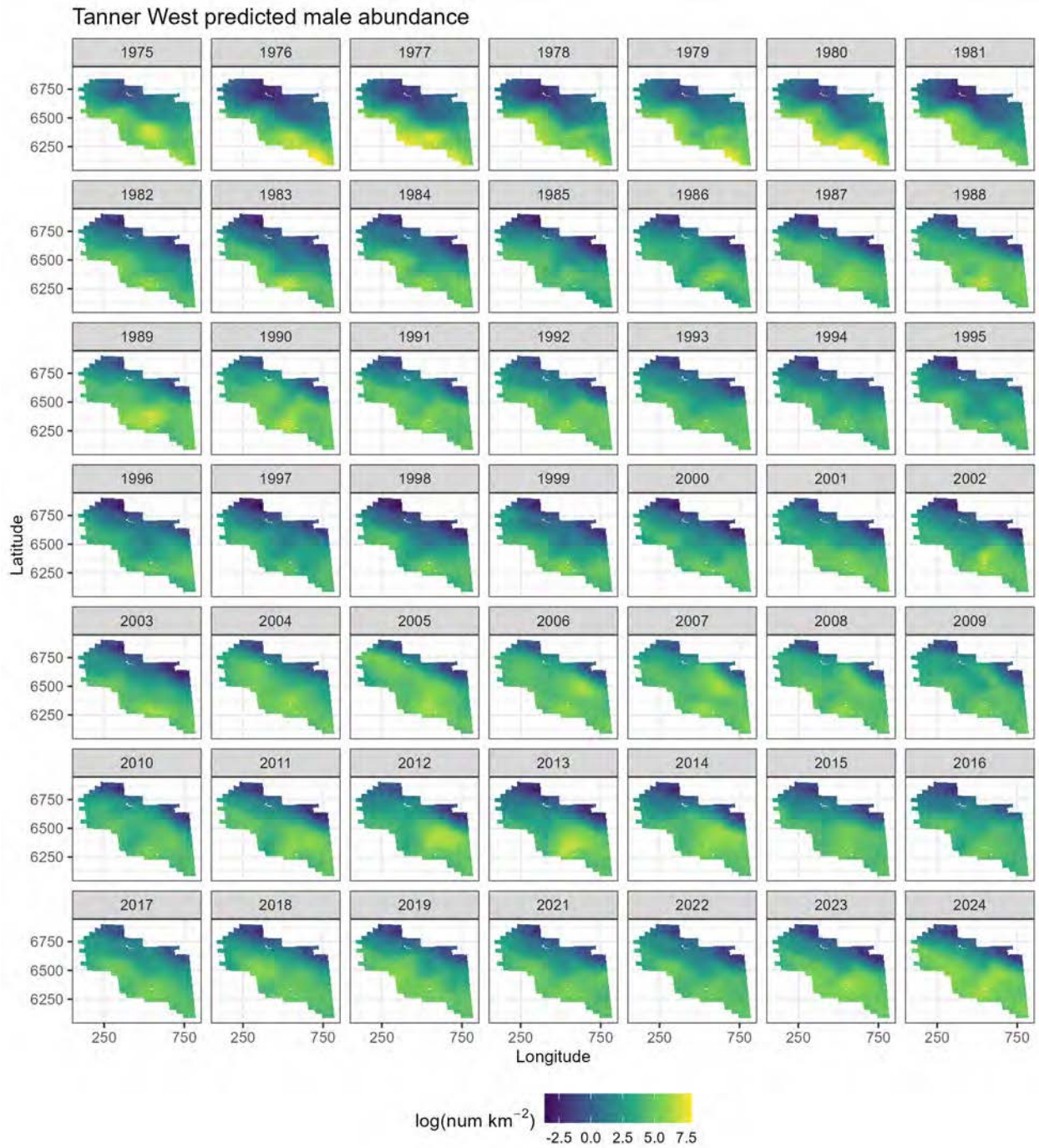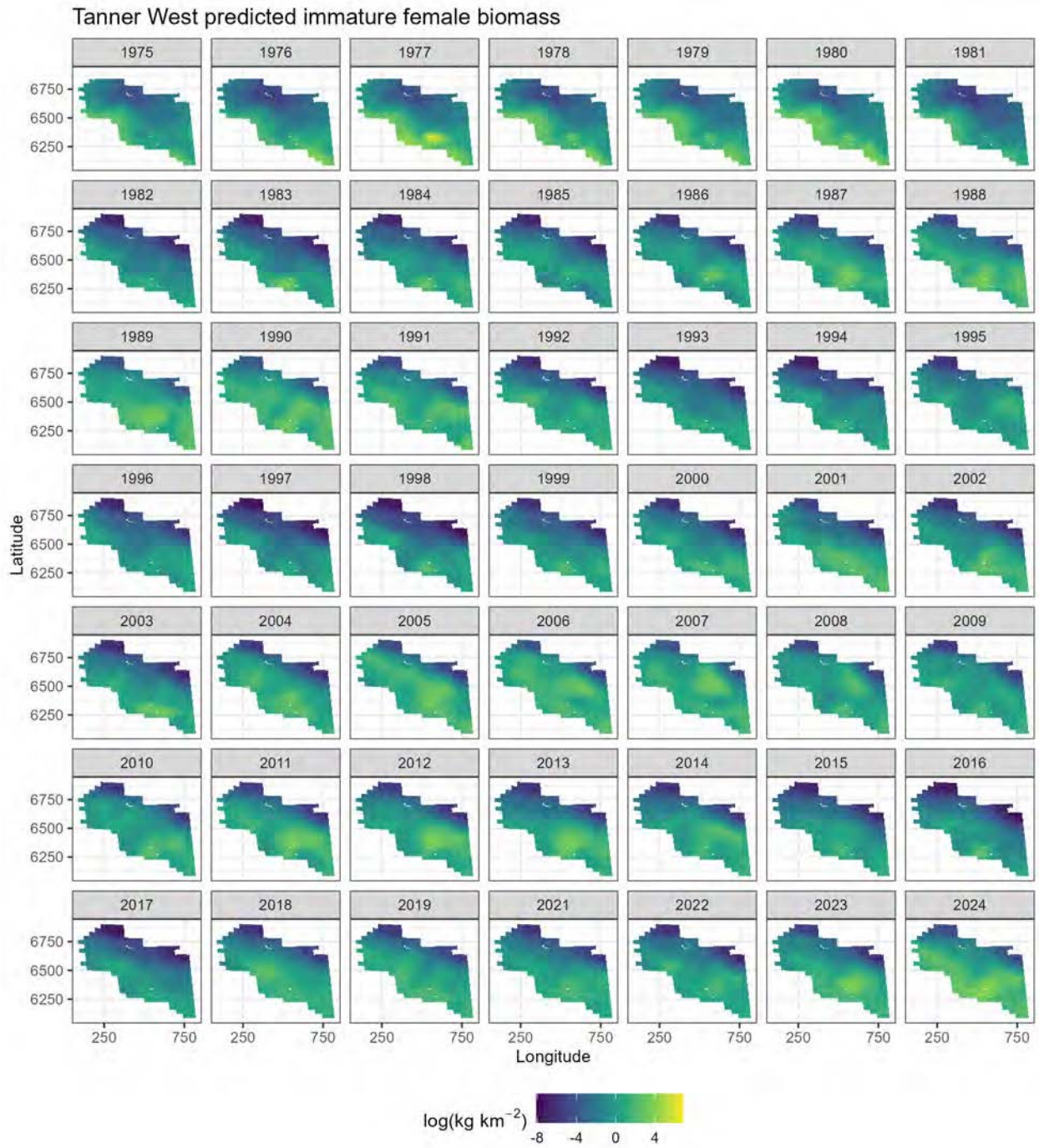
Figure 68: Spatial predictions of male abundance west of 166° using NMFS summer bottom trawl survey data before 1982 and 1982 onward with a 50-knot mesh and a delta-gamma model family. Predictions from both of these periods/models are combined in this figure.
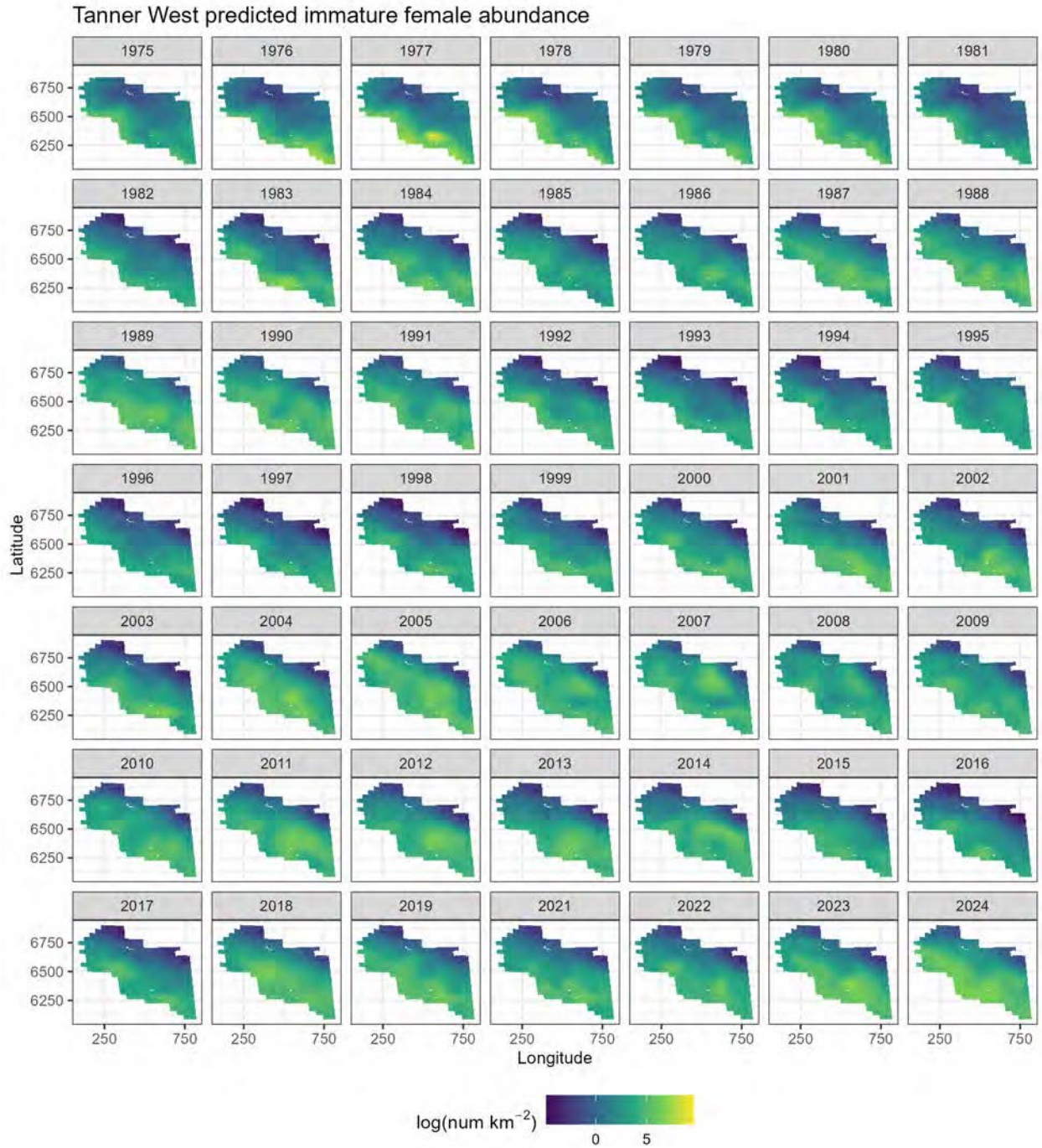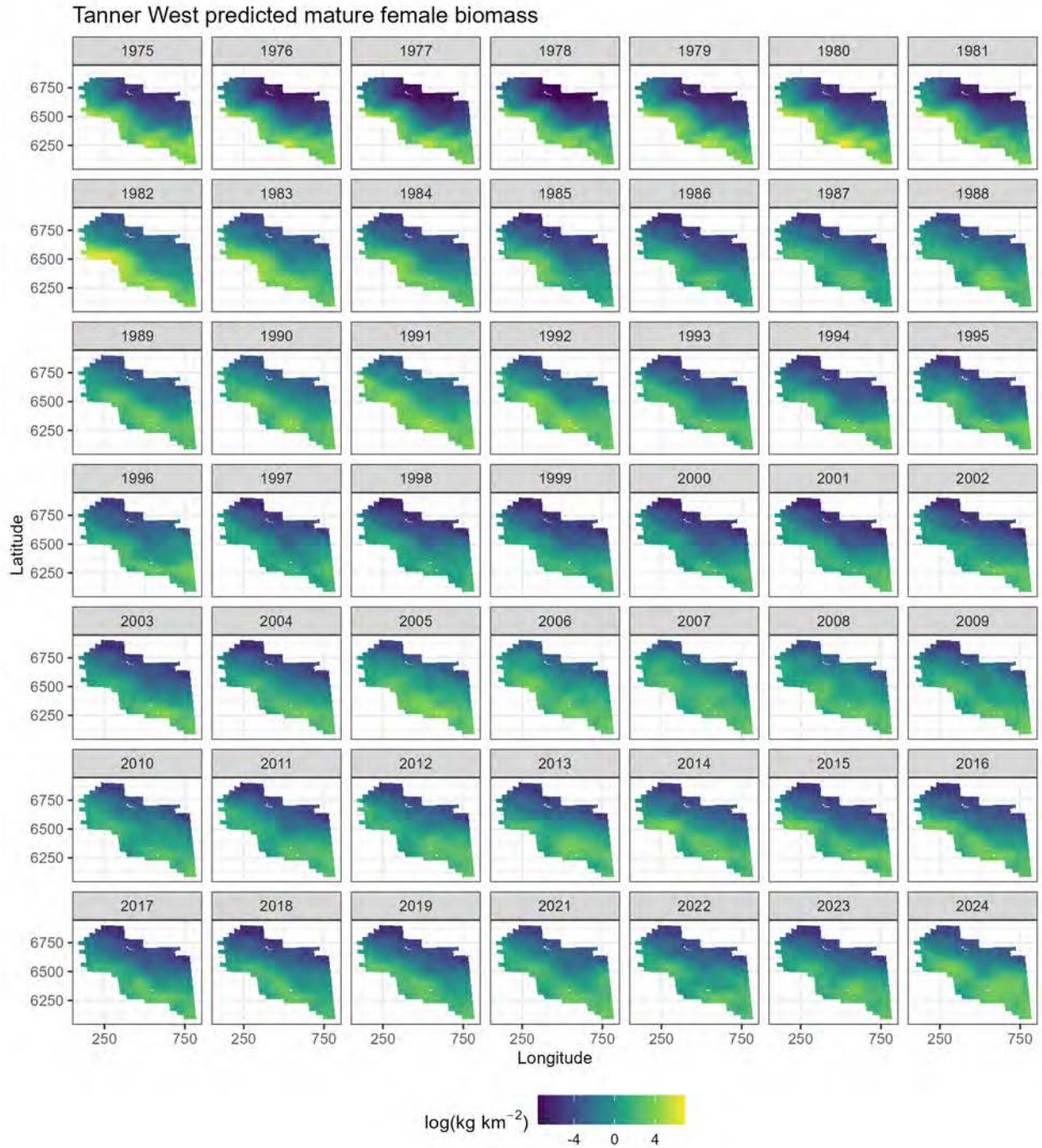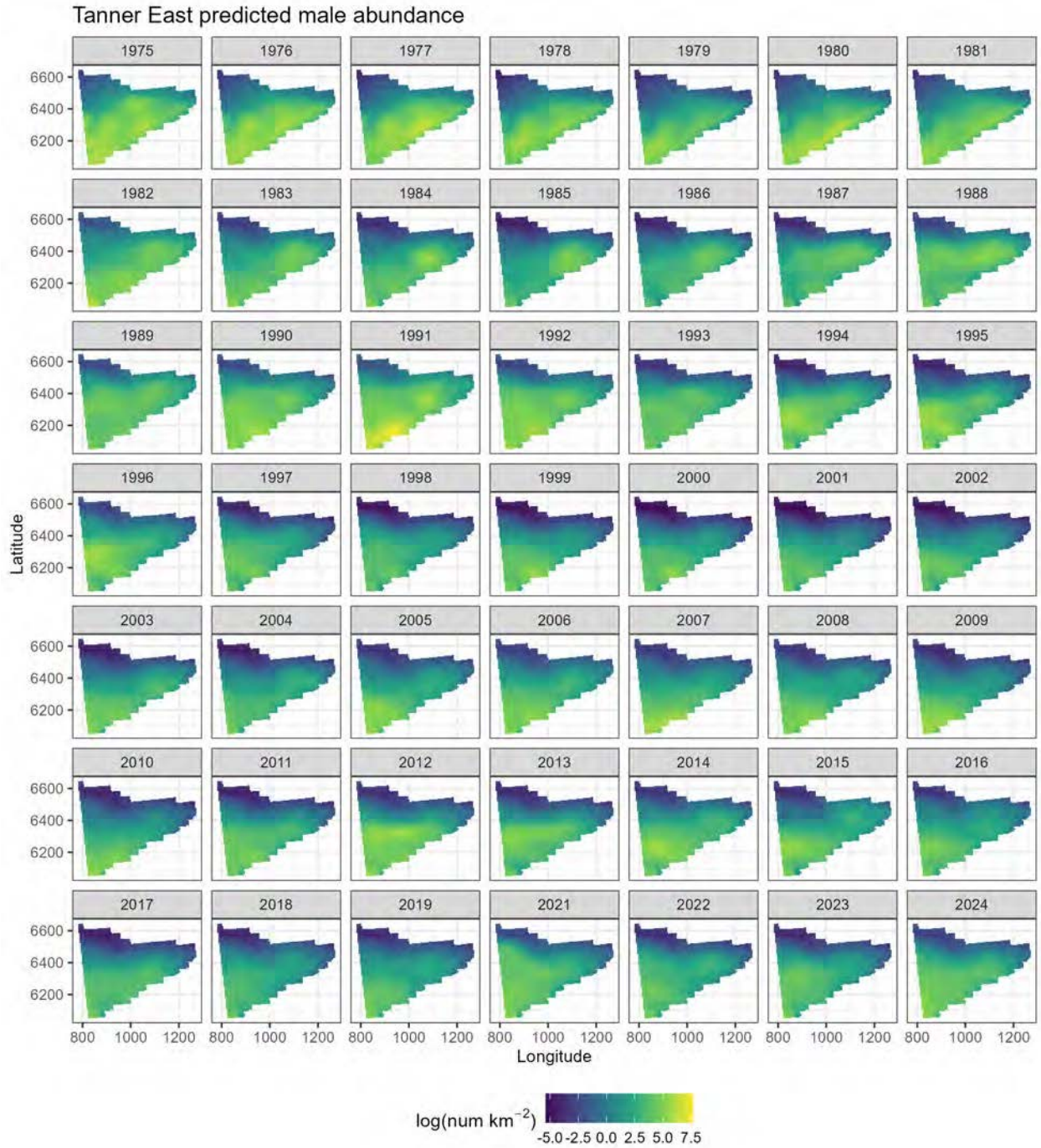
Figure 69: Spatial predictions of immature female abundance west of 166° using NMFS summer bottom trawl survey data before 1982 and 1982 onward with a 50-knot mesh and a delta-gamma model family. Predictions from both of these periods/models are combined in this figure.
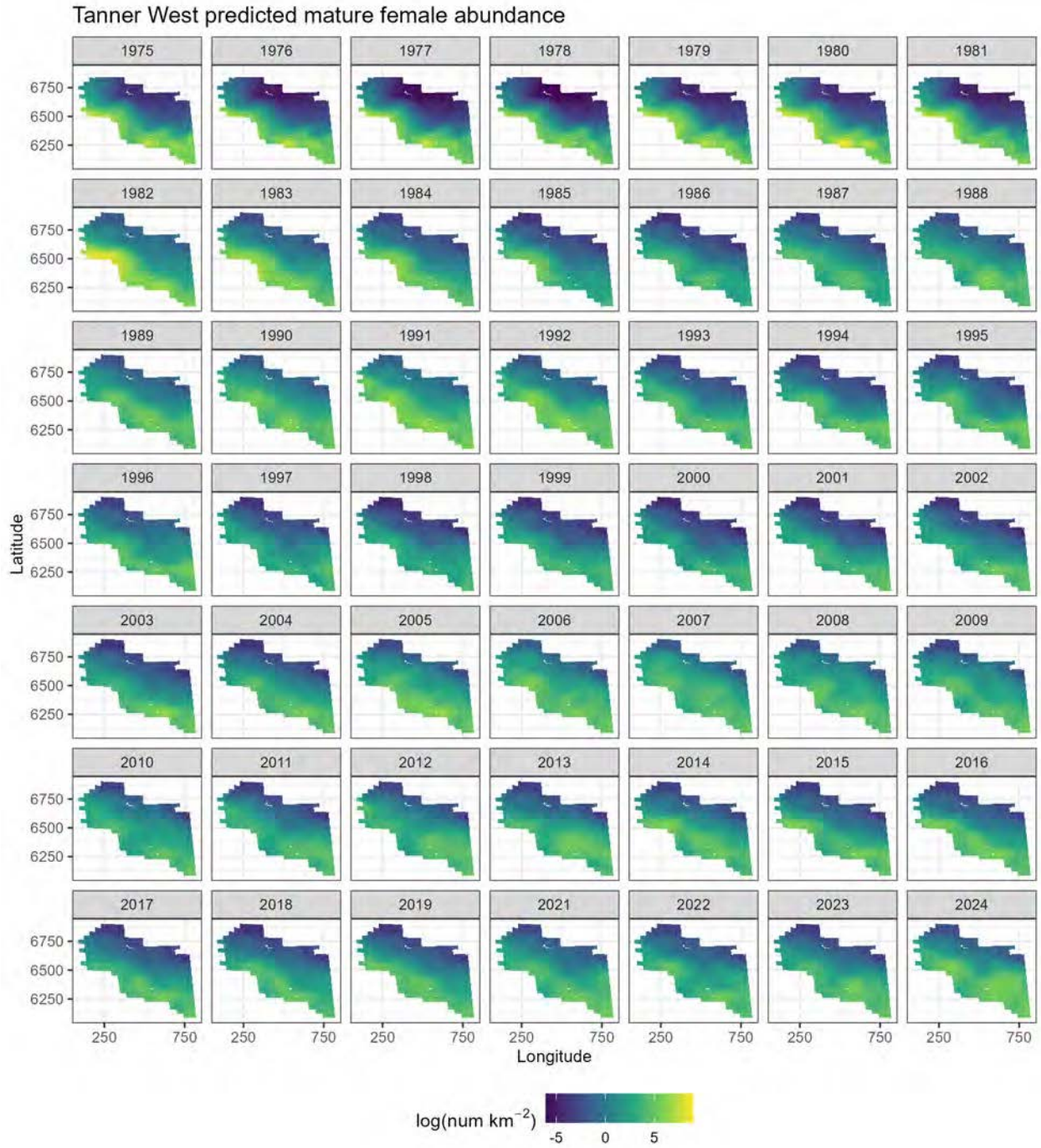
Figure 70: Spatial predictions of mature female abundance west of 166° using NMFS summer bottom trawl survey data before 1982 and 1982 onward with a 50-knot mesh and a delta-gamma model family. Predictions from both of these periods/models are combined in this figure.
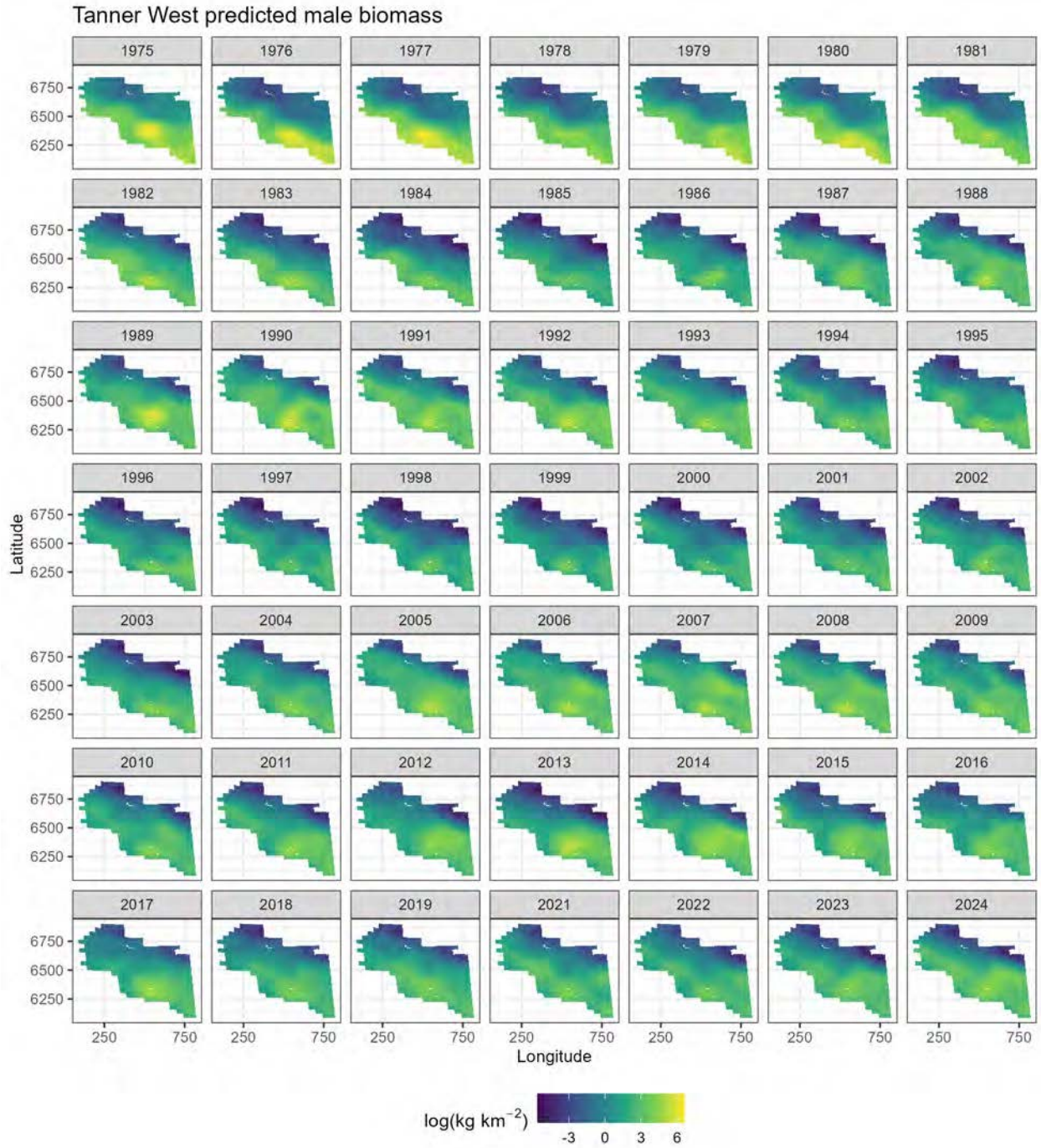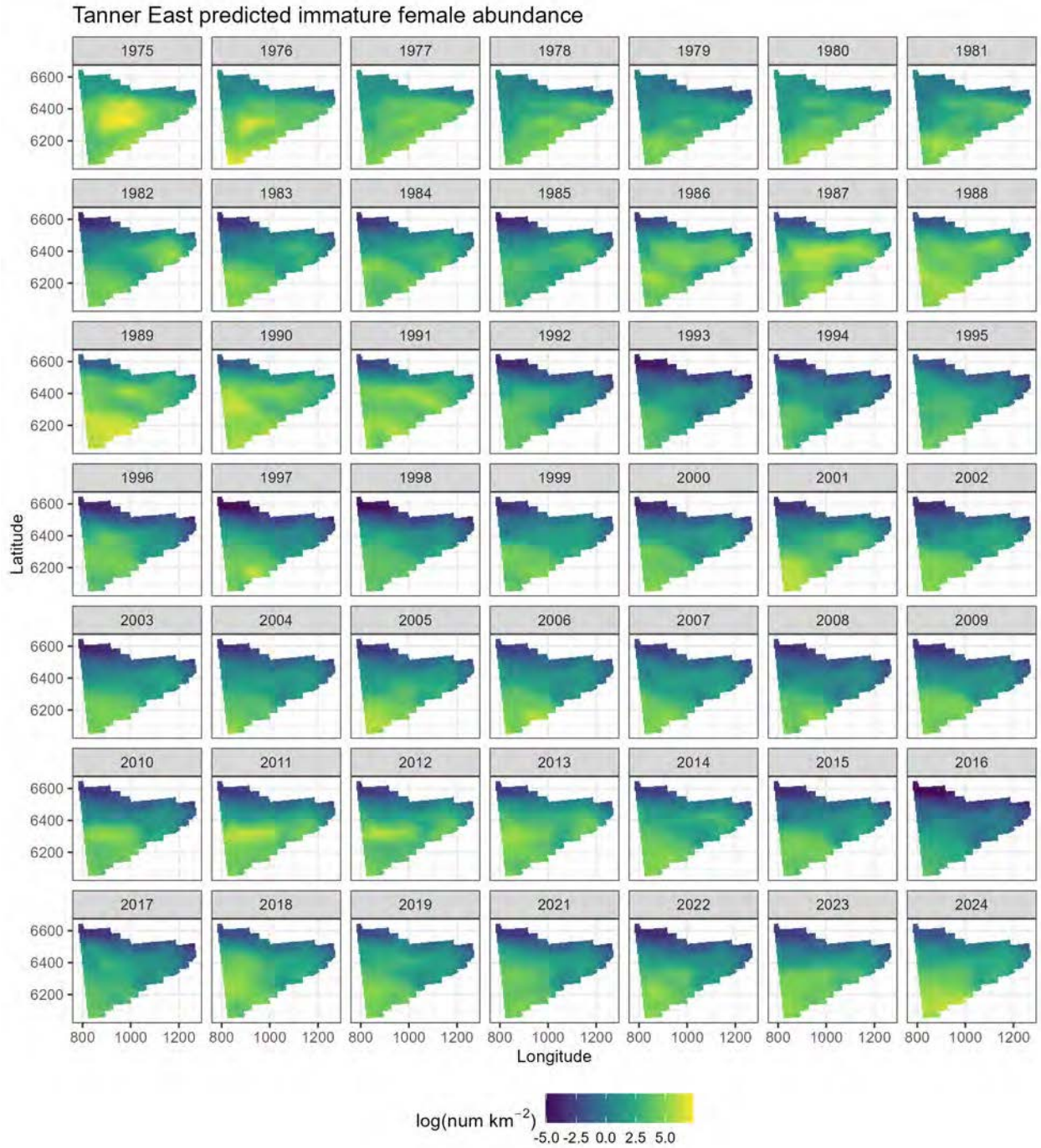
Figure 71: Spatial predictions of male biomass west of 166° using NMFS summer bottom trawl survey data before 1982 and 1982 onward with a 50-knot mesh and a delta-gamma model family. Predictions from both of these periods/models are combined in this figure.
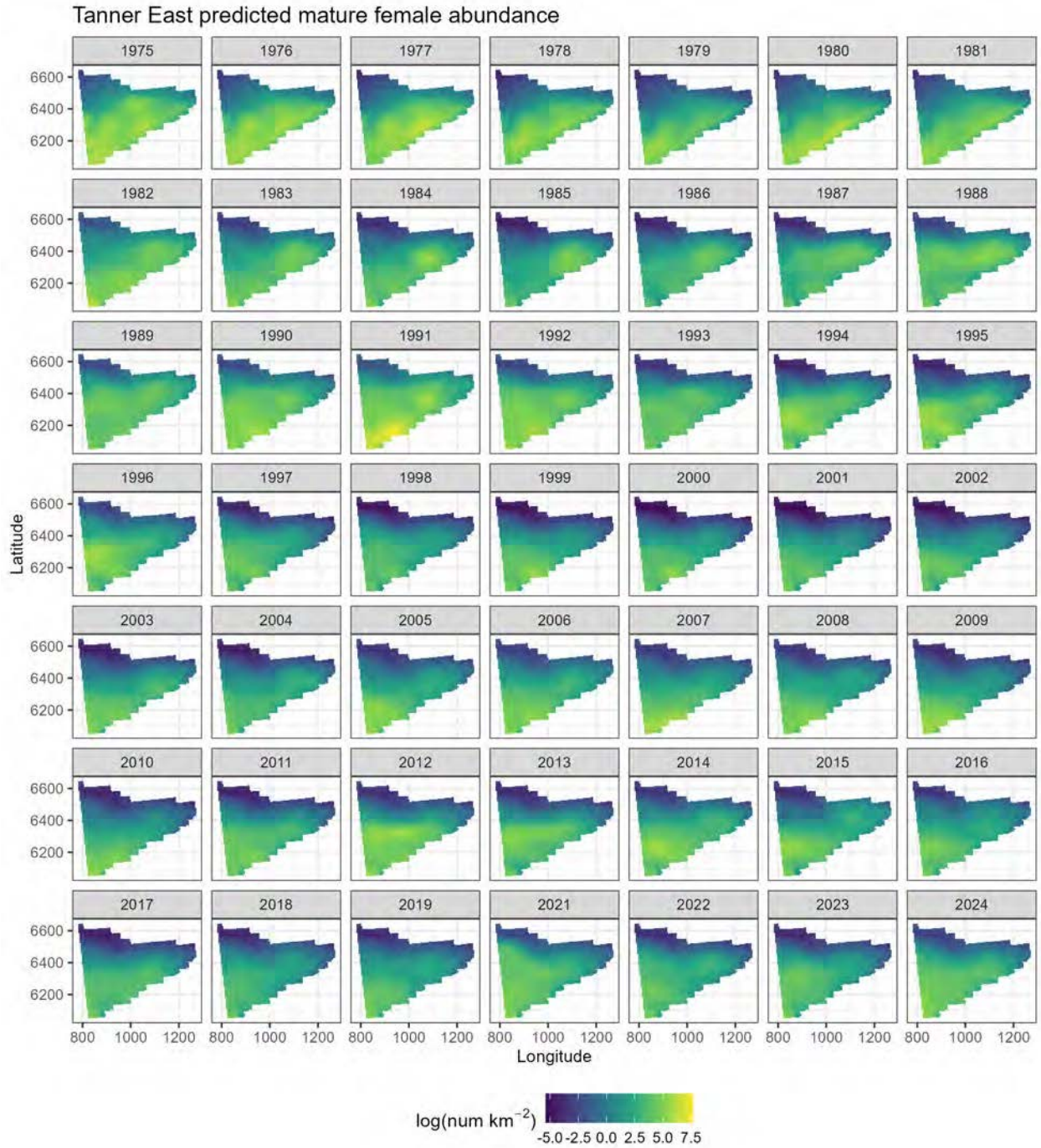
Tanner West predicted immature female biomass

Figure 72: Spatial predictions of immature female biomass west of 166° using NMFS summer bottom trawl survey data before 1982 and 1982 onward with a 50-knot mesh and a delta-gamma model family. Predictions from both of these periods/models are combined in this figure.
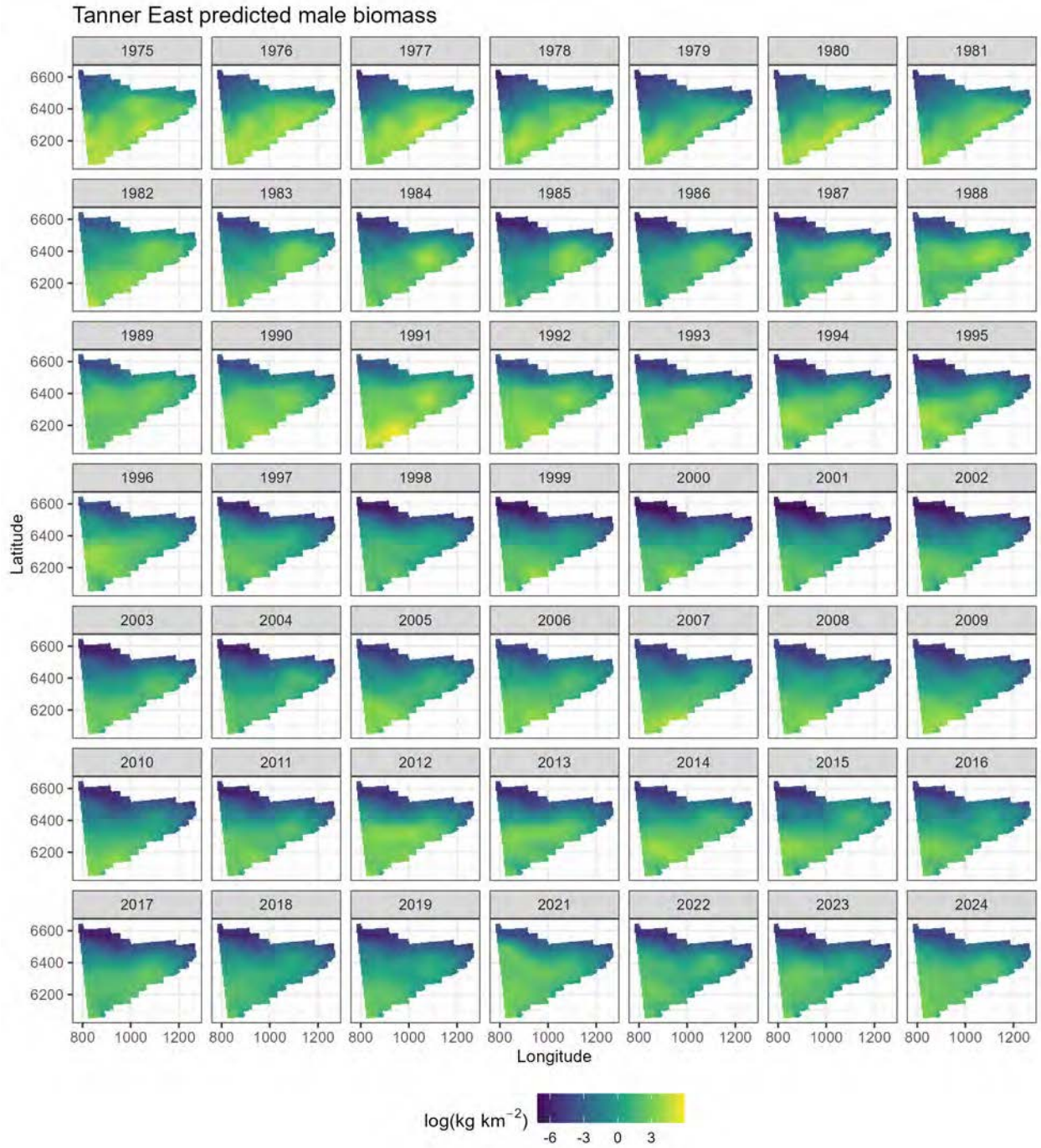
Figure 73: Spatial predictions of mature female biomass west of 166° using NMFS summer bottom trawl survey data before 1982 and 1982 onward with a 50-knot mesh and a delta-gamma model family. Predictions from both of these periods/models are combined in this figure.
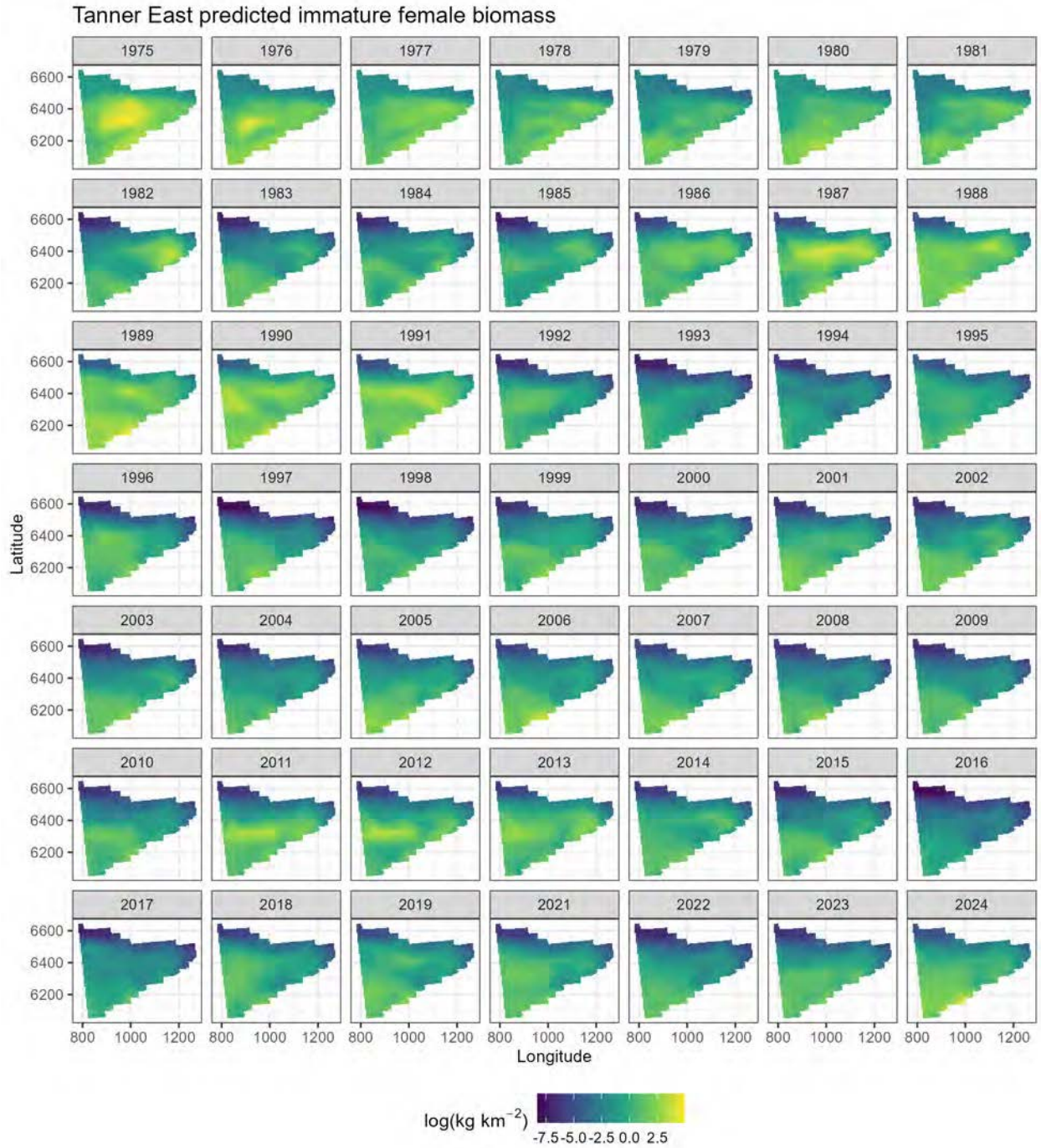
Figure 74: Spatial predictions of male abundance east of 166° using NMFS summer bottom trawl survey data before 1982 and 1982 onward with a 50-knot mesh and a delta-gamma model family. Predictions from both of these periods/models are combined in this figure.

Figure 75: Spatial predictions of immature female abundance east of 166° using NMFS summer bottom trawl survey data before 1982 and 1982 onward with a 50-knot mesh and a delta-gamma model family. Predictions from both of these periods/models are combined in this figure.
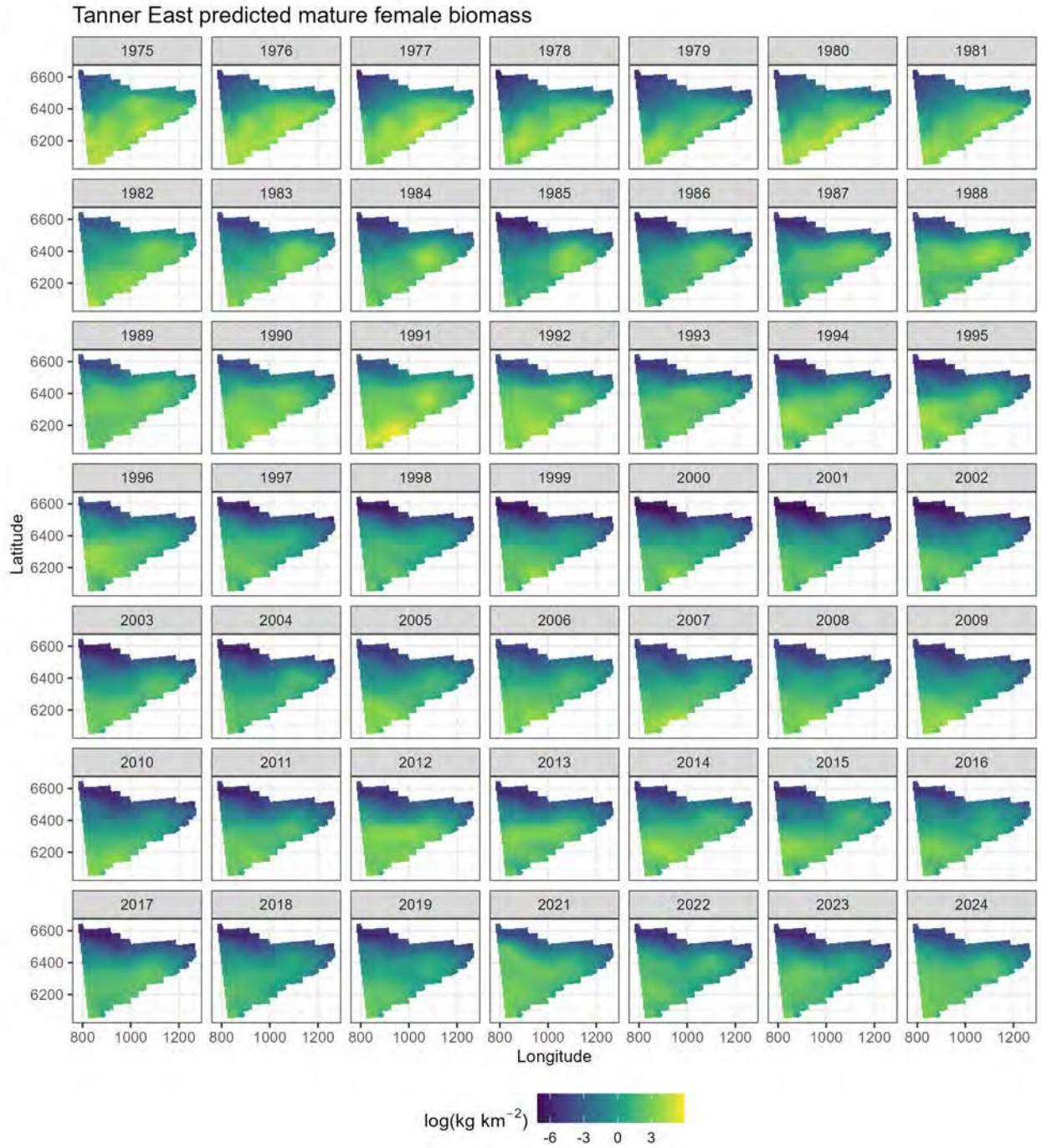
Figure 76: Spatial predictions of mature female abundance east of 166° using NMFS summer bottom trawl survey data before 1982 and 1982 onward with a 50-knot mesh and a delta-gamma model family. Predictions from both of these periods/models are combined in this figure.

Figure 77: Spatial predictions of male biomass east of 166° using NMFS summer bottom trawl survey data before 1982 and 1982 onward with a 50-knot mesh and a delta-gamma model family. Predictions from both of these periods/models are combined in this figure.

Figure 78: Spatial predictions of immature female biomass east of 166° using NMFS summer bottom trawl survey data before 1982 and 1982 onward with a 50-knot mesh and a delta-gamma model family. Predictions from both of these periods/models are combined in this figure.

Figure 79: Spatial predictions of mature female biomass east of 166° using NMFS summer bottom trawl survey data before 1982 and 1982 onward with a 50-knot mesh and a delta-gamma model family. Predictions from both of these periods/models are combined in this figure.
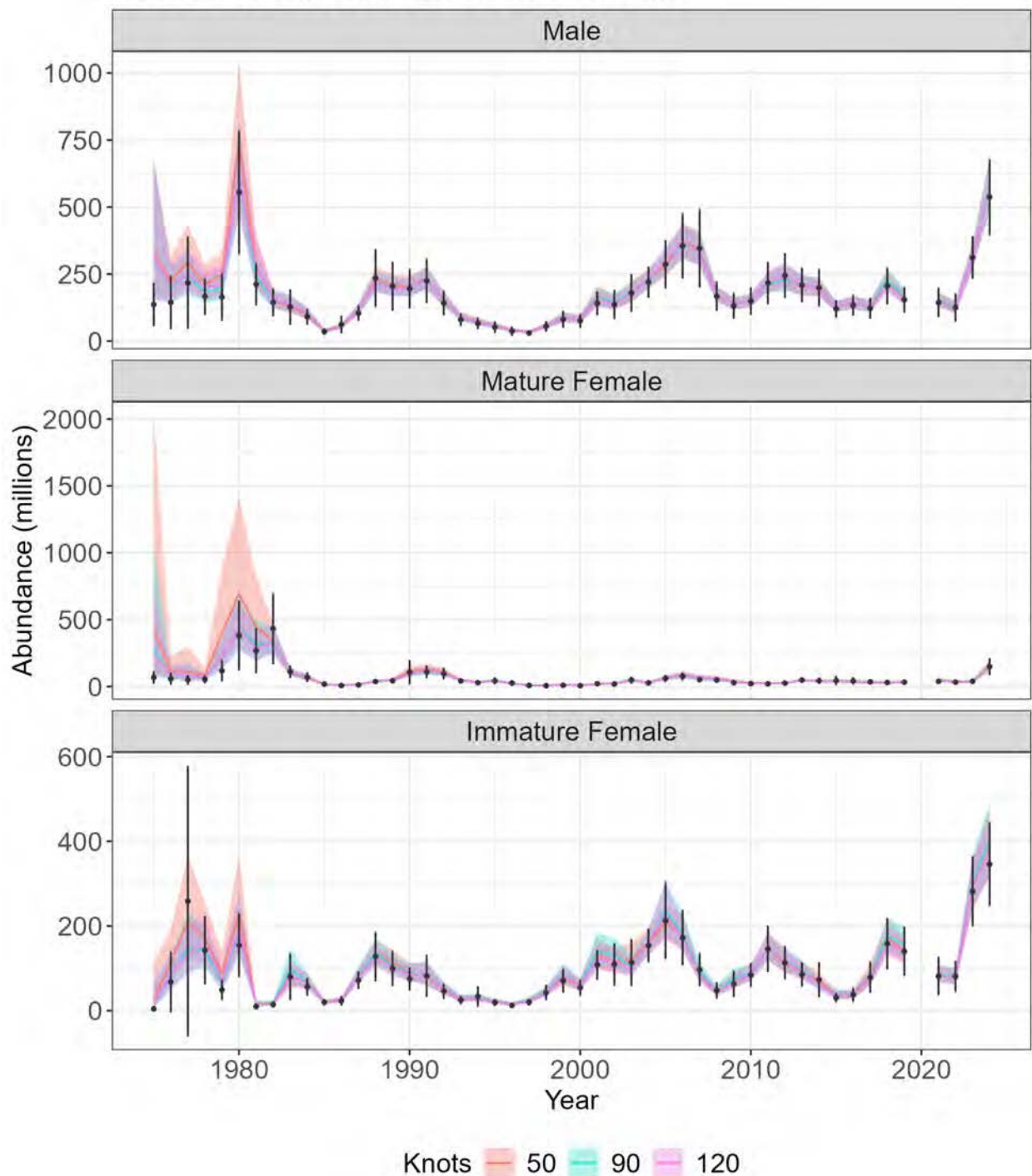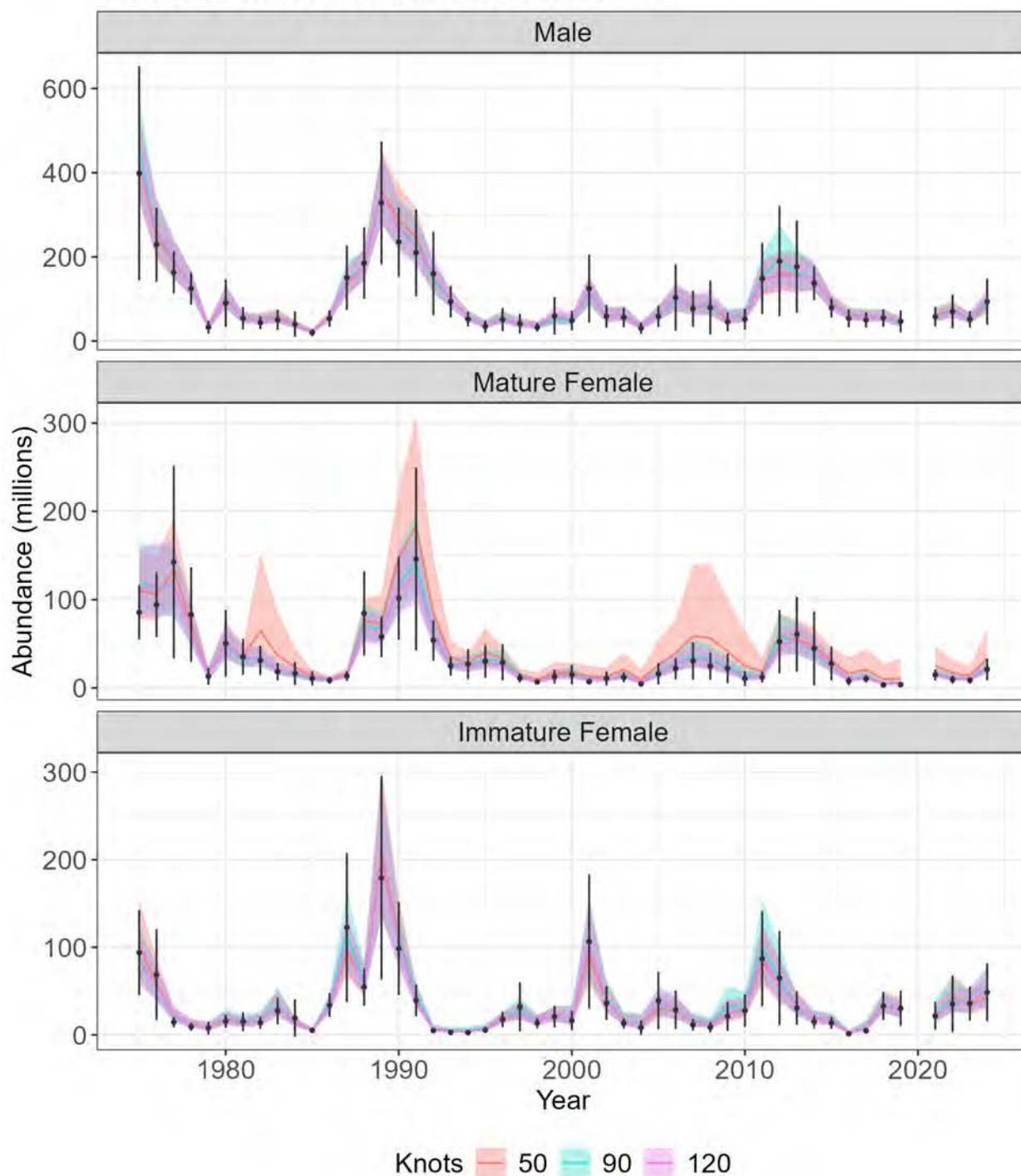
Figure 80: Estimated abundance (millions) for Tanner crab west of 166°. Colored lines represent abundance (±95% CI) estimated by sdmTMB, with orange, blue, and pink denoting models fit with a 50-, 90-, and 120-knot mesh, respectively. Black points represent abundance (±95% CI) estimated by the NMFS summer bottom trawl survey.
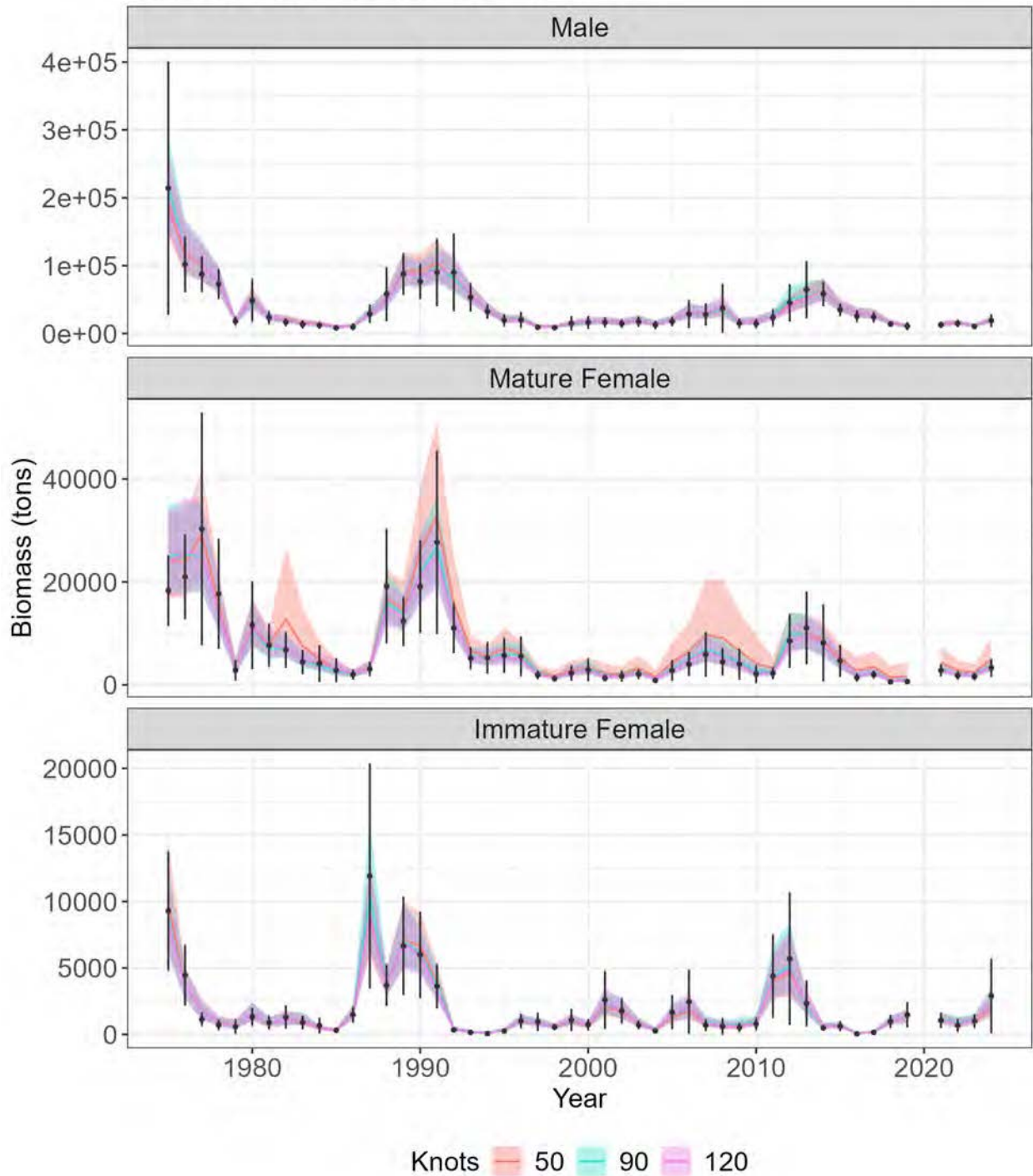
Figure 81: Estimated biomass (tons) for Eastern Bering Sea Tanner crab west of 166°. Colored lines represent abundance (±95% CI) estimated by sdmTMB, with orange, blue, and pink denoting models fit with a 50-, 90-, and 120-knot mesh, respectively. Black points represent biomass (±95% CI) estimated by the NMFS summer bottom trawl survey.

Figure 82: Estimated abundance (millions) for Tanner crab east of 166°. Colored lines represent abundance (±95% CI) estimated by sdmTMB, with orange, blue, and pink denoting models fit with a 50-, 90-, and 120-knot mesh, respectively. Black points represent abundance (±95% CI) estimated by the NMFS summer bottom trawl survey.

Figure 83: Estimated biomass (tons) for Eastern Bering Sea Tanner crab east of 166°. Colored lines represent abundance (±95% CI) estimated by sdmTMB, with orange, blue, and pink denoting models fit with a 50-, 90-, and 120-knot mesh, respectively. Black points represent biomass (±95% CI) estimated by the NMFS summer bottom trawl survey.
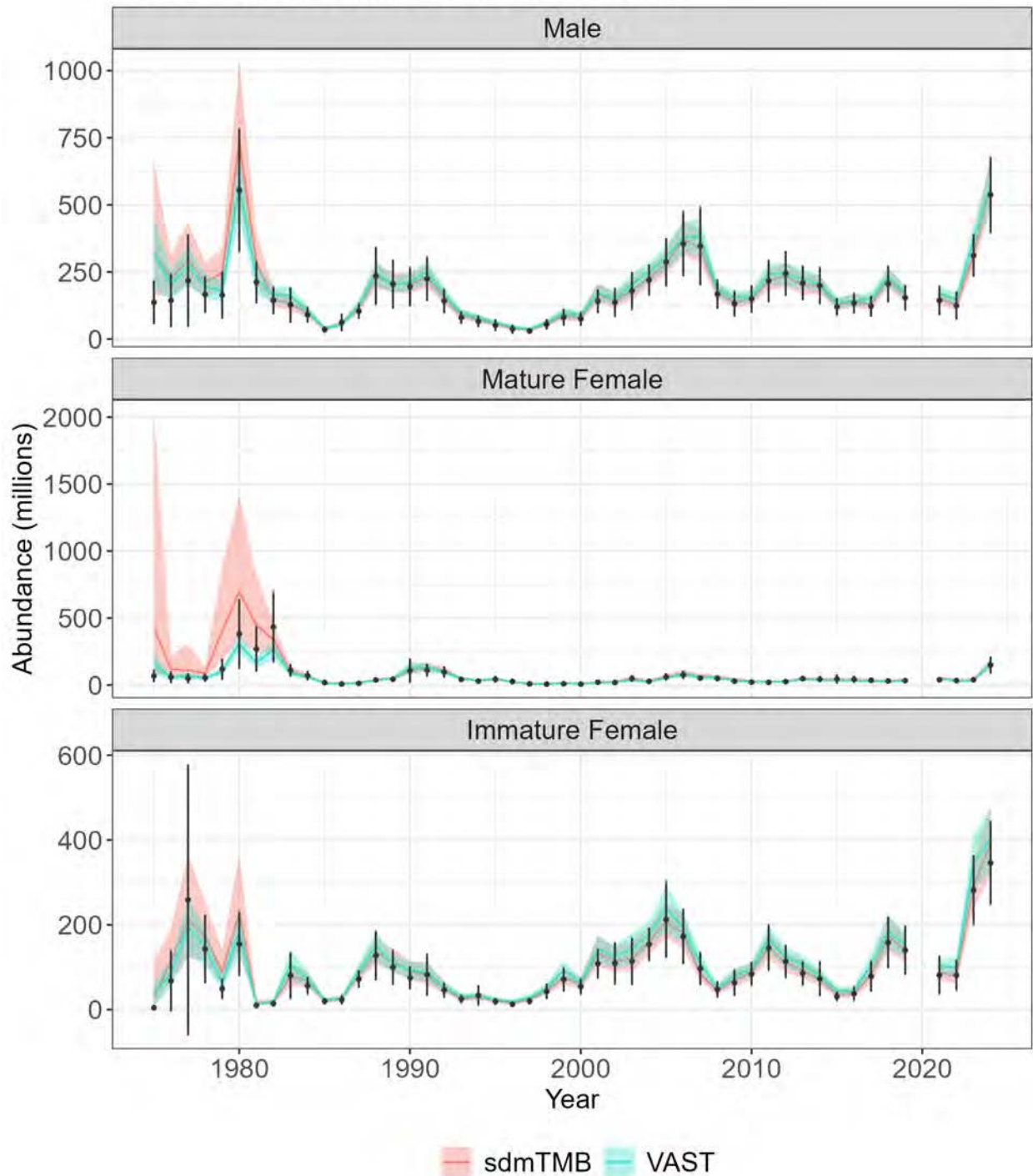
Figure 84: Estimated abundance (millions; ±95% CI) for Tanner crab west of 166° predicted using sdmTMB (pink) and VAST (blue). Both algorithms fit models using a delta-gamma family at 50 knots. Black points represent abundance (±95% CI) estimated by the NMFS summer bottom trawl survey.
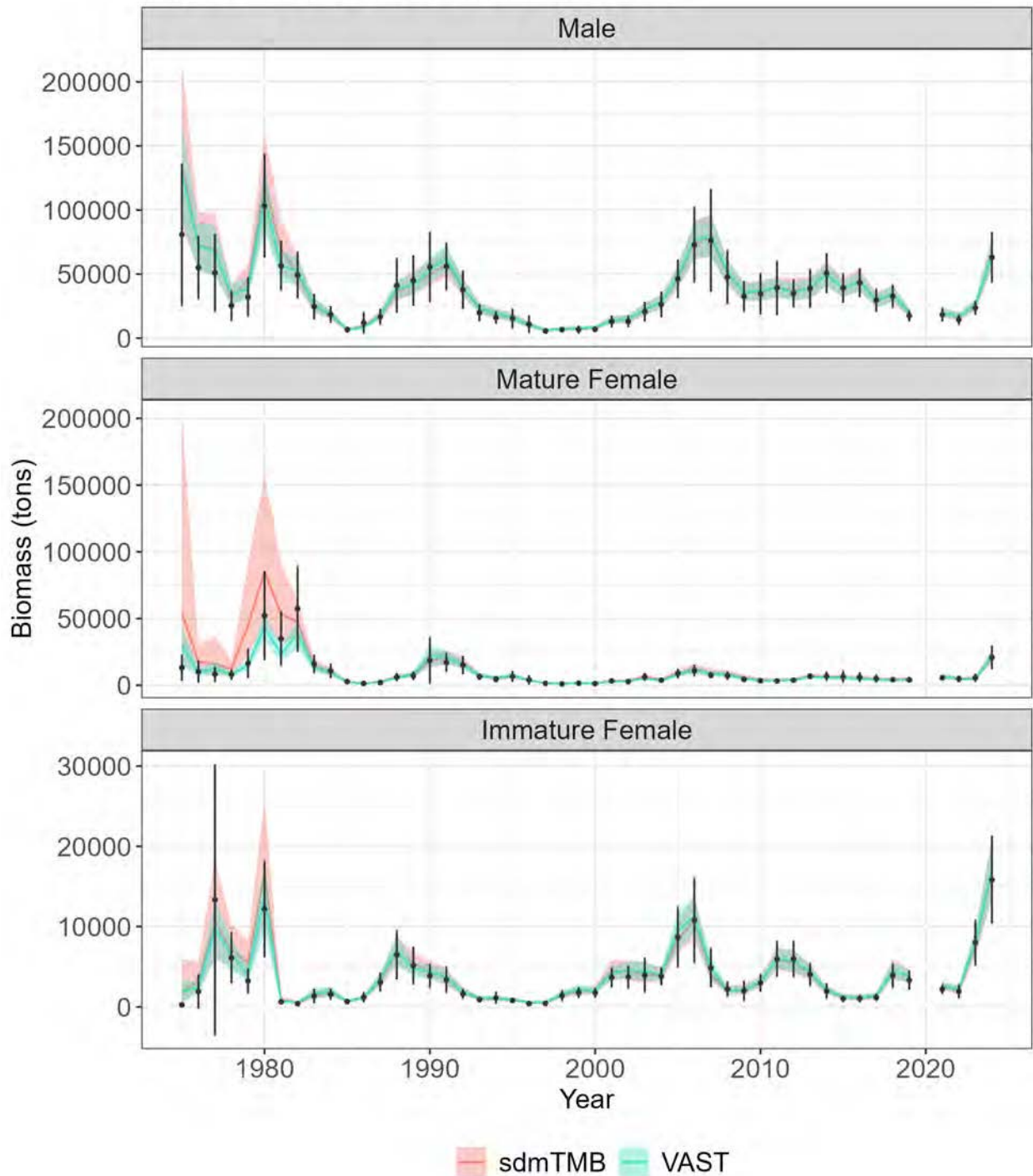
Figure 85: Estimated biomass (tons; ±95% CI) for Tanner crab west of 166° predicted using sdmTMB (pink) and VAST (blue). Both algorithms fit models using a delta-gamma family at 50 knots. Black points represent biomass (±95% CI) estimated by the NMFS summer bottom trawl survey.
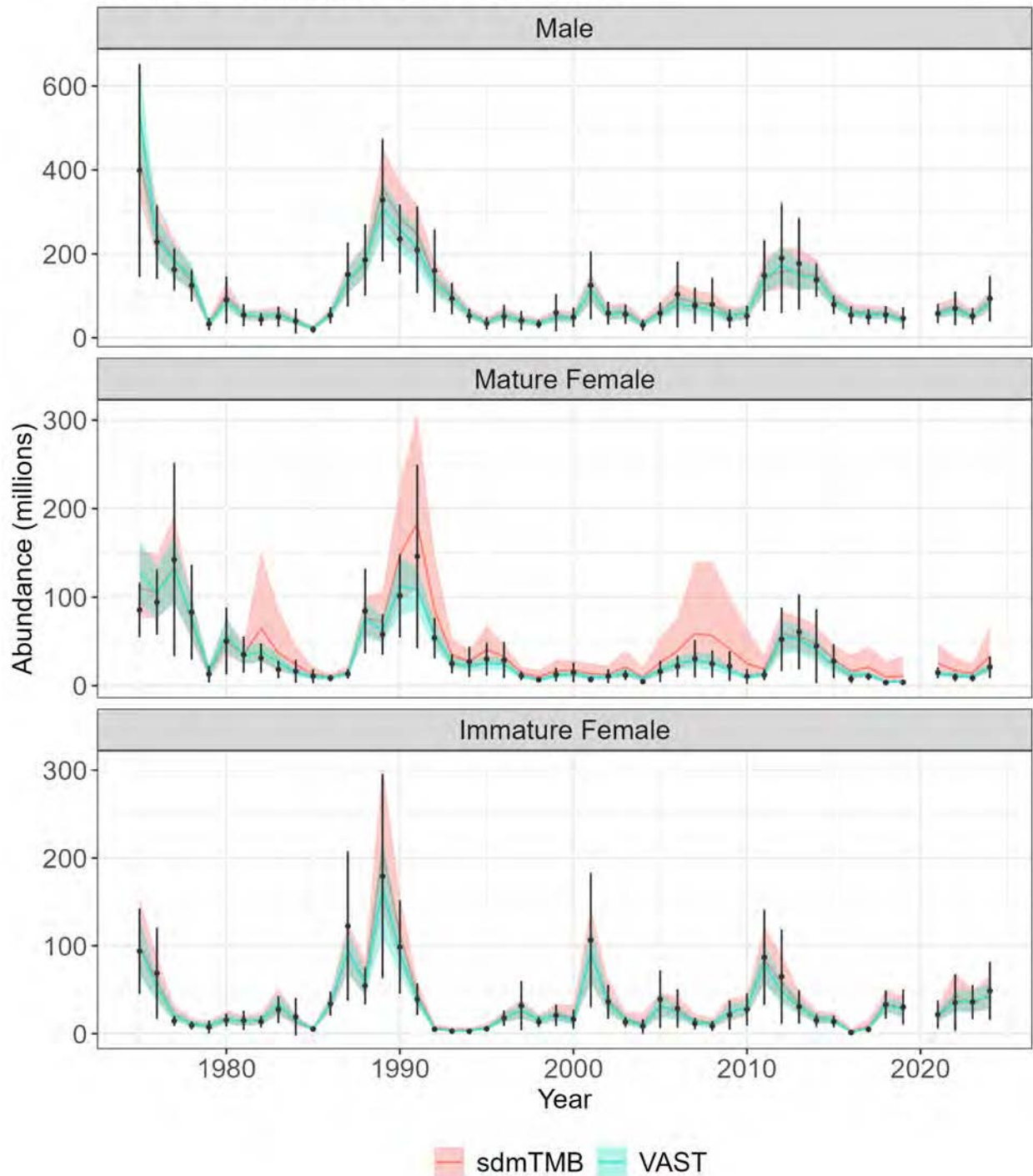
Figure 86: Estimated abundance (millions; ±95% CI) for Tanner crab east of 166° predicted using sdmTMB (pink) and VAST (blue). Both algorithms fit models using a delta-gamma family at 50 knots. Black points represent abundance (±95% CI) estimated by the NMFS summer bottom trawl survey.
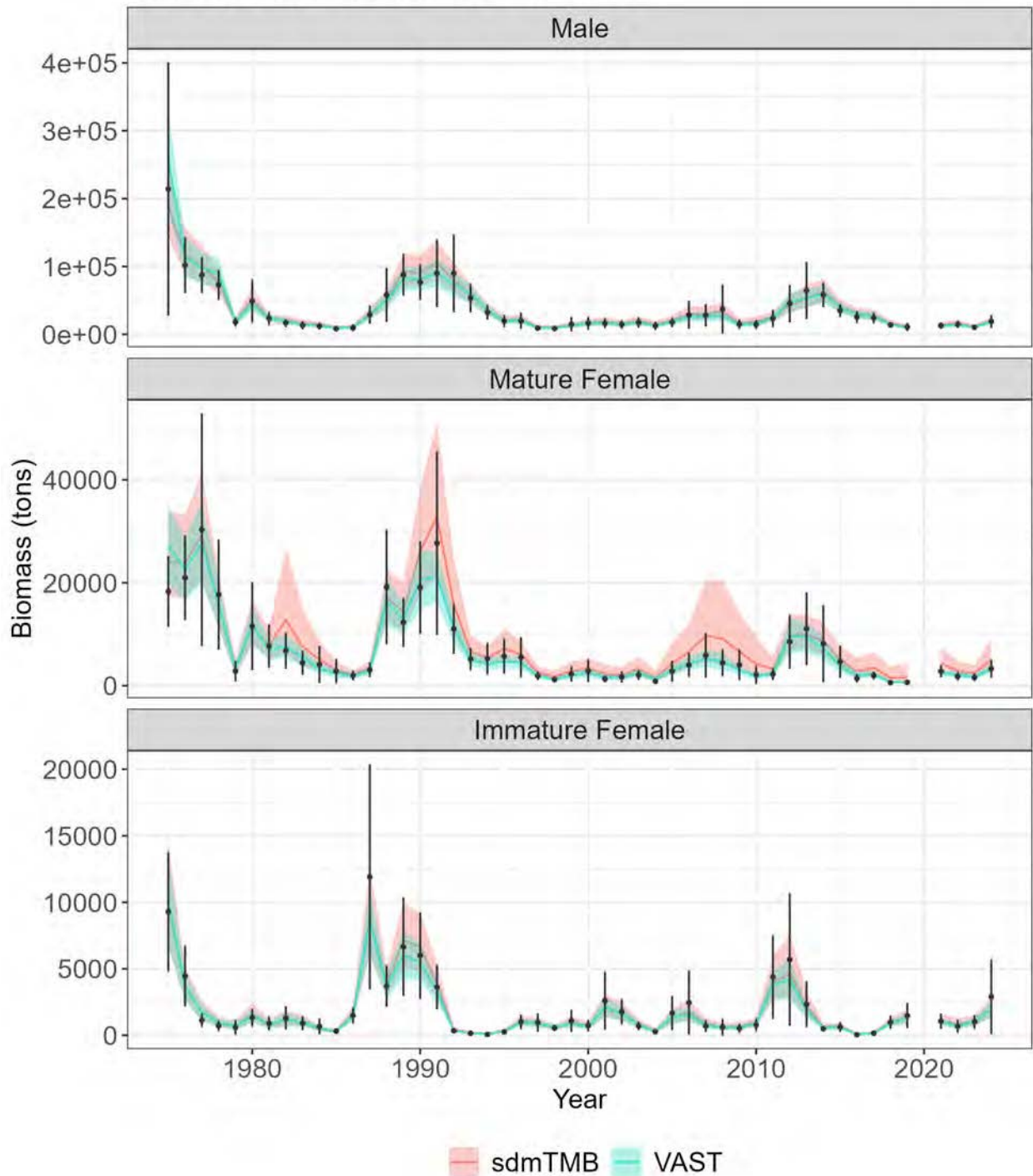
Figure 87: Estimated biomass (tons; ±95% CI) for Tanner crab east of 166° predicted using sdmTMB (pink) and VAST (blue). Both algorithms fit models using a delta-gamma family at 50 knots. Black points represent biomass (±95% CI) estimated by the NMFS summer bottom trawl survey.